3. SITE 1049[1]

Shipboard Scientific Party[2]

HOLE 1049A

Position: 30°08.5436′N, 76°06.7312′W

Date occupied: 1315 hr, 13 January 1997

Spud hole: 2100 hr, 13 January 1997

Date departed: 0400 hr, 15 January 1997

Time on hole: 38.75 hr (1 day, 14 hr, 45 min)

Seafloor (drill pipe measurement from rig floor, mbrf): 2667.3

Distance between rig floor and sea level (m): 11.2

Water depth (drill pipe measurement from sea level, m): 2656.1

Total depth (drill pipe measurement from rig floor, mbrf): 2859.2

Penetration (m): 191.9

Number of cores (including cores having no recovery): 23

Total core recovered (m): 104.32

Core recovery (%): 54.4

Oldest sediment cored:
Depth (mbsf): 191.9
Lithology: Nannofossil chalk
Age: Aptian

Comments: K/T boundary in Section 171B-1049A-17X-2

HOLE 1049B

Position: 30°08.5423′N, 76°06.7264′W

Date occupied: 0400 hr, 15 January 1997

Spud hole: 0500 hr, 15 January 1997

Date departed: 0030 hr, 16 January 1997

Time on hole: 20.5 hr (20 hr, 30 min)

Seafloor (drill pipe measurement from rig floor, mbrf): 2682.0

Distance between rig floor and sea level (m): 11.2

Water depth (drill pipe measurement from sea level, m): 2670.8

Total depth (drill pipe measurement from rig floor, mbrf): 2838.9

Penetration (m): 156.9

Number of cores (including cores having no recovery): 12

Total core recovered (m): 81.6

Core recovery (%): 73.7

Oldest sediment cored:
Depth (mbsf): 156.9
Lithology: nannofossil claystone
Age: Aptian

Comments: Drilled 0-2 and 46.5-90.7 mbsf, with K/T boundary in Section 171B-1049B-8X-2

HOLE 1049C

Position: 30°8.5370′N, 76°06.7271′W

Date occupied: 0030 hr, 16 January 1997

Spud hole: 0130 hr, 16 January 1997

Date departed: 0030 hr, 17 January 1997

Time on hole: 24 hr (1 day)

Seafloor (drill pipe measurement from rig floor, mbrf): 2682.0

Distance between rig floor and sea level (m): 11.2

Water depth (drill pipe measurement from sea level, m): 2670.8

Total depth (drill pipe measurement from rig floor, mbrf): 2840.5

Penetration (m): 158.5

Number of cores (including cores having no recovery): 13

Total core recovered (m): 88.86

Core recovery (%): 79.7

Oldest sediment cored:
Depth (mbsf): 153.29
Lithology: nannofossil chalk
Age: Aptian

Comments: Drilled intervals 0–2 and 45.0–90.0 mbsf, with K/T boundary in Section 171B-1049C-8X-5

Principal results: Site 1049 is located on the eastern margin of the Blake Nose and represents the deepest site of the Blake Nose transect. The location was chosen to recover a sedimentary section of Eocene through Aptian–Albian deep-water strata to compare with age-equivalent, but expanded, sections at shallower water depths. The site is at a present depth of 2671 m below sea level (mbsl) and is shallow enough to preclude significant dissolution in the lysocline, yet deep enough to record changes in bottom-water chemistry produced by changes in the vertical structure of deep and intermediate waters during the Paleogene and Cretaceous.

The sediments were recovered from three adjacent holes using the advanced hydraulic piston corer (APC) and extended core barrel (XCB) techniques to obtain complete recovery of the section. Although the middle Eocene, lower Paleocene–Maastrichtian, and Aptian–Albian sequences are condensed, they will be useful for paleoceanographic studies. The microfossil faunas are well preserved and, in combination with magnetostratigraphy, provide a good chronostratigraphic framework. In the upper 50 m of the section (middle Eocene), the gamma-ray attenuation porosity evaluator (GRAPE) density and magnetic susceptibility records are remarkably featureless and do not provide an unambiguous composite record. On the other hand, we observed cyclical records in all three holes from the Cretaceous/Tertiary (K/T) boundary and below that allowed us to develop a well-constrained composite Cretaceous section.

[1]Norris, R.D., Kroon, D., Klaus, A., et al., 1998. *Proc. ODP, Init. Repts.,* 171B: College Station, TX (Ocean Drilling Program).
[2]Shipboard Scientific Party is given in the list preceding the Table of Contents.

At Site 1049, the sediment/water interface is covered by a manganese sand and nodule layer that contains Pleistocene-aged planktonic foraminifers and nannofossils. Below the manganiferous sands we recovered middle Eocene to Aptian sediments that we divided into four lithologic units. Unit I is middle to lower Eocene nannofossil ooze with several ash layers. Unit II is upper to lower Paleocene nannofossil ooze with several intervals of limestone and chert. Unit III is Paleocene to upper Campanian clayey nannofossil ooze and chalk. The Cretaceous/Tertiary boundary was recovered three times within this unit and appears to be well preserved and complete. The biostratigraphically constrained boundary consists of a 0.3-cm limonitic layer containing brown yellowish spherules (and presumably microkrystites and the Ir anomaly), overlying a 9- to 17-cm normally graded bed of green clay spherules that is interpreted as microtektite ejecta. The limonitic layer is overlain by 4 cm of gray mottled clay, representing the lowermost Cenozoic. Below the K/T boundary, the 20-m-thick interval of Campanian to Maastrichtian oozes shows signs of slumping. Unit IV is lower Albian to Aptian bioturbated clayey nannofossil chalk and claystone, with high-frequency variations in color and magnetic susceptibility among light gray, dusky red, and greenish gray beds and includes a 46-cm interval of organic-rich (maximum 11.5% total organic carbon [TOC]) black shale laminated on a millimeter scale.

Middle Eocene through upper Aptian sediments are characterized by a low average sedimentation rate of ~6 m/m.y. Sedimentation rates during the lower Eocene (~11 m/m.y.) appear to have been slightly higher than those of the middle Eocene. The upper lower Eocene is separated from the middle upper Paleocene by a hiatus of at least 2 m.y., encompassing the Paleocene/Eocene boundary. Planktonic foraminifers and calcareous nannoplankton within the Paleocene are abundant and well preserved, radiolarians are absent, and benthic foraminifers are common and well preserved. Most noteworthy is the exquisite foraminifer preservation and the complete recovery of most early Danian planktonic foraminifer and calcareous nannofossil zones, including the early Danian Pα Zone (*Parvulorugoglobigerina eugubina* Zone), which is often either poorly preserved or unrecovered at other deep-sea sites containing the K/T boundary. Studies of this early Danian interval will provide a highly detailed record of paleoceanographic and evolutionary changes associated with the earliest radiation of plankton and benthos following the terminal Cretaceous extinction event.

An excellent composite record of middle Campanian through latest Maastrichtian time was also recovered. Sedimentation rates for this interval are very low, averaging about 2 m/m.y. Rhythmically bedded red and green calcareous claystones and white chalks at the base of the cored interval contain calcareous nannofossils and planktonic foraminifers of the early Albian and late Aptian. Paleodepth estimates based on benthic foraminifers revealed a deepening trend through time at Site 1049: from middle bathyal depths (~800–1000 m) during Albian times to lower bathyal depths (1000–2000 m) throughout the latest Cretaceous (Maastrichtian) and Paleogene (Paleocene to middle Eocene).

Portions from nearly all cores yielded magnetostratigraphic data, and most of these polarity intervals are reproduced at similar depth intervals in all three holes. Early to middle Eocene Chrons C19n through C22n appear to be complete, although these preliminary chron assignments may change as the shipboard middle Eocene biostratigraphy is further refined. Although the K/T interval clearly is in Chron C29r, it was not possible to delineate the exact positions of the chron boundaries. Upper Maastrichtian chrons C30n–C30r–C31n are present. A brief lower Albian reversed-polarity zone could be the elusive "M–2" reported during Leg 40. Within the Albian, an interesting "reversed-polarity" interval is adjacent to a black shale that appears to be caused by redox-induced precipitation of iron during a post-Santonian reversed-polarity period.

Sediment porosity decreases from 75% near the top of the hole to 40% at ~160 m below seafloor (mbsf). Over the same depth interval, compressional-wave velocity increases from 1500 to 1740 m/s. The compaction state of the upper sediment column suggests that about 75 m of sediment has been removed by erosion at Site 1049. The K/T boundary was well resolved with *P*-wave, magnetic susceptibility, and GRAPE data. Magnetic susceptibility increases in magnitude and GRAPE bulk density and *P*-wave velocity decrease in magnitude across the boundary. These changes may be caused by the occurrence of more iron-rich noncarbonate material, which has a coarser grain size and is less consolidated within the boundary layer. The Albian organic-rich black shale is well defined by multisensor track (MST) data that show a decrease in magnetic susceptibility and an increase in natural gamma radiation. An organic carbon-rich interval occurs in Albian variegated claystones and ranges from 1.7% to 11.5% TOC, with hydrogen indices of 451 to 699 mg hydrocarbons (HC)/g TOC. Finally, unlike the terrestrial-sourced organic matter from the Aptian–Albian of the Blake-Bahama Basin, the Albian organic matter at Site 1049 has a marine origin.

BACKGROUND AND OBJECTIVES

Background

Site 1049 is located on the eastern margin of the Blake Nose and represents the deepest site of the Ocean Drilling Program (ODP) Leg 171B Blake Nose transect. We reoccupied Deep Sea Drilling Project (DSDP) Site 390 to recover a sedimentary section of Eocene through Campanian deep-water strata to compare with age-equivalent, but more expanded, sections at shallower water depths. In particular, the middle Eocene and lower Paleocene–Maastrichtian sequences are thick enough to allow high-resolution paleoceanographic studies. The well-preserved faunas should be suitable to tie micropaleontologic events to the magnetostratigraphy, and we hope that parts of the sequence will yield a complete record of Milankovitch orbital climate cycles spanning one or more polarity zones to further refine the time scale in these periods.

About 200 m of sediment was recovered at Site 390, including 160 m of middle Eocene to Barremian pelagic sediment and 40 m of Barremian oolitic limestone. The Site 390 pelagic sediments are entirely stiff to soupy nannofossil ooze, with the exception of seven 5-cm-thick limestone and chert stringers recovered in the 30-m-thick lower Eocene and upper Paleocene sections. Eocene sediments form about 75 m of the cored section, whereas the Paleocene (35 m), Maastrichtian (28 m), Campanian (2 m), and Barremian to lower Albian (20 m) pelagic sediments make up the remainder. During rotary core barrel (RCB) drilling of Hole 390A, the penetration rate was about 50 m/hr, except in the cherts, where it dropped to about 20 m/hr. We hoped to use the results from Site 390 to guide our drilling through cherts in the lower Eocene and upper Paleocene sediments. We also hoped to determine the distribution and number of chert intervals in the stratigraphic section and to assess how difficult it would be to recover them with the APC.

Objectives

Site 1049 was included mainly to increase the total depth range of the Leg 171B transect (to about 1330 m total water-depth range) and to recover sediments deposited well within the depth range of modern Upper North Atlantic Deep Water. Site 390 has a moderately thick Paleocene–Eocene section, and we anticipated that the APC coring system could produce much better recovery of the stratigraphic section than was obtained with the Leg 44 rotary coring system. Complete recovery of the Paleogene section in multiple holes at Site 1049 was expected to provide a record useful for comparison with more expanded records of equivalent age at shallower water depths in the Leg 171B depth transect. The well-preserved microfaunas from the Paleogene should be extremely useful in reconstructing deep-water characteristics throughout this period at a reasonably high temporal resolution. Hence, this deep location along the slope is useful for obtaining information on Paleogene deep-water circulation, one of the key objectives of Leg 171B.

Drilling at Site 390 recovered an apparently biostratigraphically complete K/T boundary interval, including a spherule layer smeared by rotary drilling over about 40 cm of core in soft sediments. An im-

portant objective of drilling Site 1049 was to recover the boundary section with considerably less drilling disturbance than that achieved at Site 390. Our intention was to use the APC/XCB coring tools to recover the K/T boundary in as undisturbed a state as possible in order to obtain crucial information on the sequence of events surrounding the boundary.

Another objective of drilling at Site 1049 was to recover Campanian–Maastrichtian and Albian–Aptian sequences. Although these sequences are relatively condensed, they are useful for biomagnetostratigraphic and paleoceanographic purposes. There are few low-latitude sites where Cretaceous sediments with well-preserved calcareous microfossils have been found. The well-preserved Cretaceous fauna and flora found at Site 390 made it worthwhile to try to recover the Cretaceous sequences at Site 1049. Our main aims were to document climate cyclicity and variability in low-latitude, sea-surface temperatures and to characterize deep-water circulation during the Albian–Aptian and Campanian–Maastrichtian periods, when the North Atlantic basins were more isolated and bottom-water ventilation was more restricted. One of our particular interests was to obtain a well-developed mid-Maastrichtian section to study the response of the biota to the change in deep-water circulation observed at southern high-latitude sites. The excellent preservation of the microfaunas from shallowly buried Cretaceous oozes, combined with the magnetostratigraphy, should render Site 1049 useful for paleoceanographic reconstructions.

OPERATIONS

Transit From Bridgetown, Barbados, to Site 1049

We departed Bridgetown, Barbados, at 1515 hr on 8 January 1997, and began the 1400-nmi transit to the first site of Leg 171B. Calm seas and a following current contributed to the short transit time to the first site.

During the transit, we passed to the west of the islands of Dominica, Guadeloupe, Monserrat, Nevis, St. Kitts, St. Eustatius, Saba, and St. Martin and to the east of the Virgin Islands. A warning had been issued by the government of Monserrat that the southwestern wall of Soufriere Hill Volcano could collapse, and all ships were alerted to pass no closer than 10 nmi. The *JOIDES Resolution* sailed about 20 nmi west of the island, and we passed under the volcano's ash cloud, driven west by trade winds.

After traversing 1380 nmi at an average speed of 12.3 kt, we arrived at the beginning of the site survey over the Leg 171B drill sites at 0700 hr on 13 January. We then conducted a short seismic reflection survey over the sites, primarily to reconfirm the exact location of proposed sites BN-3 (1051) and BN-4Alt (1053). After the survey was finished (1245 hr, 13 January), we positioned the ship over the intended position of Site 1049 (proposed site BN-1 and Site 390), extended the hydrophones and thrusters, and deployed a positioning beacon at 1315 hr. Depths reported in the "Operations" sections (this chapter) are drill-pipe measurements in meters below rig floor (mbrf). The elevation of the rig floor above sea level was 11.2 m for Holes 1049A, 1049B, and 1049C.

Hole 1049A

Based on a precision depth recorder (PDR) depth of 2687.4 mbrf (corrected using Carter tables for local variations in water sound velocity), we positioned the bit ~5 m above the PDR-inferred mudline at 2682 mbrf. The bit apparently contacted the seafloor at 2682 mbrf (inferred from the weight indicator), and we raised the bit to 2681 mbrf to take the first APC mudline core. The APC did not fully stroke into the formation. When the core barrel was retrieved, the lower half of the inner barrel was missing.

Although the parting of the core barrel was a surprise, the difficulty in attaining an APC mudline core was not unexpected because RCB coring at Site 390 recovered a veneer of manganese nodules and sand that is present throughout the Blake Nose area. Farther up the slope of the Blake Nose, this surface veneer is lithified, and it is possible that the surface veneer partially deflected the APC attempt and snapped off the barrel. When the core barrel was pulled out of the formation, there was no indication of excessive pull-out force; therefore, the failure was not attributed to the core barrel being stuck in the formation. We decided to offset the vessel 10 m to the east to spud in with the XCB.

During the next attempt, we apparently contacted the seafloor at 2667.3 mbrf, based on an apparent 5000-lb reduction in drill-string weight. After advancing 20.6 m and retrieving two XCB cores with no recovery, the bit appeared to advance effortlessly into soft sediments. We then initiated APC coring and obtained Cores 171B-1049A-3H through 7H. Core 7H was not able to attain a full stroke and recovered 1.5 m of nannofossil ooze, as well as a large chert fragment jammed in the cutting shoe.

We then took XCB Core 8X, which appeared to penetrate the chert layer after advancing only 1.8 m. This core recovered 0.76 m of chert fragments and nannofossil ooze. Because the APC Core 9H attempt did not obtain a full stroke, we resumed XCB coring. With the exception of one additional piston core attempt (Core 13H, which did not attain full stroke), the remainder of the hole was XCB cored. Several zones of chert were encountered between 40 and 90 mbsf.

The K/T boundary was recovered in Section 171B-1049A-17X-2. Coring was terminated at 172.7 mbsf after meeting the objective to recover Aptian-aged sediments (Table 1). The bit cleared the mudline and Hole 1049A was officially terminated at 0400 hr on 15 January.

The seafloor depths for Hole 1049A, determined by the reduction of drill-string weight, are most likely incorrect when compared with those in Holes 1049B and 1049C. The mbsf of a marker layer, such as the limonitic interval at the top of the K/T boundary, indicates that the correlative interval in Hole 1049A (125.88 mbsf) is ~12–14 m deeper than the corresponding intervals in Holes 1049B and 1049C (111.18 and 112.99 mbsf, respectively). To compare data from Hole 1049A with the other holes at this site, the depth must be adjusted by subtracting ~12–14 m from the reported Hole 1049A mbsf depth.

Hole 1049B

We offset the ship 10 m east of Hole 1049A and spudded Hole 1049B using an XCB core barrel with a center bit. A water depth of 2682.0 mbrf was determined by the driller gently lowering the bit until he observed a gradual reduction in drill-string weight. After drilling ahead for 2 m to penetrate the surface sediments that had caused problems in Hole 1049A, we deployed an APC core barrel. APC Cores 171B-1049B-1H through 5H were taken from 2.0 to 46.5 mbsf, and, after advancing 6.5 m, Core 5H contacted the expected (based on Hole 1049A results) chert layer.

In order to avoid the poor core recovery experienced in the corresponding interval in Hole 1049 and to make up for the slower than expected penetration rates, we drilled through the chert zone (46.5 to 90.7 mbsf) using an XCB core barrel with a center bit. XCB Cores 171B-1049B-6X and 7X were then taken to 109.0 mbsf. We wanted to APC core the K/T boundary, and, fortunately, APC Core 8H recovered a full core spanning this target interval. XCB Cores 9X and 12X were then taken from 118.5 to 156.9 mbsf (Table 1). The bit was pulled out of the hole and cleared the mudline at 0030 hr on 16 January.

Hole 1049C

We offset the ship 10 m east of Hole 1049B and spudded Hole 1049C using the XCB with a center bit. Based on the drill-string weight indicator, the water depth was the same as that in Hole 1049B (2682.0 mbrf). After drilling to 2 mbsf, we took APC Cores 171B-1049C-1H through 5H (2–45 mbsf) until contact was made with the

first chert layer at 45.0 mbsf. After the hole was drilled from 45.0 to 90.0 mbsf without coring, XCB coring advanced to 120.2 mbsf. We obtained a third recovery of the K/T boundary at Site 1049 in Core 8X. Core 10H was shot at 120.2 mbsf. Although the drill bit did not achieve a full stroke, a full core was recovered, indicating that the bottom part had been sucked in. XCB Cores 11X through 13X were taken from 129.7 to the total depth of 158.5 mbsf (Table 1). We then began to retrieve the drill pipe at 1945 hr on 16 January.

When the drill bit was inspected at the surface, one cone and cone leg were missing; no other bit damage was observed. We suspect that the large heave experienced on 16 January possibly contributed to this failure by slamming the bit into the formation. Because the drillers did not observe erratic torque while drilling, the bit failure may have occurred just before (or while) pulling out of the hole.

While the vessel was coring Hole 1049C, the operator of the dynamic positioning system (DPS) observed the sudden onset of a 3.4-kt current toward the east-northeast. Simultaneously, a front passed through with southerly wind gusts as high as 35 kt. Because of the direction of the strong current, it was not possible for the ship to head directly into the wind-driven sea. As a result of the conflicting angles of the wind and current, there was considerable ship motion, with as much as 3-m heaves and 6° roll angles.

After securing the drilling equipment, we began the ~7-nmi transit to Site 1050 at 0030 hr on 17 January.

Table 1. Site 1049 coring summary.

Core	Date (January 1997)	Time (UTC)	Depth (mbsf)	Length cored (m)	Length recovered (cm)	Recovery (%)
171B-1049A-						
1X	13	0320	0.0-9.3	9.3	0.00	0.0
2X	13	0415	9.3-18.6	9.3	0.01	0.1
3H	14	0000	18.6-30.1	11.5	10.02	87.1
4H	14	0140	30.1-39.6	9.5	10.01	105.3
5H	14	0230	39.6-49.1	9.5	9.98	105.0
6H	14	0320	49.1-58.6	9.5	9.98	105.0
7H	14	0420	58.6-60.1	1.5	1.46	97.3
8X	14	0715	60.1-61.9	1.8	0.76	42.2
9H	14	0800	61.9-69.4	7.5	7.53	100.0
10X	14	1030	69.4-77.1	7.7	3.77	48.9
11X	14	1630	77.1-86.1	9.0	0.18	2.0
12X	14	1730	86.1-95.7	9.6	3.04	31.6
13H	14	1815	95.7-100.1	4.4	4.40	100.0
14X	14	1945	100.1-105.3	5.2	0.21	4.0
15X	14	2105	105.3-115.0	9.7	0.65	6.7
16X	14	2210	115.0-124.6	9.6	9.15	95.3
17X	14	2335	124.6-134.3	9.7	3.87	39.9
18X	15	0035	134.3-143.9	9.6	8.12	84.6
19X	15	0200	143.9-153.5	9.6	7.06	73.5
20X	15	0320	153.5-163.1	9.6	8.02	83.5
21X	15	0510	163.1-172.7	9.6	4.62	48.1
22X	15	0650	172.7-182.3	9.6	1.46	15.2
23X	15	0800	182.3-191.9	9.6	0.02	0.2
Coring totals:				191.9	104.32	54.4
171B-1049B-						
			*** Drilled from 0.0 to 2.0 mbsf ***			
1H	15	1145	2.0-11.5	9.5	6.91	72.7
2H	15	1230	11.5-21.0	9.5	10.01	105.3
3H	15	1315	21.0-30.5	9.5	9.96	105.0
4H	15	1430	30.5-40.0	9.5	9.75	102.0
5H	15	1520	40.0-46.5	6.5	6.48	99.7
			***Drilled from 46.5 to 90.7 mbsf ***			
6X	15	2120	90.7-100.3	9.6	9.60	100.0
7X	15	2220	100.3-109.0	8.7	0.00	0.0
8H	15	2310	109.0-118.5	9.5	9.54	100.0
9X	16	0035	118.5-128.1	9.6	9.72	101.0
10X	16	0205	128.1-137.7	9.6	0.15	1.6
11X	16	0310	137.7-147.3	9.6	3.13	32.6
12X	16	0425	147.3-156.9	9.6	6.38	66.4
Coring totals:				110.7	81.63	73.7
171B-1049C-						
			*** Drilled from 0.0 to 2.0 mbsf ***			
1H	16	0755	2.0-11.5	9.5	0.10	1.1
2H	16	0755	11.5-21.0	9.5	9.63	101.0
3H	16	0900	21.0-30.5	9.5	9.94	104.0
4H	16	0955	30.5-40.0	9.5	9.50	100.0
5H	16	1050	40.0-45.0	5.0	9.94	199.0
			***Drilled from 45.0 to 90.0 mbsf ***			
6X	16	1800	90.0-96.5	6.5	5.34	82.1
7X	16	1850	96.5-106.1	9.6	1.61	16.8
8X	16	1940	106.1-115.7	9.6	9.50	98.9
9X	16	2020	115.7-120.2	4.5	5.34	118.0
10H	16	2115	120.2-129.7	9.5	9.74	102.0
11X	16	2230	129.7-139.3	9.6	4.84	50.4
12X	16	1845	139.3-148.9	9.6	8.99	93.6
13X	17	0025	148.9-158.5	9.6	4.39	45.7
Coring totals:				111.5	88.86	79.7

Note: An expanded version of this coring summary table that includes lengths and depths of sections and comments on sampling is included on CD-ROM (back pocket, this volume).

LITHOSTRATIGRAPHY

Description of Lithologic Units

Site 1049 was drilled at the northeastern end of the Blake Nose and represents a reoccupation of Site 390. Three holes were drilled at Site 1049. We divided the recovered section into four lithologic units based on variation in clay content and fossil composition and preservation (Table 2; Fig. 1). Sediment composition was estimated from smear slides (Section 5 on CD-ROM, back pocket, this volume). The uppermost unit is a manganese oxide layer of unknown thickness that yields Pleistocene nannofossils and is designated as lithologic Subunit IA. Beneath this layer is lithologic Subunit IB, a 51-m-thick middle Eocene section of nannofossil ooze with varying levels of foraminifers and siliceous microfossils, primarily radiolarians and sponge spicules. Lithologic Unit II (45.2 m thick; lower Eocene to lower Paleocene in age) comprises interbeds of nannofossil ooze and chert. Lithologic Unit III ranges in age from early Paleocene to late Maastrichtian and is divided into four subunits that contain nannofossil ooze and chalk and vary in color: pale orange (lithologic Subunit IIIA), greenish gray (lithologic Subunit IIIB), pale yellow to yellowish green (lithologic Subunit IIIC), and white (lithologic Subunit IIID). Lithologic Unit III contains a K/T boundary section that is remarkably well preserved and relatively undisturbed by drilling. The K/T boundary was recovered in each hole drilled at Site 1049. The oldest unit recovered, lithologic Unit IV (38.2 m thick; Aptian to Albian in age), is characterized by a rhythmic alternation of reddish and green bioturbated nannofossil clay, white nannofossil chalk with clay, and yellowish green laminated nannofossil clay. This unit also contains a 46-cm-thick laminated black shale that is rich in immature organic matter (see "Organic Geochemistry" section, this chapter).

Exact section thickness is uncertain because of difficulties in determining the seafloor depth (see "Operations" section, this chapter), but is estimated to be 170 m in Hole 1049A, 157 m in Hole 1049B, and 158 m in Hole 1049C. The composite section for Site 1049 is 176.6 m thick (Fig. 2). As expected (because Site 1049 is a reoccupation of Site 390), our lithologic boundaries correspond roughly to those proposed for Holes 390 and 390A (Shipboard Scientific Party, 1978; Fig. 3). Our lithologic Subunits IA and IB match their lithologic Units 1 and 2, respectively. The top and bottom of our lithologic Unit II are defined by the first and last downhole occurrences of chert, whereas a transitional upper contact was proposed at Site 390. Furthermore, Benson, Sheridan, et al.'s Unit 3 was subdivided into two subunits based on differences in the stratigraphic distribution of chert; however, we could not resolve this change. Except for the basal 3 m, lithologic Unit 4 at Site 390 seems to correspond to our lithologic Subunit IIIA. Our lithologic Subunit IIIB includes all of their lithologic Unit 5 as well as the basal 3 m of the overlying lithologic Unit 4. Our lithologic Subunits IIIC and IIID correspond to their lithologic Unit 6, and our lithologic Unit IV (which we divided into two subunits) corresponds to their lithologic Unit 7. We did not recover sediment corresponding to their lithologic Unit 8.

Table 2. Summary of lithologic units from the three holes drilled at Site 1049.

Lithologic unit/ subunit	Hole 1049A	Hole 1049B	Hole 1049C	Age
IA	Interval 2X-1, 0 cm, to 3H-1, 2 cm 9.3-18.6 mbsf	NR	Interval 1H-CC, 0 cm, to 1H-1, 10 cm 2.0-2.1 mbsf	Holocene to Pleistocene
IB	Interval 3H-1, 2 cm, to 7H-CC, 32 cm 18.6-60.1 mbsf 41.5 m thick	Interval 1H-1, 0 cm, to 6X-CC, 44 cm 0-46.5 mbsf 46.5+ m thick (base not recovered)	Interval 1H-CC, 10 cm, to 5H-CC, 23 cm 2.1-45.0 mbsf 42.9+ m thick (base not recovered)	middle Eocene
II	Interval 8X-1, 0 cm, to 14X-CC, 21 cm 60.1-105.3 mbsf 45.2 m thick	Interval 6X-1, 0 cm, to 6X-CC, 21 cm 90.7-100.3 mbsf 9.6+ m thick (top not recovered)	Interval 6X-1, 0 cm, to 6X-2, 100 cm 90.0-92.5 mbsf 2.5+ m thick (base not recovered)	early Eocene to early Paleocene
IIIA	Interval 15X-1, 0 cm, to 16X-5, 140 cm 105.3-122.4 mbsf 17.1 m thick	6X-4, 55 cm, to 7X-CC 100.3-109.0 mbsf 8.7+ m thick (top not recovered)	Interval 6X-2, 100 cm, to 8X-1, 0 cm 90.0-106.1 mbsf 16.1 m thick	early Paleocene
IIIB	Interval 16X-5, 140 cm, to 18X-4, 13 cm 122.4-138.9 mbsf 16.5 m thick	Interval 7X-CC to 9X-5, 64 cm 109.0-125.1 mbsf 16.1 m thick	Interval 8X-1, 0 cm, to 10H-4, 95 cm 106.1-125.6 mbsf 19.5 m thick	early Paleocene to early Maastrichtian
IIIC	Interval 18X-4, 13 cm, to 19X-1, 0 cm 138.9-144.0 mbsf 5.1 m thick	Interval 9X-5, 64 cm, to 9X-6, 104 cm 125.1-127.4 mbsf 1.9 m thick	Interval 10H-4, 95 cm, to 11X-2, 85 cm 125.6-132.0 mbsf 6.4 m thick	late Maastrichtian
IIID	Interval 19X-1, 0 cm, to 19X-1, 17 cm 144.0-144.1 mbsf 17 cm thick	Interval 10X-CC, 0-7 cm 127.0-137.0 mbsf 10 cm thick	Interval 11X-2, 85 cm, to 11X-2, 102 cm 132.0-132.4 mbsf 17 cm thick	late Campanian
IVA	Interval 19X-1, 17 cm, to 21X-CC, 51 cm 144.1-172.7 mbsf 38.2 m thick	Interval 10X-CC, 7 cm, to 12X-CC, 18 cm 128.2-156.9 mbsf 28.7 m thick	Interval 11X-2, 102 cm, to 13X-CC, 49 cm 132.4-158.5 mbsf 26.1 m thick	early Albian to Aptian
IVB	Interval 22X-1, 0 cm, to 22X-CC, 35 cm 172.7-191.9 mbsf 38.2 m thick	NR	NR	Aptian

Note: NR = not recovered.

Unit I

Description: Nannofossil ooze, nannofossil ooze with foraminifers, foraminifer nannofossil ooze, nannofossil ooze with sponge spicules, calcareous ooze, nannofossil ash, and manganese oxide/phosphate nodules
Intervals: 171B-1049A-2X-1, 0 cm, to 7H-CC, 32 cm; 171B-1049B-1H-1, 0 cm, to 6X-CC, 44 cm; 171B-1049C-1H-1, 0 cm, to 5H-CC, 23 cm
Depth: 9.3–60.1 mbsf, Hole 1049A; 0–46.5 mbsf, Hole 1049B; 0–45.0 mbsf, Hole 1049C
Thickness: 50.8 m, Hole 1049A; 46.5+ m (base of unit not recovered), Hole 1049B; 45.0+ m (base of unit not recovered), Hole 1049C
Age: Holocene to middle Eocene

Lithologic Unit I is divided into two subunits: the first comprises nodules of Mn oxide and/or phosphate, and the second is the underlying sequence of middle Eocene oozes dominated by calcareous nannofossils. The base of the unit is defined as the first downhole occurrence of chert. We drilled without coring from ~50 to 90 mbsf in Holes 1049B and 1049C and consequently recovered the base of the lithologic unit only in Hole 1049A. Recovery was poor across the basal contact of lithologic Unit I in Hole 1049A.

Subunit IA

Description: Manganese oxide and phosphate nodules
Intervals: 171B-1049A-2X-1, 0 cm, to 3H-1, 2 cm; 171B-1049C-1H-CC, 0–10 cm
Depth: 9.3–18.6 mbsf, Hole 1049A; 2.0–2.1 mbsf, Hole 1049C
Thickness: a few meters?
Age: Holocene to middle Eocene

Lithologic Subunit IA comprises nodules of Mn oxide and phosphate that contain Pleistocene-aged nannofossils and Pleistocene–Holocene foraminifers. The base of Subunit IA is placed at the last occurrence of the nodules. The subunit was highly disturbed by drilling, with only a few botryoidal nodules recovered in Holes 1049A and 1049C and no recovery in Hole 1049B. Consequently, it is not possible to estimate the subunit thickness accurately.

Subunit IB

Description: Nannofossil ooze, nannofossil ooze with foraminifers, foraminifer nannofossil ooze, nannofossil ooze with sponge spicules, calcareous ooze, and ash with nannofossils
Intervals: 171B-1049A-3H-1, 2 cm, to 7H-CC, 32 cm; 171B-1049B-1H-1, 0 cm, to 6X-CC, 44 cm; 171B-1049C-1H-1, 10 cm, to 5H-CC, 23 cm
Depth: 18.6–60.1 mbsf, Hole 1049A; 0–46.5 mbsf, Hole 1049B; 2.1–45.0 mbsf, Hole 1049C
Thickness: 41.5 m, Hole 1049A; 46.5+ m (base of subunit not recovered), Hole 1049B; 42.9+ m (base of subunit not recovered), Hole 1049C
Age: middle Eocene

Lithologic Subunit IB comprises a middle Eocene section of ooze composed dominantly of calcareous nannofossils with trace to common amounts of foraminifers, sponge spicules, and radiolarians. The color varies from pale yellowish white (2.5Y 8/2) to very pale yellow (10YR 8/2). Bedding is poorly defined, and the sediment is homogeneous. This fabric is typical of thoroughly bioturbated intervals, and scattered burrow-mottled intervals confirm the presence of burrowing organisms. Pyrite flecks are disseminated throughout the unit, and millimeter-scale laminae of pyrite-rich sediments are common. A single, light gray ash layer is present in Sections 171B-1049A-6H-4 and 171B-1049B-3H-CC but was not recovered in Hole 1049C. Drilling has moderately disturbed the sediment of Unit I in Hole 1049A and moderately to highly disturbed it in Hole 1049C. The base of Unit I is placed at the first downhole occurrence of chert, as indicated by a reduction in drilling penetration rate.

Unit II

Description: Nannofossil ooze with chert interbeds

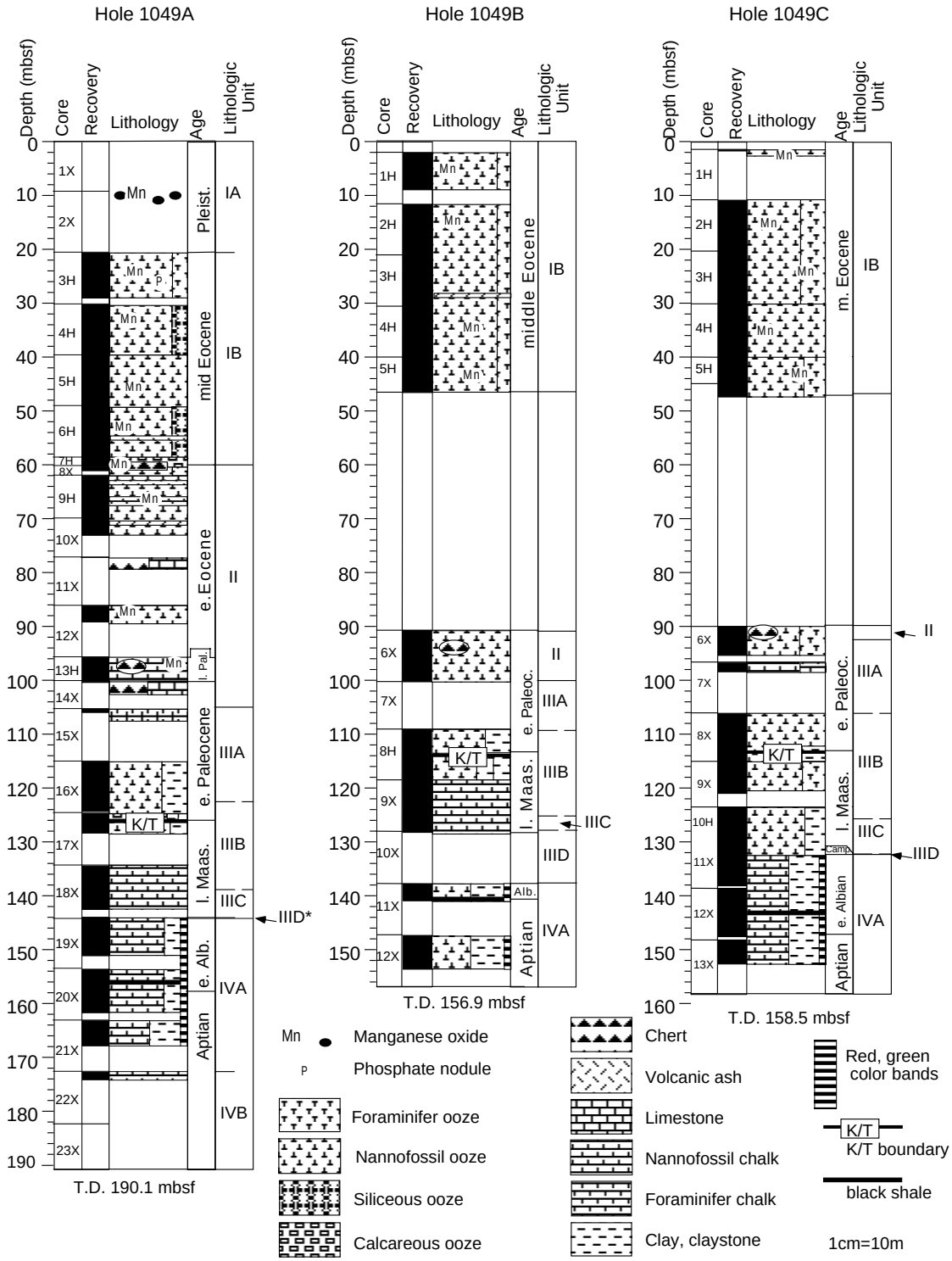

Figure 1. Summary of lithology, core recovery, and age for sediment recovered from three holes at Site 1049. * in Hole 1049A indicates that 15 cm of upper Campanian sediment is present at the top of Core 171B-1049A-19X-1. Symbols: l. = late; m. = middle; e. = early; Pleist. = Pleistocene; Paleoc. = Paleocene; Maas. = Maastrichtian; Camp. = late Campanian; Alb. = Albian. For more precise ages, see "Biostratigraphy" section, this chapter.

Intervals: 171B-1049A-8X-1, 0 cm, to 14X-CC, 21 cm; 171B-1049B-6X-1, 0 cm, to 6X-CC, 44 cm; 171B-1049C-6X-1, 0 cm, to 6X-2, 100 cm

Depth: 60.1–105.3 mbsf, Hole 1049A; 90.7–100.3 mbsf, Hole 1049B; 90.0–92.5 mbsf, 1049C

Thickness: 45.2 m, Hole 1049A; 9.6+ m (top of unit not recovered), Hole 1049B; 2.5+ m (top of unit not recovered), Hole 1049C

Age: early Paleocene to early Eocene

The sediment of lithologic Unit II consists of pinkish brown (10YR 8/2) to light gray (10YR 7/2) nannofossil ooze with varying amounts of foraminifers and chert. The nannofossil ooze is partly silicified, and chert layers or chert chips produced by drilling and the core splitting process are common throughout the unit. Pyrite micronodules with diameters ranging from <1 cm to <1 mm are common throughout. The top of Unit II is placed at the first downhole occur-

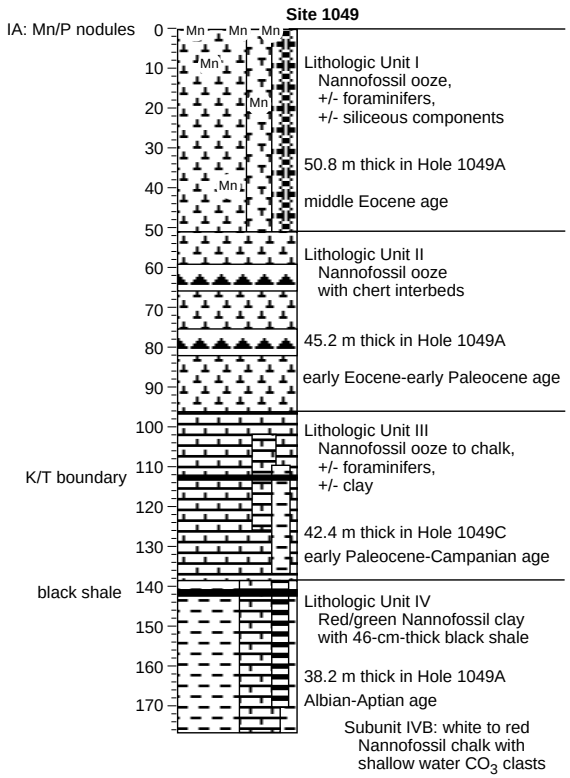

Figure 2. Composite section from the three holes drilled at Site 1049. Symbols are the same as those used in Figure 1. ± = with or without.

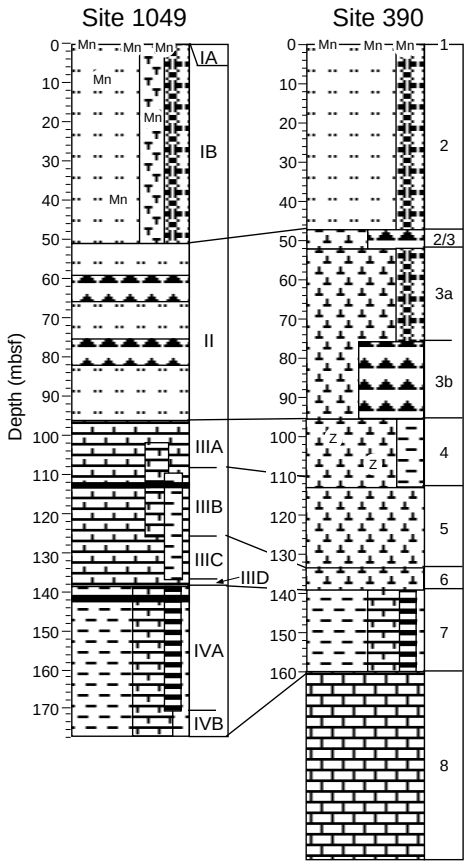

Figure 3. Correlation between Site 1049 and Site 390 lithologic units.

rence of chert (indicated by a reduction in drilling-penetration rate). In Core 171B-1049A-7H, the APC corer penetrated only 1.5 m of sediment before it had to be replaced by the XCB (see "Operations" section, this chapter). The upper 7 cm of Core 171B-1049A-8X contains pieces of the chert that presumably formed the obstacle that was not penetrated by the APC. Recovery of this unit was generally poor. The lower boundary of lithologic Unit II was placed at the last downhole occurrence of chert in Core 171B-1049A-14X. The upper and lower contacts of lithologic Unit II with Units I and III were not recovered in Holes 1049B or 1049C.

Unit III

Description: Burrow-mottled nannofossil ooze to weakly indurated nannofossil chalk with foraminifers and clay and a spherule layer, indicating the K/T boundary interval
Intervals: 171B-1049A-15X-1, 0 cm, to 19X-1, 17 cm; 171B-1049B-6X-4, 55 cm, to 10X-CC, 7 cm; 171B-1049C-6X-2, 100 cm, to 11X-2, 120 cm
Depth: 105.3–144.3 mbsf, Hole 1049A; 90.7–100.3 mbsf, Hole 1049B; 92.5–132.4 mbsf, Hole 1049C
Thickness: 38.8 m, Hole 1049A; 9.6+ m (top of unit not recovered), Hole 1049B; 39.9 m, Hole 1049C
Age: early Paleocene–Campanian

Mixed APC and XCB coring recovered as much as 42.4 m of yellowish, grayish green, creamy, and white (clayey) nannofossil oozes that we assigned to lithologic Unit III. This unit is divided into four subunits based primarily on color and subtle variations in clay content. With the exception of the K/T boundary interval, sediment composition is fairly constant. Both APC and XCB drilling introduced disturbance. The APC cores are only slightly disturbed in the upper portions but contain numerous flow-in structures (i.e., vertical pseudobedding) in the lower meter or more of each core. The XCB cores contain mainly 2- to 5-cm-long drilling biscuits.

Subunit IIIA

Intervals: 171B-1049A-15X-1, 0 cm, to 16X-5, 140 cm; 171B-1049B-6X-4, 55 cm, to 7X-CC; 171B-1049C-6X-2, 100 cm, to 8X-1, 0 cm
Depth: 105.3–122.4 mbsf, Hole 1049A; 100.3–109.0 mbsf, Hole 1049B; 90.0–106.1 mbsf, Hole 1049C
Thickness: 17.1 m, Hole 1049A; 8.7+ m (top of subunit not recovered), Hole 1049B; 16.1 m, Hole 1049C
Age: early Paleocene

Subunit IIIA comprises a succession of massive, very pale orange (10YR 8/1) to grayish orange (10YR 7/3) nannofossil ooze and chalk of early Paleocene age, with decimeter-scale alternations between darker and lighter sediments. The top of this subunit is defined as the deepest occurrence of chert, but the nature of the contact is not known because of poor recovery. The base of the subunit is marked by a change from yellowish to greenish sediment. Bioturbation is slight to moderate, with *Chondrites* most commonly observed (Fig. 4). Faint lamination occurs in Section 171B-1049A-16X-4, 38–48 cm. Pyrite flecks occur throughout, and yellow (limonite?) blebs occur in Section 171B-1049A-16X-3.

Subunit IIIB

Intervals: 171B-1049A-16X-5, 140 cm, to 18X-4, 13 cm; 171B-1049B-7X-CC, 0 cm, to 9X-5, 64 cm; 171B-1049C-8X-1, 0 cm, to 10H-4, 95 cm
Depth: 122.4–138.9 mbsf, Hole 1049A; 109.0–125.1 mbsf, Hole 1049B; 106.1–125.6 mbsf, Hole 1049C
Thickness: 16.5 m, Hole 1049A; 16.1 m, Hole 1049B; 19.5 m, Hole 1049C
Age: early Paleocene to early Maastrichtian.

Subunit IIIB consists of greenish gray (5GY 6/1), light gray (5Y 7/2), and pale green (10GY 7/1) clayey nannofossil ooze and clayey

nannofossil chalk that is laminated to slightly bioturbated. Both the upper and lower contacts of this unit are defined at fairly sharp color transitions; Subunit IIIB is composed of sediments that are various shades of light green, and both the over- and underlying subunits are yellowish. Normal microfaults (Fig. 5) and chaotic bedding occur throughout the unit but are especially pervasive in sediment beneath the K/T boundary. Some of the disturbance is clearly the result of drilling; however, much of it appears to be of natural origin.

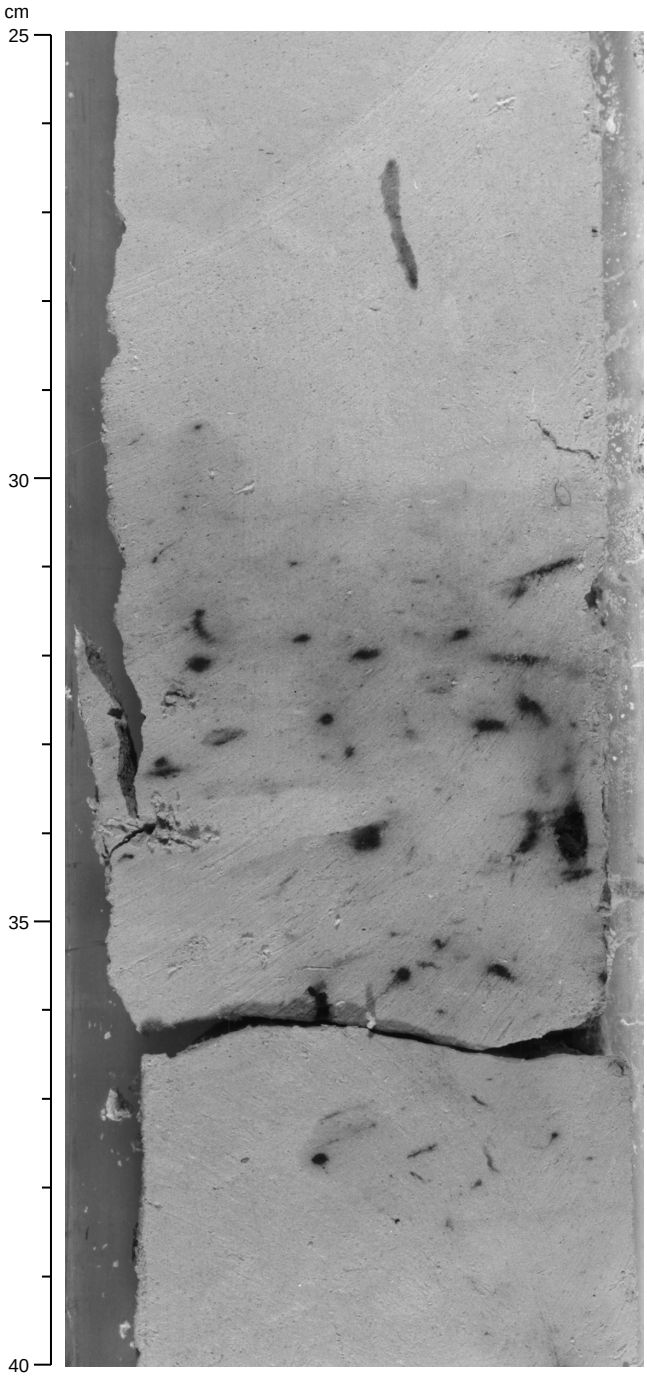

Figure 4. Section 171B-1049A-15X-1, 25–40 cm. Darker interval in lithologic Subunit IIIA (30–38 cm) = a nannofossil chalk with Mn oxide–filled burrows.

The K/T boundary interval was recovered in Holes 1049A, 1049B, and 1049C (Sections 171B-1049A-17X-2, 58–75 cm [126.08 mbsf], 171B-1049B-8H-2, 64–75 cm [111.25 mbsf], and 171B-1049C-8X-5, 87–97 cm [113.07 mbsf]). The Maastrichtian sequence is highly disturbed immediately below the K/T boundary. Bioturbation is indistinct. Bedding, revealed by color variation, dips at high angles to the core and is obviously contorted throughout the upper Maastrichtian section in all holes. Thus, the boundary intervals are 17, 9, and 10 cm thick in Holes 1049A, 1049B, and 1049C, respectively. The boundary interval exhibits the same sequence of four beds in each hole (Fig. 6). The lowest bed is a graded, faintly laminated layer consisting almost entirely of green spherules ranging in size from 2 to 3 mm at the base to <1 mm at the top. The spherule bed in Hole 1049A is more than twice as thick as the bed in Hole 1049B. The lower contact of the spherule bed is sharp in all holes and is obviously irregular in Hole 1049B; however, this may be a reflection of drilling disturbance. The spherule bed in Holes 1049A and 1049C contains clasts of hard gray chalk as much as 1 cm in diameter. A 1-mm-thick orange limonitic layer caps the spherule and contains flat goethite concretions. The upper 1 cm of the spherule bed is stained orange, perhaps because of remobilization of material from the limonitic layer or oxidation of the upper part of the spherule layer. The limonitic layer is overlain by 3 to 7 cm of dark, burrow-mottled clay, which contains planktonic foraminifers indicative of foraminifer Zone Pα (see "Biostratigraphy" section, this chapter). The final bed in the sequence is a 5- to 15-cm-thick white foraminifer nannofossil ooze that is also foraminifer Zone Pα in age. The lower contact of the white foraminifer nannofossil ooze is burrowed, whereas the upper contact is sharp with the overlying greenish gray foraminifer nannofossil ooze.

Subunit IIIC

Intervals: 171B-1049A-18X-4, 13 cm, to 19X-1, 0 cm; 171B-1049B-9X-5, 64 cm, to 9X-6, 104 cm; 171B-1049C-10H-4, 95 cm, to 11X-2, 85 cm
Depth: 138.9–144.0 mbsf, Hole 1049A; 125.1–127.4 mbsf, Hole 1049B; 125.6–132.0 mbsf, Hole 1049C
Thickness: 5.1 m, Hole 1049A; 1.9 m, Hole 1049B; 6.4 m, Hole 1049C
Age: late Maastrichtian

Subunit IIIC consists of laminated pale yellow (10Y 8/1) foraminifer nannofossil ooze and very pale yellowish green (10GY 8/1) foraminifer nannofossil chalk (Fig. 7). Trace amounts of pyrite occur throughout. The upper contact is best preserved in Hole 1049C, where the interval is laminated and the color shift occurs over a 3- to 5-cm interval. Similarly, the base of the subunit is well preserved only in Hole 1049C, where it is a red burrowed horizon developed on the white nannofossil ooze below (Fig. 8). As in Subunit IIIB, Subunit IIIC contains numerous microfaults and contorted beds indicative of both ductile and brittle deformation, some of which is difficult to distinguish from drilling disturbance.

Subunit IIID

Intervals: 171B-1049A-19X-1, 0 cm, to 19X-1, 17 cm; 171B-1049B-10X-CC, 0 cm, to 7 cm; 171B-1049C-11X-2, 85 cm, to 11X-2, 102 cm
Depth: 144.0–144.0 mbsf, Hole 1049A; 127.0–137.0 mbsf, Hole 1049B; 132.0–132.4 cm mbsf, Hole 1049C
Thickness: 17 cm, Hole 1049A; 10 cm, Hole 1049B; 17 cm, Hole 1049C
Age: late Campanian

Subunit IIID consists of a white nannofossil ooze (N7) that is coarser grained (because of a higher abundance of foraminifers) and has a disconformable contact with both the overlying and underlying units. The contacts are well preserved only in Hole 1049C, where they are burrowed intervals (Figs. 8, 9).

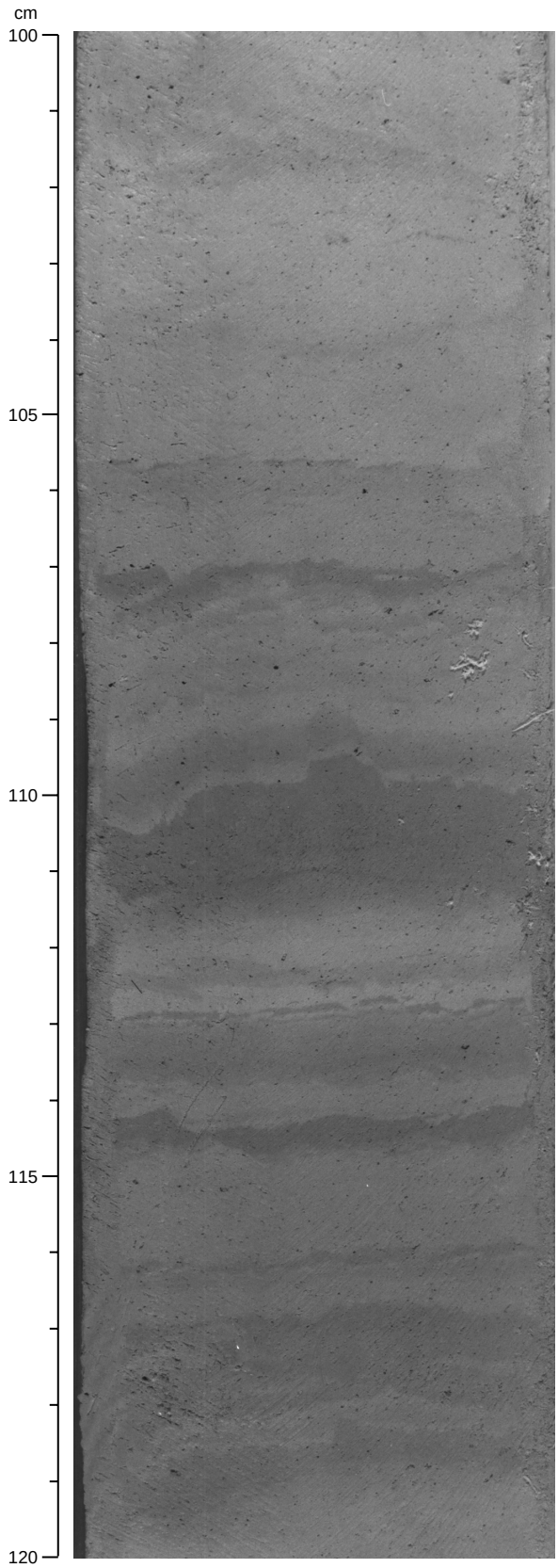

Figure 5. Section 171B-1049A-18X-2, 100–120 cm. Microfaults in lithologic Subunit IIIB, late Maastrichtian in age, between 106 and 115 cm.

Unit IV

Description: Nannofossil chalk, clayey nannofossil chalk, nannofossil clay, clay, and an organic-rich black shale
Intervals: 171B-1049A-19X-1, 17 cm, to 22X-CC, 35 cm; 171B-1049B-10X-CC, 7 cm, to 12X-CC, 18 cm; 171B-1049C-11X-2, 102 cm, to 13X-CC, 49 cm
Depth: 144.1–190.9 mbsf, Hole 1049A; 128.2–153.7 mbsf, Hole 1049B; 132.4–153.3 mbsf, Hole 1049C
Thickness: 38.2 m, Hole 1049A; 28.7 m, Hole 1049B; 26.1 m, Hole 1049C
Age: middle Albian to Aptian

XPC coring of lithologic Unit IV recovered as much as 21.0 m of middle Albian to Aptian clayey nannofossil chalk and clay over a cored interval of 38.2 m. Drilling disturbance was slight to moderate, but there were recovery gaps (Fig. 1). However, MST data indicate that the entire section was recovered over the three holes (see "Core-Core Integration" section, this chapter). Lithologic Unit IV was divided into two subunits. Subunit IVA comprises a varicolored succession of greenish gray (5GY 5/1) to dusky red (2.5YR 3/6) to light gray (N7) clayey nannofossil chalk and clay. The subunit contains subordinate light yellowish brown (10YR 6/4) laminated intervals, a 46-cm-thick laminated organic-rich black shale, and several hardgrounds. Subunit IVB comprises light green to pink nannofossil chalks with bivalve and echinoderm fragments scattered throughout.

Subunit IVA

Description: Clayey nannofossil chalk, nannofossil clay, clay, and an organic-rich black shale
Intervals: 171B-1049A-19X-1, 17 cm, to 21X-CC, 51 cm; 171B-1049B-10X-CC, 7 cm, to 12X-CC, 18 cm; 171B-1049C-11X-2, 120 cm, to 13X-CC, 49 cm
Depth: 144.1–172.7 mbsf, Hole 1049A; 128.2–156.9 mbsf, Hole 1049B; 132.4–158.5 mbsf, Hole 1049C
Thickness: 38.2 m, Hole 1049A; 28.7 m, Hole 1049B; 26.1 m, Hole 1049C
Age: middle Albian late Aptian

Subunit IVA is dominated by decimeter-scale rhythmic alternations between greenish and reddish clayey nannofossil chalk and nannofossil clay (Fig. 10), with minor occurrences of yellowish green laminated nannofossil clay (Fig. 11). The top of lithologic Subunit IVA is unconformably overlain by lithologic Subunit IIID, a white nannofossil ooze of Campanian age, and in Hole 1049C (where the contact is best preserved), it is represented by a slightly drilling-disturbed hardground with filled borings and Fe-enriched sediment (Fig. 9). The material in the borings appears to match sediment in lithologic Subunit IIID. Toward the base of lithologic Subunit IVA, lighter colors dominate, and the concentration of shell fragments (bivalves and echinoderms) increases. Lithologic Subunit IVB is also characterized by lighter colors and macrofossil fragments, but the contact between the subunits was not recovered. In general, lighter intervals of lithologic Subunit IVA seem to be more intensively bioturbated than darker intervals. Among the trace fossils, *Phycoides*, *Chondrites*, and *Zoophycos* were identified. *Phycoides* seems to be more prevalent in intervals with less burrow mottling. The best preserved trace fossils were observed around transitions between light and dark intervals, probably because the piped sediment contrasts most strongly with the surrounding material. Color appears to be at least partly a result of diagenetic enhancement (e.g., redox reactions localized by burrows).

A 46-cm-thick laminated black shale layer interrupts the rhythmic alternations ~10 m below the top of Subunit IVA (Sections 171B-1049A-20X-2, 62–108 cm, 171B-1049B-11X-CC, 8–21 cm, and 171B-1049C-12X-3, 44–90 cm) and is well preserved in both Holes 1049A and 1049C (Fig. 12). The shale contains distinct, light, millimeter-scale laminae composed of rhombic calcite, alternating with

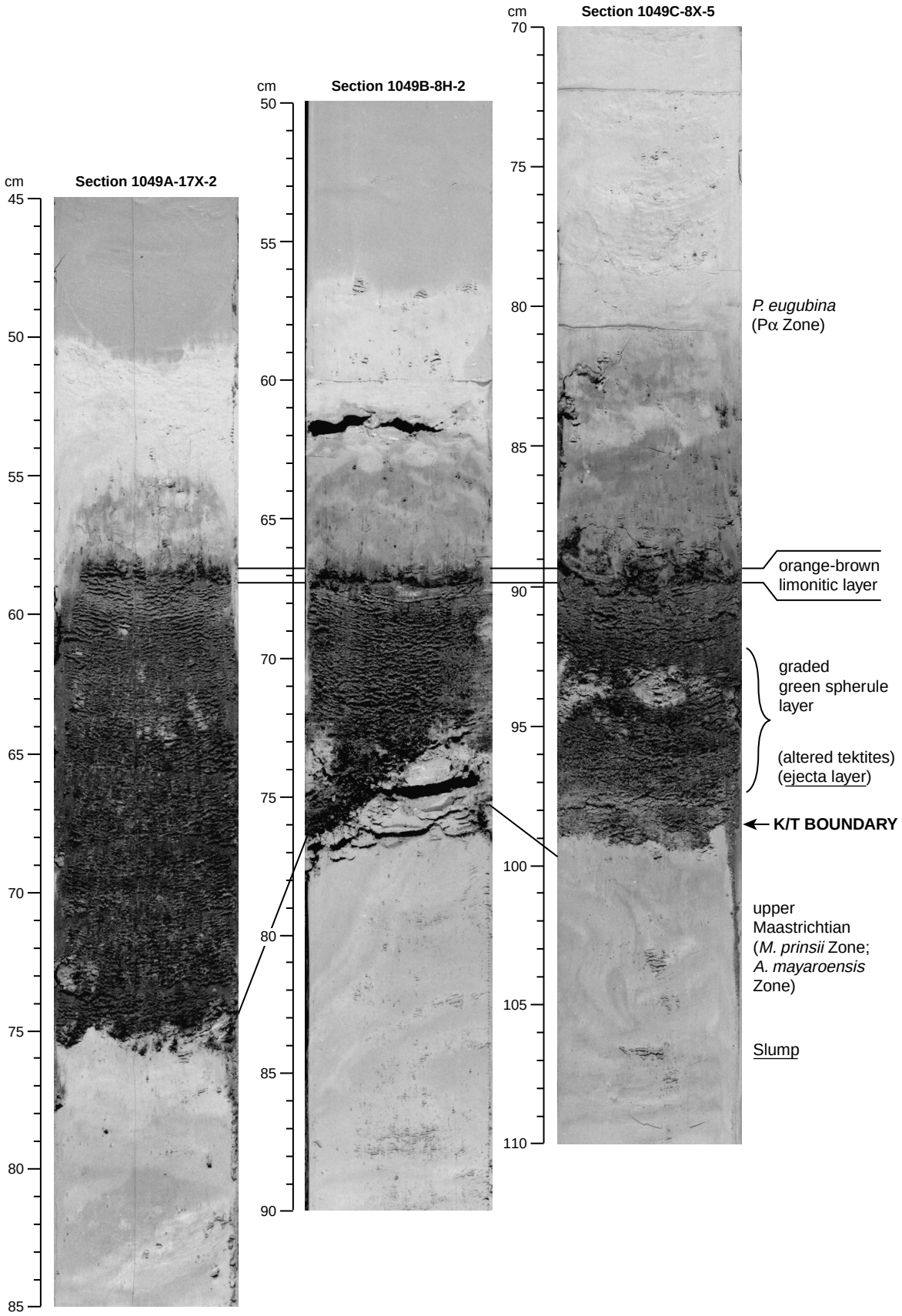

Figure 6. The K/T boundary interval from the three holes drilled at Site 1049.

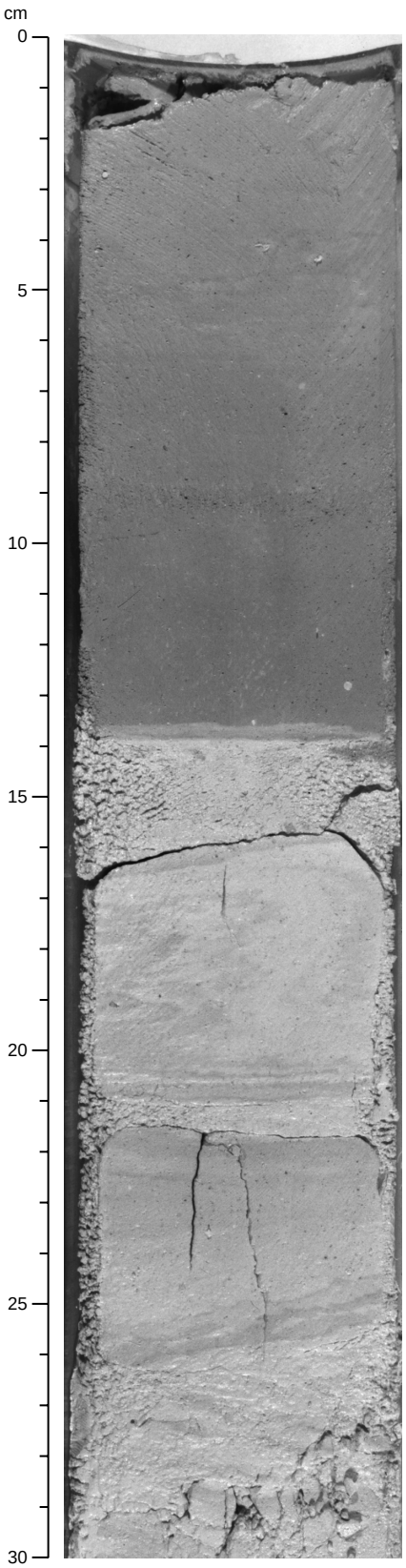

Figure 7. Section 171B-1049A-18X-4, 0–30 cm. Contact between overlying lithologic Subunit IIIB, a lower Maastrichtian gray nannofossil chalk, and lithologic Subunit IIIC, a pale yellow lower Maastrichtian nannofossil ooze to chalk with chaotic bedding (17–21 cm in photograph).

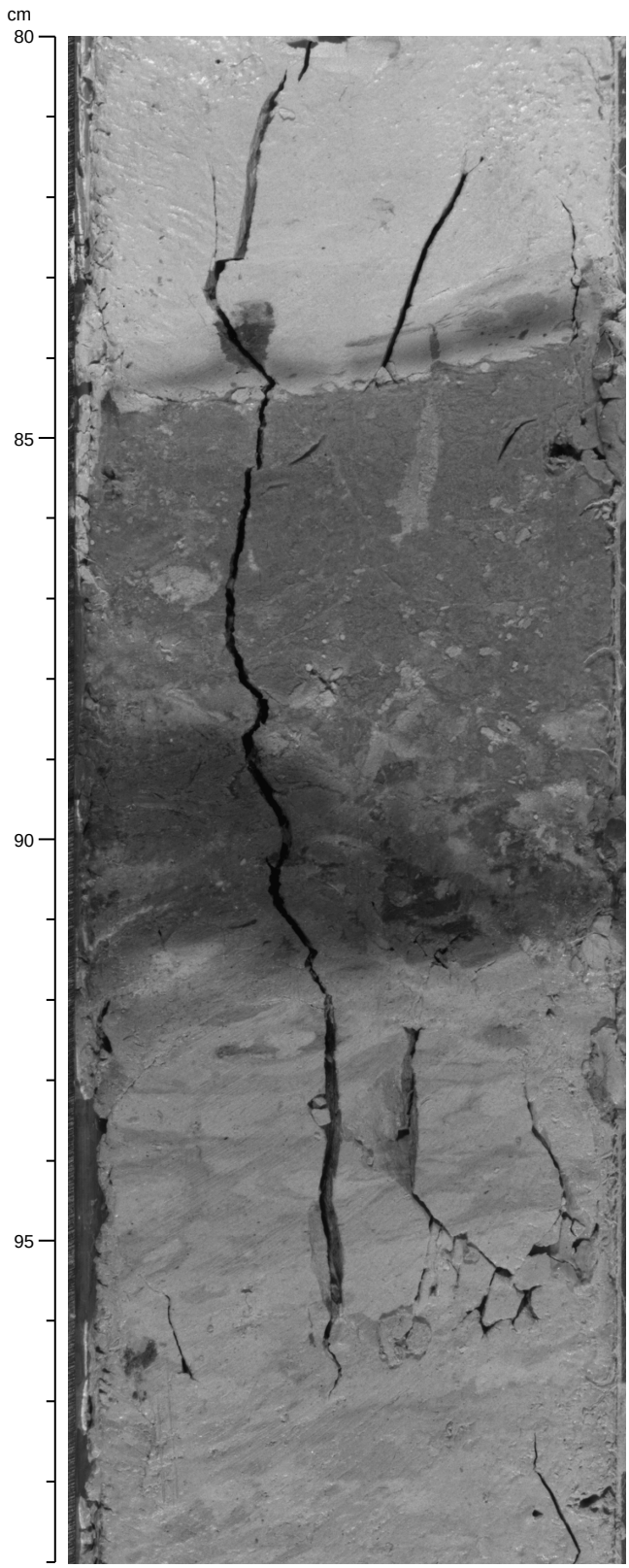

Figure 8. Section 171B-1049C-11X-2, 80–99 cm. Contact between lithologic Subunits IIIC (to 84 cm) and IIID, showing iron oxide–rich hardground between lower Maastrichtian and upper Campanian nannofossil chalk.

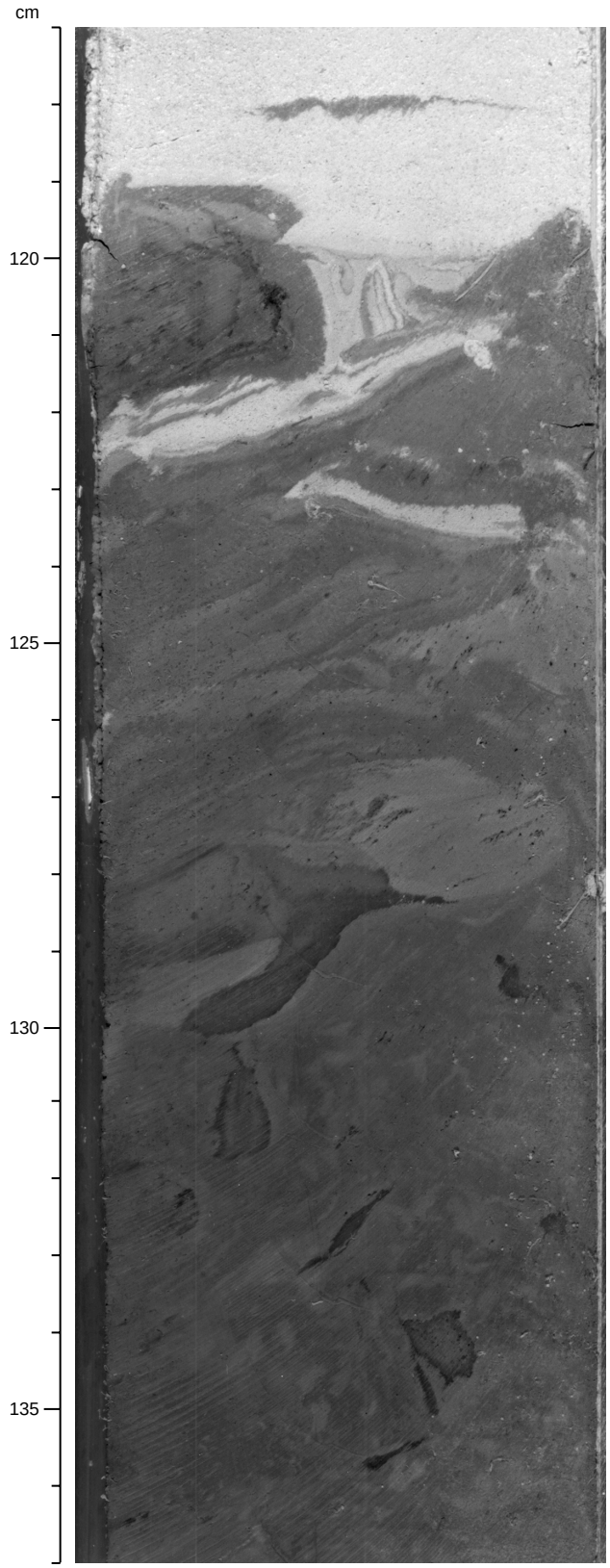

Figure 9. Section 171B-1049C-11X-2, 117–137 cm. Drilling-disturbed contact between the overlying upper Campanian nannofossil chalk and the underlying Albian bright red nannofossil clay.

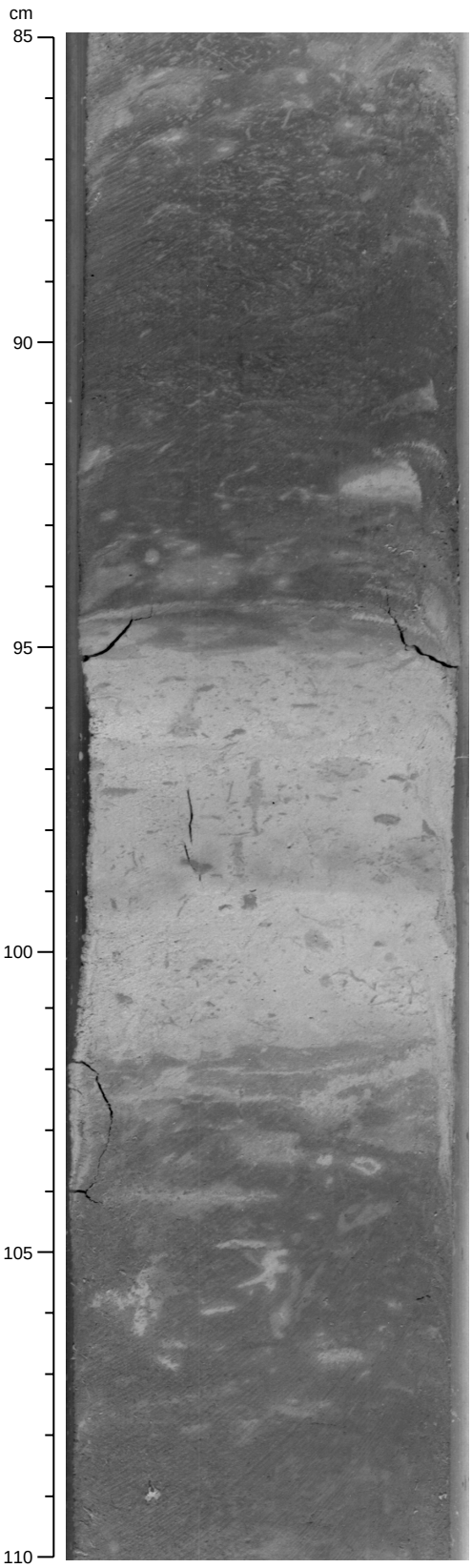

Figure 10. Section 171B-1049A-19X-2, 85–110 cm. Albian lithologic Subunit IVA, showing alternations of bright red nannofossil clay with green burrows (85–95 and 102–110 cm) and white nannofossil chalk (95–102 cm).

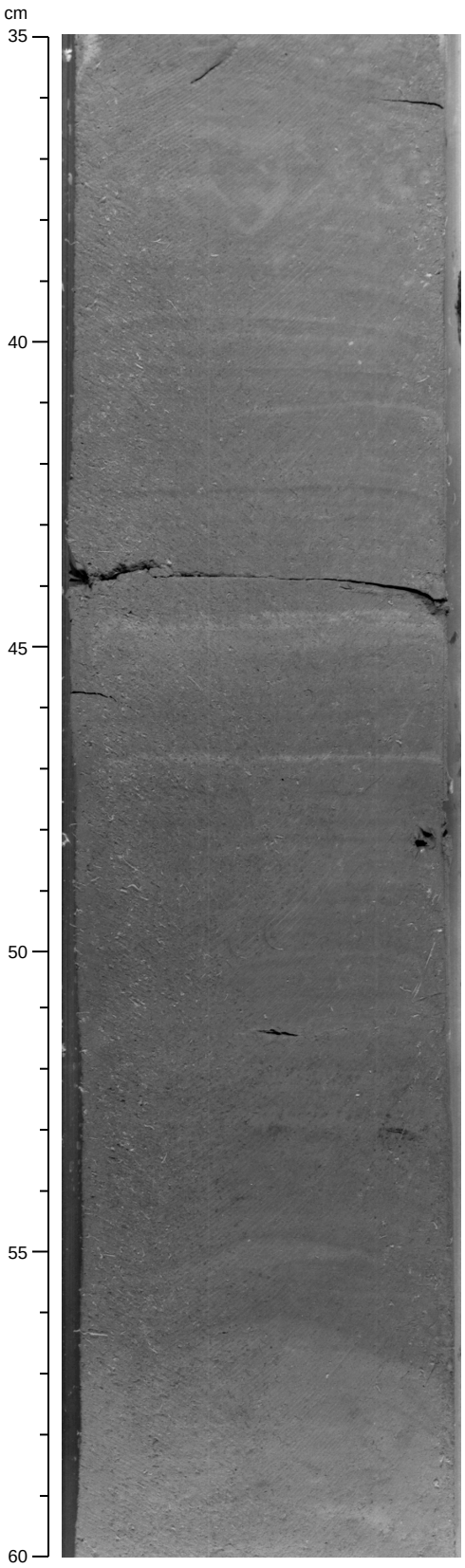

Figure 11. Section 171B-1049A-19X-3, 35–60 cm. Yellowish green laminated nannofossil clay occurs cyclically with the bright red to green bioturbated lithology illustrated in Figure 8.

organic-rich black laminae and pyritic nodules. Above the black shale, the sediments grade into brownish (oxidized?) laminated shales and then olive green clays. A 10-cm layer of green clay was recovered below the black shale. It is proposed that the black shale may represent the local expression of the globally recognizable early Albian Oceanic Anoxic Event 1b.

Drilling in Hole 1049C seems to have recovered the least disturbed record of lithologic Subunit IVA, and in this hole, hardgrounds occur 20, 30, and 308 cm below the base of the black shale (Sections 171B-1049C-12X-3, 110 cm, 12X-3, 120 cm, and 12X-5, 98 cm, respectively). In each case, the hardgrounds are characterized by a concentration of Mn flakes and specks along the contact with the underlying, slightly lithified, whitish sediments.

Subunit IVB

Description: Nannofossil chalk
Interval: 171B-1049A-22X-1, 0 cm, to 22X-CC, 35 cm
Depth: 172.7–191.9 mbsf
Thickness: 38.23 m
Age: Aptian

Subunit IVB occurs only in Core 171B-1049A-22X and is a light-colored nannofossil chalk. Neither the top of the subunit nor its base was recovered. Besides a change in color to light, creamy variations of green and red, a distinct decrease in clay content, and a relatively high abundance of calcareous shell debris (bivalves and echinoderms) clearly separate this subunit from Subunit IVA.

Discussion

The lithologic succession recovered at Site 1049 records an Aptian–Albian pelagic basin that received some carbonate platform debris in addition to clay and iron oxides (possibly iron-coated clays) from the adjacent continent. Bottom-water conditions were generally conducive to supporting a flourishing benthos (intervals represented by bioturbated sediments), but episodically burrowing organisms were absent (intervals represented by laminated sediments), which we attribute to bottom-water anoxia. A single major anoxic event near the Aptian/Albian boundary is indicated by the 46-cm-thick black shale. After the Albian and before the Campanian, Site 1049 was cut off from most terrigenous input. Since the Campanian, the area has intermittently received sediment dominated by biogenic components. During the Late Cretaceous, these biogenic grains were dominantly calcareous. Site 1049 felt the effects of the K/T boundary impact event, as recorded by the boundary beds and, possibly, by slumping (indicated by the microfaulting and contorted bedding) of Maastrichtian sediment.

Siliceous biogenic input increased in the early Paleocene, as indicated by the presence of chert and remnants of radiolarians and sponge spicules. This input persisted into the middle Eocene, with better preservation of siliceous microfossils in the middle Eocene section. Nondeposition or erosion of sediment has persisted from the late middle Eocene to the present. Mn oxide and phosphate nodules have been forming at the surface since at least the Pleistocene.

BIOSTRATIGRAPHY

The sedimentary sequence in Hole 1049A was sampled extensively for calcareous nannofossils to establish the biostratigraphic framework. Sample spacing is typically one per section (~1.5 m) in the cores from this hole. A list of chronostratigraphically significant biohorizons derived from this detailed examination is presented in Table 3. The sedimentary sequences from Holes 1049B and 1049C were sampled only from the core catchers to provide biostratigraphic correlation between the holes. The nannofossil biostratigraphy for these duplicate holes is presented in Figure 13. In general, calcareous

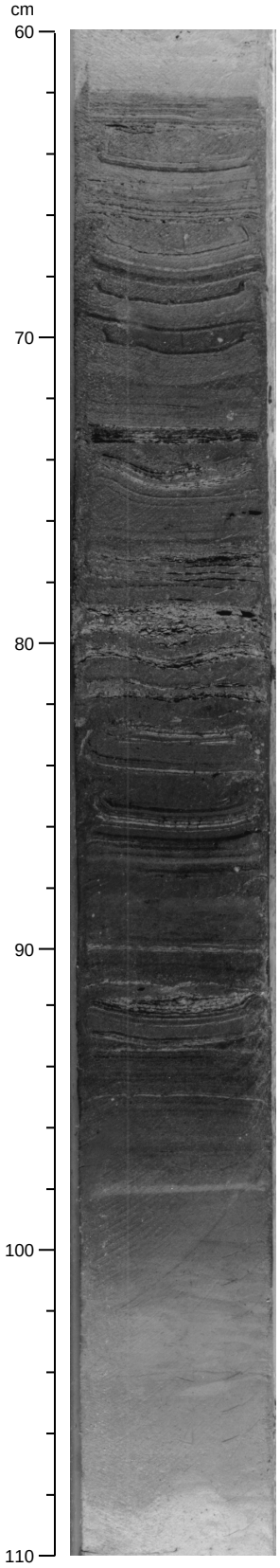

Figure 12. Section 171B-1049A-20X-2, 60–110 cm. Finely laminated black shale interval in lithologic Subunit IVA.

Table 3. Calcareous nannofossil biohorizons and stratigraphic placements in Hole 1049A.

Core, section, interval (cm)	Datum	Species	Age (Ma)	Occurrence depth (mbsf)	Error depth (mbsf)
171B-1049A-					
6H-6, 65-70	FO	*C. gigas*	46.1	57.3	58.7
7H-1, 65-70	FO	*R. inflata*	48.5	59.3	60.0
9H-4, 67-72	FO	*D. sublodoensis*	49.7	67.1	68.6
10X-2, 65-70	LO	*T. orthostylus*	50.6	72.9	71.6
12X-1, 65-70	FO	*D. lodoensis*	52.9	86.8	88.2
12X-CC	FO	*T. orthostylus*	53.6	89.1	96.4
13X-2, 64-69	FO	*D. mohlerii*	57.5	97.8	100.1
13X-CC	FO	*S. primus*	60.6	100.1	100.3
14X-CC	FO	*E. macellus*	62.2	100.3	105.9
16X-2, 65-70	FO	*C. danicus*	63.8	117.2	118.7
16X-4, 64-69	FO	*C. tenuis*	64.5	120.1	124.1
17X-2, 3-10	FO	*C. primus*	64.8	125.3	125.5
17X-2, 76-78.5	LO	Cretaceous spp.	65.0	126.1	125.9
18X-4, 10-12	FO	*M. prinsii*	66.0	138.9	139.0
18X-4, 10-12	FO	*M. murus*	68.5	138.9	139.0
19X-1, 16-16.5	LO	*E. eximius*	75.2	144.1	142.4
19X-1, 16-16.5	FO	*Q. trifidum*	76.1	144.1	144.1
19X-CC	FO	*C. ehrenbergii*	110.3	151.0	154.0
20X-3, 102-106	FO	*P. columnata*	112.5	157.6	159.3
22X-1, 60-63	LO	*M. hoschulzii*	114.2	173.3	167.7

Notes: FO = first occurrence; LO = last occurrence. These data reflect post-cruise modifications and are, thus, more up to date than data presented in the range charts and in the biostratigraphy and sedimentation rate figures (this chapter).

nannofossils are abundant and well to moderately preserved throughout the sedimentary sequence.

The early Pleistocene *Gephyrocapsa caribbeanica* Subzone (CN14a) is represented only by material adhering to manganese nodules in Section 171B-1049A-2X-CC (9.30 mbsf). Other remnants of Neogene sediments are contained within these nodules, as evidenced by cursory examination of broken nodules, but the exact biostratigraphic placement of this material is unknown at this time. This upper Cenozoic material disconformably overlies the Paleogene at this site.

At least a part of the middle Eocene at this site is so contaminated by reworked calcareous nannofossils that detailed biostratigraphy is difficult, if not impossible. The sequence from Core 171B-1049A-3H through Section 4H-2 has enough in situ nannofossils to yield a reliable age of Subzone CP14a. This is consistent with age determinations based on planktonic foraminifer and radiolarian stratigraphy. In a similar fashion, Core 171B-1049A-6H yields a reliable biostratigraphy, including Subzones CP13b and 12b. Subzone CP13a is either very thin (<1.5 m) or is missing in this hole. Most of Core 171B-1049A-4H and all of Core 171B-1049A-5H contain assemblages thoroughly tainted by reworked material. These recycled assemblages include fossils from both Subzone CP13b (middle Eocene) and Zones CP10 to CP11 (early Eocene). Correlations with planktonic foraminifer assemblages from this interval suggest that both Subzones CP12b and CP13a may be within this interval of intense reworking. However, it is questionable whether samples with sufficiently low levels of reworking can be located within this interval to establish the nannofossil biostratigraphy. Consequently, this interval with intense reworking is given an indeterminate age assignment in Figure 13.

The lower Eocene at this site contains a relatively complete succession of nannofossil assemblages spanning Subzones CP9b through CP12a, although the basal Eocene Subzone CP9a was not recognized. It is possible that this subzone occurs within an interval of nonrecovery between Cores 171B-1049A-11H and 12H. The correlative interval in Holes 1049B and 1049C was washed, so it is not possible to test this hypothesis by additional sampling. The upper Paleocene Zones CP7 and CP8 also were not recovered. In addition, at least one-half of the upper part of Zone CP6 (above the first occurrence [FO] of *Heliolithus riedelii*) was not recovered. This also may be the result of a disconformity at the Paleocene/Eocene boundary or

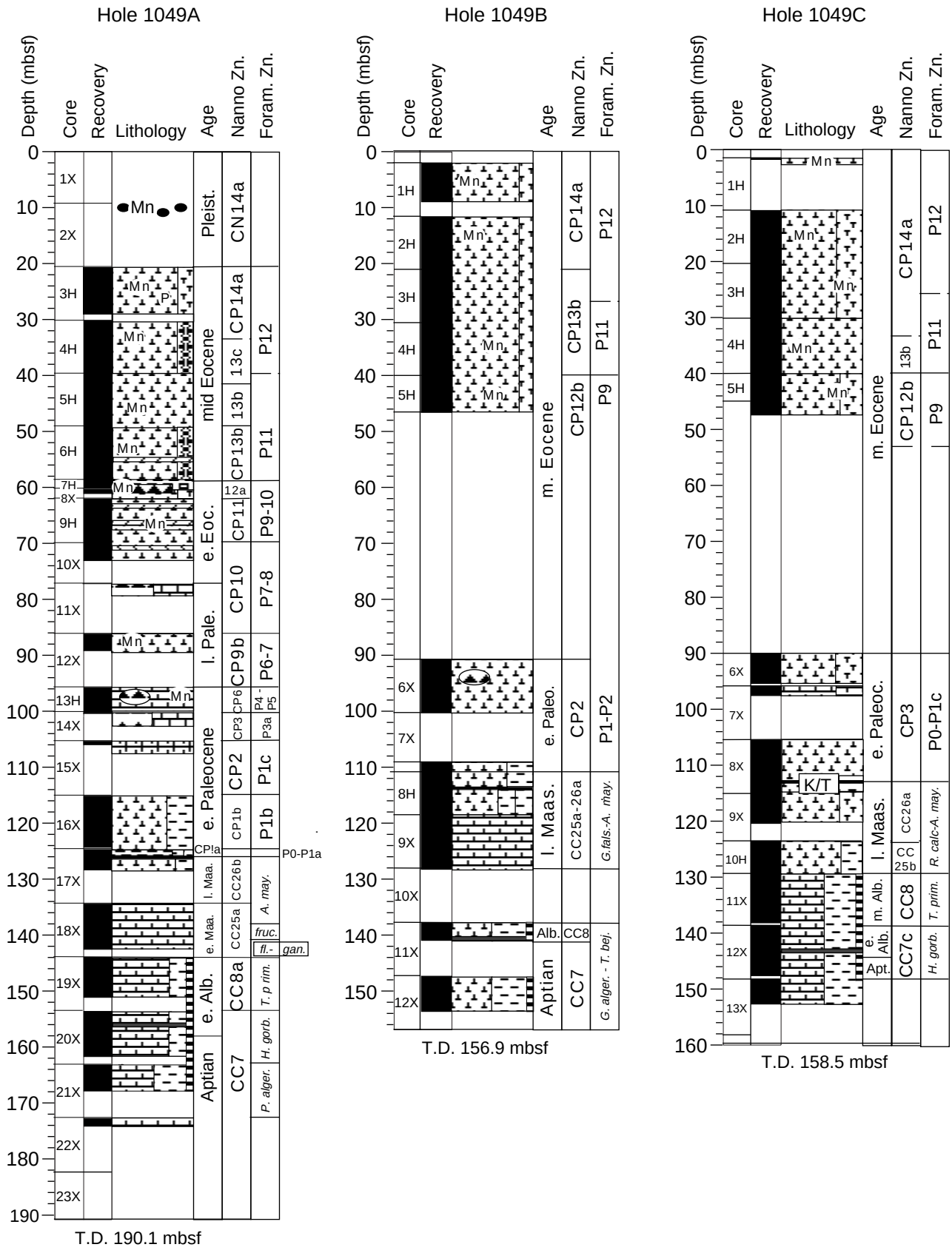

Figure 13. Biostratigraphic summary for Site 1049. See Figure 1 for explanation of lithologic symbols. Refer to the nannofossil and foraminifer datum tables (this chapter) for biostratigraphic data that reflect post-cruise additions and modifications to range data.

a thick zone without recovery (~6.5 m) from Core 171B-1049A-12X. The duration of the missing stratigraphic interval is ~3.7 m.y. Assuming that the missing stratigraphic sequence filled the entire interval of nonrecovery, this would imply an average sediment accumulation rate of ~1.75 m/m.y. This assumed rate is significantly lower than others seen at this site and suggests that a disconformity is more likely than mere nonrecovery.

Despite poor core recovery in some intervals, the record of the early Paleocene is probably complete. All of the calcareous nannofossil zones and most of the subzonal intervals are present in Hole 1049A, and examination of the records from Holes 1049B and 1049C suggests a complete succession. Sedimentary rocks from Zones CP2 and CP3 and Subzone CP1b contain abundant, beautifully preserved Danian assemblages with minor amounts of reworked Cretaceous specimens. Assemblages from Subzone CP1a contain substantially more reworked Cretaceous specimens. Bloom events of both *Thoracosphaera* and *Braarudosphaera* are evident from the records at this site. In addition, fluctuations in dominance by various small species of *Praeprinsius, Biscutum,* and *Prinsius* are well preserved in the Site 1049 record. All indications suggest that the sedimentary sequence recovered at Site 1049 may be one of the finest records of the K/T boundary ever recovered from the deep sea.

Nannofossil assemblages from the late Maastrichtian also are well preserved at this site. Most important, the uppermost Maastrichtian sedimentary record includes *Micula prinsii, M. murus, Cylindralithus oweinii, Ceratolithoides kamptnerii, Lithraphidites kennethii,* and *Pseudomicula quadrata.* The presence of all of these taxa strongly suggests a complete boundary sequence. The rest of the upper Maastrichtian record is more fragmentary because of poor recovery and (possibly) a disconformity separating Subzones CC25b and CC26b. A disconformity is suggested by the concurrent FO of *M. murus* and *M. prinsii* in Sample 171B-1049A-18X-4, 10–12 cm (Table 3). Subzone CC25a is apparently rather thin (<5 m) at this site and is underlain by a very thin (<1 m) interval of upper Campanian chalk (Zone CC22 to Subzone CC23a). Upper Campanian chalk disconformably overlies a sequence of lower Albian to Aptian nannofossil claystones and chalks. This rhythmically interbedded sequence of red nannofossil claystones, green nannofossil claystones, and white chalks in Cores 171B-1049A-19X through 23X represents ~10 m.y. of deposition. The red nannofossil claystones contain beautifully preserved nannofossil assemblages, whereas the assemblages in the green claystones exhibit moderate preservation, and the white chalk assemblages are severely corroded and overgrown. A prominent laminated black claystone interval (Section 171B-1049A-20X-2) lies just above the Aptian/Albian boundary and is bracketed by nannofossil assemblages that indicate an earliest Albian age.

Planktonic Foraminifers

A total of 61 samples from Site 1049 were studied on the ship. Zonal assignments are summarized in Figure 13 and Table 4. Distribution charts for the three holes are presented in Tables 5, 6, and 7. Planktonic foraminifer data indicate successive sequences at Site 1049 that span from the middle to lower Eocene, the upper Paleocene to Maastrichtian, and the lower Albian to upper Aptian. Preservation of planktonic foraminifers is very good in the middle Eocene, moderate to good in the lower Eocene and Paleocene, and good to very good in the Cretaceous.

The Zone P12/P11 boundary (middle Eocene) is defined on the last occurrence (LO) of *Morozovella aragonensis,* which was found one core below the FO of *M. lehneri* at all three Site 1049 holes. The base of Zone P11 was identified only tentatively in the three holes, based on the co-occurrence of *M. aragonensis, Subbotina inaequispira, S. linaperta, Truncorotaloides rohri, Acarinina bullbrooki, Globigerinatheka mexicana,* rare *Hantkenina mexicana,* and *Guembelitrioides higginsi.* The marker species for the lower zonal boundary (*Turborotalia pessagnoensis*) was not identified. The Zone P10/P9 boundary could not be distinguished at any of the holes because of the absence of the zonal marker, *H. nuttali.* Zone P9 was tentatively identified by the co-occurrence of *M. aragonensis, M. caucasica, T. rohri, A. bullbrooki, S. inaequispira, G. senni,* and rare *Globigerinatheka subconglobata micra.* Similarly, the top of Zone P8 could not be determined using the Berggren et al. (1995) definition because the defining marker, *Planorotalites palmarae,* was not found in any of the samples. This zone was tentatively identified based on the co-occurrence of *A. broedermanni, M. formosa,* and *M. lensiformis.* The Zone P8–P7 interval was assigned to Sample 171B-1049A-10X-CC (73.1 mbsf), which yielded *M. aragonensis, M. formosa, M. subbotinae, A. soldadoensis,* and *A. primitiva.* The FO of *M. aragonensis* was used to identify the base of Zone P7 in all three holes at Site 1049. The Zone P6 interval was identified based on the co-occurrence of *M. subbotinae, M. marginodentata, M. gracilis, A. primitiva, S. patagonica,* and *G. senni;* however the LO of *M. velascoensis* was not recorded at any of the Site 1049 holes because of poor core recovery in Holes 1049A and 1049B and a disconformity separating Zones P6 and P4 in Hole 1049A.

Subzone P3a and Zone P4 were recovered only in Hole 1049A. A typical Zone P4 assemblage, including *Morozovella velascoensis, Planorotalites pseudomenardii, Subbotina patagonica, S. triangu-*

Table 4. Planktonic foraminifer biohorizons and their stratigraphic placements at Site 1049.

Core, section, interval (cm)	Datum	Species	Age (Ma)	Occurrence depths (mbsf)	Error depth (mbsf)
171B-1049A-					
4H-CC	FO	*M. lehneri*	43.50	40.09	49.56
5H-CC	LO	*M. aragonensis*	43.60	49.56	40.09
10X-CC	FO	*M. aragonensis*	52.30	73.14	89.11
10X-CC	FO	*M. formosa formosa*	54.00	73.14	89.11
12X-CC	LO	*M. marginodentata*	52.50	89.14	88.29
13H-CC	LO	*M. velascoensis*	54.70	100.08	97.89
13H-CC	LO	*G. pseudomenardii*	55.90	100.08	97.89
13H-CC	FO	*A. soldadoensis*	56.50	100.08	100.29
13H-CC	FO	*G. pseudomenardii*	59.20	100.08	100.29
13H-CC	FO	*M. velascoensis*	60.00	100.08	100.29
14X-CC	FO	*M. conicotruncata*	60.90	100.29	105.93
15X-CC	LO	*P. varianta*	59.20	105.95	100.31
17X-2, 40-42	LO	*P. eugubina*	64.70	125.71	125.53
17X-2, 56-58	FO	*P. eugubina*	64.97	125.87	125.81
18X-4, 10-12	FO	*A. mayaroensis*	68.25	138.90	138.96
18X-4, 10-12	FO	*C. contusa*	69.60	138.90	138.96
18X-4, 10-12	FO	*R. fructicosa*	69.60	138.90	138.96
19X-CC	FO	*T. primula*	109.00	150.93	154.03
19X-CC	FO	*T. primula*	109.00	150.93	154.03
171B-1049B-					
2H-CC	FO	*M. lehneri*	43.50	21.49	30.93
3H-CC	LO	*M. aragonensis*	43.60	30.96	21.51
5H-CC	FO	*M. aragonensis*	52.30	46.20	100.28
6X-CC	FO	*P. inconstans*	63.00	100.28	117.70
6X-CC	FO	*S. triloculinoides*	64.30	100.28	117.70
8H-CC	FO	*R. fructicosa*	69.60	118.52	128.20
8H-CC	FO	*C. contusa*	69.60	118.52	128.20
171B-1049C-					
2H-CC	LO	*G. index*	42.9	21.13	2.1
3H-CC	FO	*M. lehneri*	43.5	30.91	39.98
3H-CC	LO	*M. aragonensis*	43.6	30.94	21.13
5H-CC	FO	*M. aragonensis*	52.3	49.91	95.31
7X-CC	LO	*P. varianta*	59.2	98.01	95.34
7X-CC	FO	*G. compressa*	63	98.01	112.79
7X-CC	FO	*P. inconstans*	63	98.01	112.79
7X-CC	FO	*P. varianta*	63	98.01	112.79
7X-CC	FO	*S. triloculinoides*	64.3	98.01	112.79
8X-4, 52-54	LO	*P. eugubina*	64.7	111.43	111.31
8X-5, 87-89	FO	*P. eugubina*	64.97	112.88	112.97
9X-CC	FO	*A. mayaroensis*	68.25	121.02	129.93
9X-CC	LO	*R. fructicosa*	69.6	121.02	129.93
9X-CC	FO	*C contusa*	69.6	121.02	129.93
11X-2, 113-115	LO	*R. calcarata*	75.2	132.33	131.97
11X-2, 113-115	FO	*R. calcarata*	75.7	132.33	134.53

Notes: FO = first occurrence; LO = last occurrence. These data reflect post-cruise modifications and are, thus, more up to date than data presented in the range charts and in the biostratigraphy and sedimentation rate figures (this chapter).

Table 5. Planktonic foraminifer distribution in Hole 1049A.

Age	Zone	Core, section, interval (cm)	Depth (mbsf)	Abundance	Preservation	*Globigerinelloides algerianus*	*Globigerinelloides ferreolensis*	*Hedbergella delrioensis*	*Hedbergella trocoidea*	*Hedbergella planispira*	*Ticinella primula*	*Contusotruncana fornicata*	*Globigerinelloides prairiehillensis*	*Globigerinelloides subcarinatus*	*Globotruncana aegyptiaca*	*Globotruncana arca*	*Globotruncana dupeublei*	*Globotruncana falsostuarti*	*Globotruncana linneiana*	*Globotruncanella petaloidea*	*Globotruncanita stuarti*	*Gublerina acuta*	*Hedbergella monmouthensis*	*Heterohelix globulosa*	*Laeviheterohelix glabrans*	*Planoglobulina multicamerata*	*Pseudotextularia nuttalli*	*Racemiguembelina fructicosa*	*Rugoglobigerina rotundata*	*Rugoglobigerina rugosa*	*Globotruncanita stuartiformis*	*Abathomphalus mayaroensis*	*Contusotruncana contusa*	*Globotruncanella minuta*	*Heterohelix punctulata*	*Pseudoguembelina palpebra*	*Pseudotextularia elegans*	*Globotruncana esnehensis*	*Heterohelix striata*	*Planoglobulina acervulinoides*	*Rosita plicata*	*Rugoglobigerina hexacamerata*	*Chiloguembelina midwayensis*	*Eoglobigerina edita*	*Eoglobigerina eobulloides*	*Globoconusa daubjergensis*	*Guembelitria cretacea*	*Parasubbotina pseudobulloides*	*Parvularugoglobigerina eugubina*	*Woodringina claytonensis*
		171B-1049A-																																													
middle Eocene	P12	3H-CC	30.60																																												
middle Eocene	P12	4H-3	33.75	A	G																																										
middle Eocene	P12	4H-5	36.75	A	G																																										
middle Eocene	P12	4H-CC	40.09	A	G																																										
middle Eocene	P12-P11	5H-CC	49.56	A	G																																									
middle Eocene	P11	6H-CC	59.06	A	G																																									
Eocene	P9-P10	7H-CC	60.04	A	M																																									
Eocene	P9-P10	8X-CC	60.83	A	M																																									
Eocene	P9-P10	9H-CC	69.40	A	G																																									
early Eocene	P8-P7	10X-CC	73.14	A	G																																									
early Eocene	P6-P7	12X-CC	89.11	A	M																																									
late Paleocene	P4a-P4b	13H-CC	100.08	A	M																																									
late Paleocene	P3a	14X-CC	100.29	A	P																																									
early Paleocene	P1c	15X-CC	105.93	A	M																																								A	
early Paleocene	P1b	16X-CC	124.12	A	VG																																							A	
early Paleocene	P1a	17X-2, 3-10	125.34	A	VG																																					A	F	A	F	A	
early Paleocene	P1a	17X-2, 22-24	125.53	A	VG																																					A	F	A	F	A	
early Paleocene	P1a	17X-2, 40-42	125.71	A	VG																																					A	R	F	R	F	
Maastrichtian	*A. mayaroensis*	17X-CC	128.46	A	G								R	R	R	R	R			R				A		F	F	F	R	F	F	P	R					F	R	F	F	F	P	P					
Maastrichtian	*A. mayaroensis*	18X-3, 65-67	137.95	A	VG										R						A	R						A	R		P	F	R	R			F	R									
Maastrichtian	*R. fructicosa*	18X-4, 10-12	138.90	A	G												R	F		R						F	A			F																
Maastrichtian	*R. fructicosa*	18X-4, 16-18	138.96	A	G													F		F						F	F				A															
Maastrichtian	*G. gansseri-G. falsostuarti*	18X-CC	142.39	A	G							F	R	F	P	F	R	R	R	R	F	R	P	A	P	F	F	A	P	R															
Albian	*T. primula*	19X-CC	150.93	A	VG			F			A																																				
Aptian	*H. gorbachikae*	20X-CC	161.49	A	G		R	F	A	R																																				
Aptian	*G. algerianus*	21X-CC	167.70	A	G	R	F	R	F																																					

Notes: Abundance: A = abundant; R = rare; F = few; P = present. Preservation: G = good; M = moderate; P = poor; VG = very good.

Table 5 (continued).

Age	Zone	Core, section, interval (cm)	Depth (mbsf)	Abundance	Preservation	*Woodringina hornerstownensis*	*Globanomalina archeocompressa*	*Parvularugoglobigerina alabamensis*	*Chiloguembelina crinita*	*Praemurica taurica*	*Chiloguembelina morsei*	*Globanomalina planocompressa*	*Parasubbotina varianta*	*Praemurica inconstans*	*Subbotina triloculinoides*	*Morozovella angulata*	*Morozovella conicotruncata*	*Praemurica uncinata*	*Subbotina triangularis*	*Acarinina mckannai*	*Acarinina soldadoensis*	*Globanomalina pseudomenardii*	*Morozovella apanthesma*	*Morozovella velascoensis*	*Pseudohastigerina wilcoxensis*	*Subbotina hornibrooki*	*Subbotina patagonica*	*Subbotina velascoensis*	*Globigerinatheka senni*	*Morozovella gracilis*	*Morozovella marginodentata*	*Morozovella subbotinae*	*Acarinina primitiva*	*Morozovella aragonensis*	*Morozovella formosa formosa*	*Acarinina bullbrooki*	*Globigerina senni*	*Morozovella caucasica*	*Subbotina inaequispira*	*Truncorotaloides rohri*	*Hantkenina mexicana*	*Globigerinatheka index*	*Globigerinatheka mexicana*	*Hantkenina dumblei*	*Morozovella lehneri*	*Morozovella spinulosa*	*Pseudohastigerina micra*	*Guembelitrioides higginsi*	*Acarinina coalingensis*	*Globigerapsis index*
		171B-1049A-																																														
middle Eocene	P12	3H-CC	30.60																																R			R	F									
middle Eocene	P12	4H-3	33.75	A	G																											R			F			R	F		F	F	R	R	R		
middle Eocene	P12	4H-5	36.75	A	G																											P			F			R	F		F	F	R	R	P		
middle Eocene	P12	4H-CC	40.09	A	G																														F				F		F	F	R				
middle Eocene	P12-P11	5H-CC	49.56	A	G																												F		F			F		F							
middle Eocene	P11	6H-CC	59.06	A	G																												F		F			F	F	F							
Eocene	P9-P10	7H-CC	60.04	A	M																												R	R	R			R	R	F							
Eocene	P9-P10	8X-CC	60.83	A	M																												A		F			F									
Eocene	P9-P10	9H-CC	69.40	A	G																												F	F	F	R	F									
early Eocene	P8-P7	10X-CC	73.14	A	G																F									F	R	F	F												
early Eocene	P6-P7	12X-CC	89.11	A	M																					F		F	F	F	F															
late Paleocene	P4a-P4b	13H-CC	100.08	A	M					R					R				F	F	R	F	F	F	P	R	A	R																		
late Paleocene	P3a	14X-CC	100.29	A	P										F	F	F	F	R																												
early Paleocene	P1c	15X-CC	105.93	A	M								F	F	F																																
early Paleocene	P1b	16X-CC	124.12	A	VG	F				F	F	R																																		
early Paleocene	P1a	17X-2, 3-10	125.34	A	VG	A	F	R	R	F																																				
early Paleocene	P1a	17X-2, 22-24	125.53	A	VG	A	R	F																																						
early Paleocene	P1a	17X-2, 40-42	125.71	A	VG	A																																								
Maastrichtian	*A. mayaroensis*	17X-CC	128.46	A	G																																									
Maastrichtian	*A. mayaroensis*	18X-3, 65-67	137.95	A	VG																																									
Maastrichtian	*R. fructicosa*	18X-4, 10-12	138.90	A	G																																									
Maastrichtian	*R. fructicosa*	18X-4, 16-18	138.96	A	G																																									
Maastrichtian	*G. gansseri-G. falsostuarti*	18X-CC	142.39	A	G																																									
Albian	*T. primula*	19X-CC	150.93	A	VG																																									
Aptian	*H. gorbachikae*	20X-CC	161.49	A	G																																									
Aptian	*G. algerianus*	21X-CC	167.70	A	G																																									

Table 6. Planktonic foraminifer distribution in Hole 1049B.

Age	Zone	Core, section, site, hole	Depth (mbsf)	Preservation	*Hedbergella trocoidea*	*Globigerinelloides ferreolensis*	*Hedbergella delrioensis*	*Hedbergella gorbachikae*	*Hedbergella planispira*	*Contusotruncana contusa*	*Globotruncana arca*	*Globotruncana dupeublei*	*Globotruncana insignis*	*Globotruncanella petaloidea*	*Globotruncanita stuarti*	*Globotruncanita stuartiformis*	*Pseudotextularia elegans*	*Racemiguembelina fructicosa*	*Rugoglobigerina rotundata*	*Trinitella scotti*	*Morozovella trinidadensis*	*Parasubbotina pseudobulloides*	*Praemurica inconstans*	*Subbotina triloculinoides*	*Acarinina bullbrooki*	*Globigerintheca subcoinglobata*	*Morozovella aragonensis*	*Morozovella caucasica*	*Subbotina inaequispira*	*Truncorotaloides rohri*	*Globigerinatheka mexicana*	*Guembelitrioides higginsi*	*Hantkenina mexicana*	*Hantkenina dumblei*	*Morozovella spinulosa*	*Acarinina primitiva*	*Globigerinatheka index*	*Morozovella lehneri*	*Pseudohastigerina micra*	*Globigerapsis index*
		171B-1049B-																																					
middle Eocene	P12	1H-CC	8.88	G																					F			R	F	F	R		F	R	R		F	R	F
middle Eocene	P12	2H-CC	21.49	G																					F			R	F		R	F	R	R	R	F	F	R	
middle Eocene	P12-P11	3H-CC	30.93	G																					F	F	R	F	F		P	R	R	R			F	R	
middle Eocene	P11	4H-CC	40.22	G																					F		R		F	R	R	R							
early Eocene	P8-P10	5H-CC	46.2	G																					F	R	R	F	F										
Paleocene	P2-P1	6X-CC	100.28	G																	R	F	R	F															
Maastrichtian	*A. mayaroensis*	8H-CC	118.52	VG						R	R	F	F	F	R	F	F	F	F	R																		
Aptian	*T. bejaouaensis-G. algerianus*	11X-CC	140.8	G	A	R	F	P	R																													
Albian	*T. bejaouaensis-G. algerianus*	12X-CC	153.66	M	F																																	

Notes: Preservation: G = good; VG = very good; M = moderate. Abundance: A = abundant; F = few; R = rare; P = present.

Table 7. Planktonic foraminifer distribution in Hole 1049C.

Age	Zone	Core, section, interval (cm)	Depth (mbsf)	Abundance	Preservation	*Globotruncana arca*	*Hedbergella infracretacea*	*Rosita patelliformis*	*Globigerinelloides ferreolensis*	*Hedbergella gorbachikae*	*Hedbergella trocoidea*	*Contusotruncana patelliformis*	*Globotruncana linneiana*	*Globotruncanita stuartiformis*	*Pseudotextularia nuttalli*	*Radotruncana calcarata*	*Contusotruncana fornicata*	*Globigerinelloides prairiehillensis*	*Heterohelix globulosa*	*Globotruncana dupeublei*	*Globotruncana falsostuarti*	*Globotruncanella havanensis*	*Globotruncanita stuarti*	*Abathomphalus mayaroensis*	*Contusotruncana contusa*	*Globigerinelloides subcarinatus*	*Globotruncana aegyptiaca*	*Racemiguembelina fructicosa*	*Planoglobulina multicamerata*	*Pseudotextularia elegans*	*Rugoglobigerina hexacamerata*	*Guembelitria cretacea*	*Hedbergella monmouthensis*	*Parvularugoglobigerina alabamensis*
		171B-1049C-																																
middle Eocene	P12	1H-CC	2.09	A	M																													
middle Eocene	P12	2H-CC	21.1	A	G																													
middle Eocene	P11	3H-CC	30.91	A	G																													
middle Eocene	P11	4H-CC	39.98	A	G																													
early Eocene	P9	5H-CC	49.91	A	G																													
early Paleocene	P1c	6X-CC	95.31	A	G																													
early Paleocene		7X-CC	98.01	A	G	P																												
Paleocene	Pa	8X-5	112.79	A	VG																												F	F
Paleocene	Pa	8X-5	112.88	A	VG																												F	F
Paleocene	P0	8X-5	112.97	A	VG																												F	F
Maastrichtian	*A. mayaroensis*	8X-CC	115.59	A	G										F					R			A	P	F		R	A	F	R	F			
Maastrichtian	*R. fructicosa*	9X-CC	121.02	A	G														A					A	F	F	F	F						
Campanian-Maastrichtian	*G. gansseri-G. falsostuarti*	10H-CC	129.93	A	G							F								R	F	R	F											
Campanian-Maastrichtian	*G. gansseri-G. falsostuarti*	11X-2, 77-79	131.97	A	M							F	F				F	R	F															
Campanian	*G. calcarata*	11X-2, 113-115	132.33	A	G	F						F	F	A	F	R																		
Aptian	*H. gorbachikae*	12X-CC	148.28	A	VG				R	F	A																							
Aptian		13X-CC	153.28	R	M	P	F	P																							F			

Notes: Abundance: A = abundant; R = rare; F = few; P = present. Preservation: M = moderate; G = good; VG = very good.

Table 7 (continued).

Age	Zone	Core, section, interval (cm)	Depth (mbsf)	Abundance	Preservation	*Parvularugoglobigerina eugubina*	*Acarinina bullbrooki*	*Chiloguembelina midwayensis*	*Eoglobigerina edita*	*Eoglobigerina eobulloides*	*Globanomalina compressa*	*Morozovella lensiformis*	*Parasubbotina pseudobulloides*	*Parasubbotina varianta*	*Praemurica inconstans*	*Praemurica taurica*	*Subbotina triloculinoides*	*Subbotina trivialis*	*Globigerinatheka mexicana*	*Morozovella aragonensis*	*Rectoguembelina cretacea*	*Subbotina triangularis*	*Globigerinatheca subcoinglobata*	*Morozovella caucasica*	*Subbotina inaequispira*	*Guembelitrioides higginsi*	*Truncorotaloides rohri*	*Hantkenina dumblei*	*Morozovella lehneri*	*Morozovella spinulosa*	*Globigerapsis index*	*Pseudohastigerina micra*	*Acarinina primitiva*	*Globigerinatheka index*
		171B-1049C-																															
middle Eocene	P12	1H-CC	2.09	A	M		F												F						F		F	R	R				
middle Eocene	P12	2H-CC	21.1	A	G		F												R				F		F	R	F	R	R	R	R	R	
middle Eocene	P11	3H-CC	30.91	A	G		F													P			F		F	P	F	R	R	R			
middle Eocene	P11	4H-CC	39.98	A	G		F												R	R					F	P	F						
early Eocene	P9	5H-CC	49.91	A	G		F													R			R	F	F								
early Paleocene	P1c	6X-CC	95.31	A	G		P				R	P			A		R		P	P	R	F											
early Paleocene		7X-CC	98.01	A	G		P	A	R	F	R	P	F	F	A	F	F	F															
Paleocene	Pa	8X-5	112.79	A	VG	A																											
Paleocene	Pa	8X-5	112.88	A	VG	A																											
Paleocene	P0	8X-5	112.97	A	VG																												
Maastrichtian	*A. mayaroensis*	8X-CC	115.59	A	G																												
Maastrichtian	*R. fructicosa*	9X-CC	121.02	A	G																												
Campanian-Maastrichtian	*G. gansseri-G. falsostuarti*	10H-CC	129.93	A	G																												
Campanian-Maastrichtian	*G. gansseri-G. falsostuarti*	11X-2, 77-79	131.97	A	M																												
Campanian	*G. calcarata*	11X-2, 113-115	132.33	A	G																												
Aptian	*H. gorbachikae*	12X-CC	148.28	A	VG																												
Aptian		13X-CC	153.28	R	M																												

laris, Acarinina soldadoensis, A. mckannai, and *Chiloguembelina crinita,* was identified in Sample 171B-1049A-13H-CC (100.1 mbsf). Subzone P3b was not identified, perhaps because it occurs in the unrecovered interval of Core 171B-1049A-14X. A Subzone P3a assemblage includes *S. triloculinoides, S. triangularis, Praemurica inconstans,* and *M. conicotruncata,* which were recorded in the core-catcher sample of this core.

A biostratigraphically complete K/T boundary transition from Zones Pα, P1a, and P1b through P1c was recovered in all three holes at Site 1049 (Fig. 6). Surface scraping samples from the K/T core sections of Holes 1049A and 1049C reveal that all the zonal marker species and characteristic planktonic foraminifer assemblages for these zones are present and well preserved (Table 5). The Pα Zone, defined by the total range of *Parvularugoglobigerina eugubina,* is ~20 cm thick in Hole 1049A. It extends from immediately above the K/T boundary tektite layer to Sample 171B-1049A-17X-2, 40–42 cm. At the base of this zone are abundant *Chiloguembelina midwayensis,* few woodringinids, rare Danian hedbergellids, and other parvulorugoglobigerinids. The nominate species of the Pα Zone, *Guembelitria cretacea,* occurs consistently and is quite common in the basal Danian sediments, but its co-occurrence with *P. eugubina* at the top of the tektite layer suggests that Zone Pα is missing. The absence of Zone Pα is puzzling because there is no evidence of a hardground, winnowing, or bioturbation through the thin limonitic horizon that bounds the top of the tektite layer and the base of the Pα Zone (Fig. 6). Perhaps Zone Pα is recognizable only in shallower settings where sedimentation rates are higher, or where *P. eugubina* may have been biogeographically excluded.

Dwarfed specimens of *Heterohelix navarroensis* are rare to common from Zone Pα through lower Zone P1a. Also recorded in this interval are sporadic occurrences of other Cretaceous species including a variety of other heterohelicids, globotruncanids, rugoglobigerinids, and *Globigerinelloides.* Most, if not all, of these post-boundary occurrences may be the result of reworking because Cretaceous species were also sporadically identified within Paleocene–Eocene cores.

The tektite layer contains only Maastrichtian planktonic foraminifers. Preservation within this interval ranges from moderate to poor because a number of specimens are preserved as internal molds of smectite, probably as a result of the devitrification of the glass spherules. The biomarker that is characteristic of the uppermost Maastrichtian, *Plummerita hantkenoides,* was not found in a Maastrichtian scraping sample immediately below the tektite layer, nor in the core-catcher samples of the K/T boundary cores. Further investigation of larger samples from immediately below the tektite layer should reveal the presence of this species if the uppermost Maastrichtian interval is complete.

A 13-m interval of Maastrichtian sediments comprising the *A. mayaroensis* Zone occurs below the K/T boundary at Site 1049. A sharp color change at the base of the *A. mayaroensis* Zone (138.92 mbsf in Hole 1049A) marks a major hiatus that spans the entire *R. fructicosa* and *G. gansseri* Zones. It is uncertain how much of the lower *A. mayaroensis* Zone is truncated by this hiatus. Assemblages below this level down to the base of Subunit IIIC (132.0 mbsf in Hole 1049C) are assigned to the *G. falsostuarti* Zone. Inoceramid prisms are common within this zone but are absent in the *A. mayaroensis* samples above the hiatus (except for Sample 171B-1049A-18X-4, 10–12 cm, which contains very rare prisms). The white nannofossil ooze that forms Subunit IIID contains well-preserved and common specimens of *Radotruncana calcarata* and is assigned to the upper Campanian *R. calcarata* Zone.

A sharp contact between the base of the *R. calcarata* Zone and the variegated nannofossil claystone below marks a major disconformity between the Campanian and mid-Albian at Sample 171B-1049C-11X-2, 120 cm. A well-preserved middle Albian assemblage, assigned to the *T. primula* Zone, occurs in the variegated claystone. This assemblage is dominated by *T. primula* and *Hedbergella delrioensis* and includes common *H. planispira* and rare *H. gorbachika*e. The *T. primula* Zone was not identified in Hole 1049B, probably because it occurs within an unrecovered interval between core catchers.

The upper Aptian was recovered in all three holes at Site 1049, and the preservation of foraminifers is as good as in the Albian. Samples 171B-1049A-20X-CC (161.5 mbsf) and 171B-1049C-12X-CC (148.2 mbsf) yielded abundant *Hedbergella trocoidea, H. delrioensis, H. planispira, H. gorbachikae,* and *Globigerinoides ferreolensis* and are assigned to the *H. gorbachikae* Zone. Sample 171B-1049A-21X-CC (167.7 mbsf) contains *Hedbergella trocoidea, H. delrioensis, Globigerinelloides ferreolensis,* and *G. algeriana,* the index of the *G. algeriana* Zone. This zone was tentatively identified in Hole 1049B (Core 171B-1049B-12X) in a sample containing only rare specimens that are tentatively identified as *Hedbergella infracretacea*. The upper Aptian *Ticinella bejaouaensis* Zone was recorded only at Hole 1049B (Sample 171B-1049B-11X-CC). The *T. bejaouaensis* assemblage includes abundant *Hedbergella trocoidea,* common *H. delrioensis* and *H. planispira,* and rare *H.* cf. *gorbachikae* and *Globigerinelloides ferreolensis.* No foraminifers were recovered from the deepest core that was drilled at Site 1049 (Section 171B-1049A-22X-CC), and thus no age assignment was possible for this sample.

Benthic Foraminifers

Benthic foraminifers were generally well preserved with increasing abundances downward in Hole 1049A (see Table 8). The low abundances of benthic foraminifers throughout the middle Eocene interval (planktonic foraminifer Zones P6–P12) are probably the result of high abundances of radiolarians and/or lithified material that diluted most of these samples. The Paleocene interval is marked by common abundances of benthic foraminifers, except for a cherty sample (171B-1049A-14X-CC) where they are absent. The two samples of Maastrichtian age (171B-1049A-17X-CC and 18X-CC) contain common to abundant benthic foraminifers. An abundant Lower Cretaceous (lower Albian) benthic foraminifer fauna of excellent preservation is present at the base of Hole 1049A (Sample 171B-1049A-19X-CC), whereas the upper Aptian (Sample 171B-1049A-22X-CC) is almost barren of benthic foraminifers. Paleodepth estimates based on benthic foraminifers reveal a deepening trend through time, from middle bathyal depths (~800–1000 m) during the Albian to lower bathyal depths (1000–2000 m) throughout the latest Cretaceous (Maastrichtian) and Paleogene (Paleocene to middle Eocene).

The middle to late early Eocene fauna from Cores 171B-1049A-3H through 10X is marked by typical post-Paleocene/Eocene benthic extinction taxa including *Aragonia semireticulata, Bulimina* sp. cf. *B. semicostata, B. macilenta, B. semicostata, B. thanetensis, Buliminella grata, Karreriella subglabra, Osangularia mexicana,* and *Vulvulina spinosa,* along with *Buliminella beaumonti* and *Globocassidulina subglobosa.* An additional component of the Eocene fauna is represented by several taxa, ranging from the Maastrichtian–early Paleocene into the middle Eocene, including pleurostomellids, *B. trinitatensis, Oridorsalis* spp., and abundant *Nuttallides truempyi.*

A number of taxa that became extinct at the Paleocene/Eocene boundary worldwide (e.g., Tjalsma and Lohmann, 1983; Van Morkhoven et al., 1986) characterize the Maastrichtian to Paleocene fauna (Cores 171B-1049A-13X through 18X) and are represented by *Aragonia velascoensis, Bolivinoides delicatulus, Bulimina spinea, Coryphostoma midwayensis, Gavelinella beccariiformis, Osangularia velascoensis, Paralabamina hillebrandti,* and *P. lunata.* All of these taxa are also absent in the Eocene in Hole 1049A. Other taxa were encountered only in the Maastrichtian samples (e.g., *Allomorphina trochoides, Boldia*? sp., *Bulimina velascoensis, Cibicidoides hyphalus, Goesella rugosa, Praebulimina reussi, Pyramidina rudita, Reussella szajnochae,* and *Osangularia navarroana*).

Gavelinella beccariiformis, which is known to dominate many Upper Cretaceous–Paleocene deep-sea sequences throughout the world's oceans, is represented by remarkably few specimens in Hole

Table 8. Hole 1049A samples examined for benthic foraminifers.

Core, section	Age	Depth (mbsf)	Abundance	Preservation
171B-1049A-				
3H-CC	middle Eocene	30.6	Rare	Moderate
4H-CC	middle Eocene	40.09	Barren	
7H-CC	middle Eocene–early Eocene	60.04	Few	Moderate
8X-CC	middle Eocene–early Eocene	60.83	Rare	Poor
9H-CC	middle Eocene–early Eocene	69.4	Few	Moderate
10X-CC	early Eocene	73.14	Abundant	Good
12X-CC	early Eocene	89.11	Barren	
13H-CC	late Paleocene	100.08	Common	Moderate
14X-CC	early Paleocene	100.29	Barren	
16X-CC	early Paleocene	124.12	Common	Good
17X-CC	late Maastrichtian	128.46	Common	Moderate
18X-CC	early Maastrichtian	142.39	Common	Moderate
19X-CC	early Albian	150.93	Abundant	Very good
22X-CC	late Aptian	174.01	Trace	Poor

1049A. This is significant, considering the dominance of *Nuttallides truempyi* in the assemblage. Although *G. beccariiformis* and *N. truempyi* had a similar depth range (bathyal–abyssal), the former has been suggested to depend on rather well-oxygenated conditions, whereas the latter was more tolerant of sluggish deep-water circulation and thereby able to tolerate lower oxygen concentrations (Widmark, 1995; Widmark and Speijer, in press). Thus, the dominance of *N. truempyi* may indicate that the benthic foraminifer community at Site 1049 on the Blake Nose was more influenced by low-oxygen, warm, saline, deep-water circulation than were benthic foraminifer faunas elsewhere—especially relative to those of the high southern latitudes where *G. beccariiformis* is the dominant faunal component during Maastrichtian through Paleocene times.

An exquisitely well-preserved early Albian fauna (Sample 171B-1049A-19X-CC) was found in the red claystone, rhythmically interbedded with green claystones and white chalks, near the base of the cored interval. This rich Albian fauna is dominated by *Osangularia utaturensis* and *Gyroidinoides primitiva*, along with *Gavelinella ammonoides, G. intermedia, Lenticulina* spp., thick-walled lagenids (such as *Marginulina* spp. and *Margulinopsis* spp.), *Nodosaria* spp., *Osangularia insigna, Pleurostomella* spp., *Tristix excavatus, Valvulineria intracretacea/parva,* and a few specimens belonging to *Ammodiscus* sp. and *Glomospira gordialis.* One sample (171B-1049A-22X-CC) from white Aptian chalk, on the other hand, provided only a few minute, poorly preserved lagenids (*Dentalina* spp. and *Lenticulina* spp.), indicating that the state of benthic foraminifer preservation in the Lower Cretaceous is diagenetically controlled at Site 1049.

Radiolarians

Radiolarian recovery at Site 1049 was confined to the lower and middle Eocene. Core-catcher samples were processed and examined for radiolarians from Sections 171B-1049A-3H-CC through 23X-CC, 171B-1049B-1H-CC through 23H-CC, and 171B-1049C-1H-CC through 12H-CC. Sections 171B-1049C-13H-CC through 23H-CC were not examined because of time constraints. The radiolarians are generally well preserved, although some cores have sparse faunas because of dissolution and reworking. The zonal scheme of Riedel and Sanfilippo (1978) was used for zonal assignments, and the biostratigraphically important taxa are discussed below. An earlier study by Weaver and Dinkleman (1978) discussed the radiolarians recovered from DSDP Leg 44, Holes 390 and 390A. Hole 390A yielded the majority of their radiolarians, and all but one of their faunas came from selected parts of Sections 44-390A-2-1 through 7-4 and not from the core catchers.

Sample 171B-1049A-3H-CC contains radiolarians assignable to the middle Eocene *Podocyrtis ampla* Zone (Fig. 13). Species common to this zone, along with *P. ampla,* include *Dictyopora mongolfieri,* early morphotypes of *Eusyringium fistuligerum, P. papalis, P. sinuosa,* and *Theocotylissa ficus.* Samples 171B-1049A-4H-CC and 5H-CC are assignable to the *Thyrsocyrtis tricantha* Zone and contain key marker taxa including *Eusyringium lagena, P. diamesa, P. sinuosa, Thyrsocyrtis hirsuta,* and *T. tricantha.* Distinctive middle Eocene taxa, such as *Calocyclas hispada, Dictyopora mongolfieri, Phormocyrtis striata striata, P. papalis,* and *Theocyrtis rhizodon,* also are common. Poorly preserved and fragmented radiolarians were recovered in Sample 171B-1049A-7H-CC but could only be assigned a general age range of early to middle Eocene. Sample 171B-1049A-8X-CC contains a well-preserved fauna assignable to the *Thyrsocyrtis cryptocephala* Zone of earliest middle Eocene age. Zonal markers include *Theocotyle cryptocephala, Calocyclomma castrum, Podocyrtis acalles, Thyrsocyrtis hirsuta,* and *T. tensa.* The next core catcher (Sample 171B-1049A-9H-CC) contains a late early Eocene fauna that is assignable to the *P. striata striata* Zone. This zone is defined by the FO of *P. striata striata*; other common taxa include *Theocotyle nigriniae* and *Thyrsocyrtis rhizodon.* Sample 171B-1049A-10X-CC contains traces of reworked radiolarians, as do a few samples downhole. Unfortunately, all samples contain nondiagnostic fragments.

Samples from Hole 1049B also contain well-preserved middle Eocene radiolarians. Samples 171B-1049B-1H-CC to 2H-CC contain forms assignable to the *Podocyrtis ampla* Zone, whereas Samples 3H-CC and 4H-CC are slightly older and are assigned to the *Thyrsocyrtis tricantha* Zone (Fig. 13). Samples 171B-1049B-5H-CC and 6H-CC contain radiolarians that are sparse, heavily oxidized, and nearly completely broken. Several Paleogene samples downhole contain traces of radiolarians, but all observed forms were nondiagnostic.

The same radiolarian distribution was found in Hole 1049C. Although Sample 171B-1049C-1H-CC contains only a few pieces of radiolarians and rare planktonic foraminifers in strewn-slide view, Samples 171B-1049C-2H-CC and 3H-CC contain taxa assignable to the *Podocyrtis ampla* Zone. Sample 171B-1049C-4H-CC contains the most abundant fauna of all samples examined at Site 1049, with taxa assignable to the *Thyrsocyrtis tricantha* Zone. Preservation of the radiolarians in Sample 171B-1049C-5H-CC is only fair, and abundance is low. Therefore, the sample could only be bracketed to the lower part of the middle Eocene and assigned to the *Thyrsocyrtis tricantha* down to the *Theocotyle cryptocephala* Zone.

Extremely few Cretaceous radiolarians were found in any of the holes from Site 1049. Several poorly preserved forms were found near the K/T boundary interval in Section 171B-1049C-8X-CC. Also, in Sample 171B-1049B-10X-CC, radiolarians were recovered including poorly preserved forms assignable to the genera *Dictyomitra, Pseudodictyomitra,* and *Stichomitra.* Their general form resembles Aptian/Albian taxa reported from the western United States and Europe. Rare, poorly preserved radiolarians were also noted in Samples 171B-1049A-10X-CC, 13H-CC, 14X-CC, and 16X-CC through 18X-CC.

Sediment Accumulation Rates

Sediment accumulation rates were calculated based upon biostratigraphic age determinations from calcareous nannofossils and planktonic foraminifers (Fig. 14). Data used in these calculations are shown in Tables 3 and 4.

Sediment accumulation rates are difficult to calculate for the upper 60 m of the site, which includes most of the middle Eocene, because of large-scale reworking and poor recovery. Lower Eocene sedimentary rock accumulated at ~12 m/m.y. A disconformity or period of low sediment accumulation spanned the Paleocene/Eocene boundary. Sediment accumulation during the late Maastrichtian and Paleocene was steady but slow, with a rate of ~3.6 m/m.y. Essentially no sediment accumulation occurred for ~30 m.y. from the mid-Albian through the late Campanian. Sediment accumulation during the Aptian and early Albian occurred at a rate of ~6 m/m.y.

Summary

Drilling at Site 1049 recovered a sequence of pelagic and hemipelagic sediments spanning the middle Eocene through upper Aptian. Middle Eocene calcareous nannofossils, planktonic foraminifers, and radiolarians at this site (Cores 171B-1049A-3H through 8X) are generally well preserved and abundant. A relatively low-average sediment accumulation rate of ~6 m/m.y. suggests that low-productivity conditions were predominant at this site during the middle Eocene. Chert and porcellanite in the lower Eocene (Cores 171B-1049A-9H through 12X) prevented recovery of a complete sedimentary record, although coring results suggest that only the upper part of the lower Eocene is present at this site. Sediment accumulation rates during this time (~11 m/m.y.) appear to have been slightly higher than those of the middle Eocene, but they still reflect relatively low rates of productivity. The upper lower Eocene is separated from the mid-upper Paleocene by a significant disconformity that eliminated the boundary. Drilling results at this site suggest the occurrence of a hiatus of at least 2 m.y. that encompasses the Paleocene/Eocene boundary. Benthic foraminifers were absent to few throughout the middle Eocene interval; this is probably because high abundances of radiolarians diluted most of these samples.

The mid-Paleocene is incomplete because of poor core recovery, but a continuous composite record of the lower Paleocene was obtained. Planktonic foraminifers and calcareous nannoplankton within the Paleocene are abundant and well preserved, radiolarians are absent, and benthic foraminifers are common and well preserved—except for a cherty sample (171B-1049A-14X-CC) where they are absent. Most noteworthy is the excellent foraminifer preservation and complete recovery of most lower Danian planktonic foraminifer and calcareous nannofossil zones, including the early Danian Pα Zone. Studies of this early Danian interval will provide a highly detailed record of the paleoceanographic and evolutionary changes associated with the earliest radiation of plankton and benthos following the terminal Cretaceous extinction event.

An excellent composite record of mid-Campanian through latest Maastrichtian time was also recovered. Throughout this interval, planktonic foraminifers and calcareous nannoplankton are well preserved and abundant, benthic foraminifers are common, and radiolarians are very rare to absent. Integration of biostratigraphic, chemostratigraphic, magnetostratigraphic, and cyclostratigraphic data from this interval will allow considerable refinements to be made to biostratigraphic schemes and chronostratigraphic correlation for this time period.

Rhythmically bedded red and green calcareous claystones and white chalks at the base of the cored interval contain calcareous nannofossils and planktonic foraminifers of the early Albian and late Aptian. Microfossil preservation varies directly with lithology, with beautiful calcareous preservation in the red claystones, moderate preservation in the green clay chalks, and poor preservation in the white chalks. The latter are dominated by nannoconids, suggesting that the occurrence and preservation of calcareous microfossils may be a diagenetically enhanced paleoceanographic phenomenon. A rich (abundant) Early Cretaceous (early Albian) benthic foraminifer fauna of excellent preservation was found at the base of Hole 1049A (Sample 171B-1049A-19X-CC), whereas the late Aptian (Sample 171B-1049A-22X-CC) was almost barren of foraminifers.

Paleodepth estimates based on benthic foraminifers revealed a deepening trend through time at Site 1049, from middle bathyal depths (~800–1000 m) during Albian times to lower bathyal depths (1000–2000 m) throughout the latest Cretaceous (Maastrichtian) and Paleogene (Paleocene–middle Eocene).

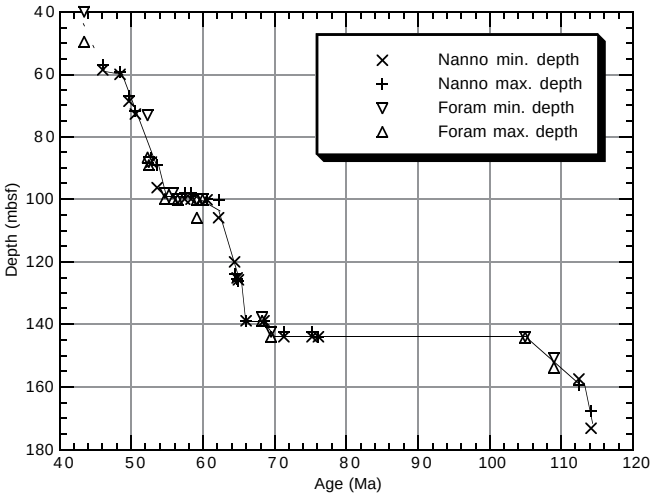

Figure 14. Age-depth relationship in Hole 1049A.

PALEOMAGNETISM

Laboratory Procedures and Interpretations

Portions from nearly all cores yielded useful magnetostratigraphic data, and the polarity intervals were reproduced at similar depth intervals from the three holes. Measurements were made using the pass-through cryogenic magnetometer on the archive half of all core sections that had recovery >40 cm. Each section was measured at 10-cm intervals at natural remanent magnetization (NRM) and after 10- and 20-mT alternating-field (AF) demagnetization steps. Higher resolution measurement steps were applied to sections with scattered intact blocks or intervals of special interest (such as the K/T boundary zone). Discrete samples taken from Hole 1049A (approximately three oriented cylinders or plastic cubes per section) to enhance the magnetostratigraphic reliability were analyzed post-cruise using progressive thermal and AF demagnetization. Thermal demagnetization results and polarity interpretations from 130 discrete samples analyzed at the paleomagnetics laboratories at the University of Oxford and the University of Michigan are included in this *Initial Reports* volume (tabulated in Tables 9 [ASCII format], 10 [PDF format] on CD-ROM, back pocket, this volume). Progressive thermal demagnetization was generally at 30°C increments from ~140° through 360°C, with continuation to higher thermal steps for the more stable samples.

All NRM measurements show variable degrees of drilling-induced overprint, an artifact that has always plagued DSDP and ODP paleomagnetic studies. These overprints have a ubiquitous downward (high positive inclination) and radially inward orientation (e.g., the series of investigative studies made by the frustrated paleomagnetists during Leg 154, as summarized in successive site chapters in Curry, Shackleton, Richter, et al., 1995). This radial-inward overprint is exhibited as an apparent preferential declination toward 0° ("north") when measuring the archive half of each split section.

The majority of these overprints were removed by applying 20-mT AF demagnetization to the shipboard cores or 200° thermal demagnetization to the minicores. The main exceptions to the shipboard measurements are those sediments that are severely distorted during coring or are surrounded by drilling slurry in the core liners. We did not apply higher alternating-demagnetization steps to the intact archive halves to avoid significantly degrading the magnetic record for

future studies. In the majority of these intervals in Hole 1049A, the discrete minicores provided the polarity interpretations.

Interpretation of the magnetostratigraphy from the pass-through magnetometer was based mainly on the clustering of positive inclinations (normal polarity) and negative inclinations (reversed polarity) after the 20-mT demagnetization step. There was insufficient time to make detailed examinations of the demagnetization characteristics of each portion of these cores. Therefore, the 20-mT data were filtered before being plotted: all measurements with inclinations >75° were assumed to be dominated by the drilling overprint; measurements of weakly magnetized samples near the noise limits of the cryogenic magnetometer were omitted; intervals of anomalously high intensity were eliminated (these are usually associated with rust particles within the drilling slurry); and data from the uppermost 20 cm of the disturbed top of each core were removed. A three-point moving mean was applied to the inclination record to smooth artifacts before plotting the data (Figs. 15–17). Careful cross-comparison of the data with the observed disturbances in the cored sediments and occurrences of rust particles in the liners would probably remove additional artifacts. However, in nearly all intervals, the shipboard interpretations were supported by post-leg analysis of minicores.

The polarity intervals are best defined in Hole 1049A, which also was the only continuously cored hole (Fig. 15). The suite of discrete samples clarified the polarity zones. APC Cores 171B-1049-3H through 7H were oriented using the tensor tool, and initial examinations of the computed declinations supports the initial polarity interpretations, based on inclination clustering.

Biomagnetostratigraphy

Polarity Zones and Chron Assignments

Assignment of polarity chrons to the interpreted polarity intervals relies on the shipboard micropaleontology datums (especially nannofossil zones) and the chronostratigraphy of Berggren et al. (1995) and Gradstein et al. (1995). For comparison among the holes, the K/T boundary was used for alignment, implying that the uppermost 13–15 m of "no recovery" in Hole 1049A is above the sediment surface of Holes 1049B and 1049C (Fig. 18; see "Operations" section, this chapter).

Paleogene

The downhole pattern of N-R-N-R in the continuous record of Cores 171B-1049A-3H through 6H is consistent in age (nannofossil Zones CP14a to upper CP13b of the upper–middle Eocene) and relative duration with Chrons C19n through C20r. A cluster of positive inclinations in the upper portion of Core 171B-1049A-6H was shown by the discrete samples to be spurious (Fig. 15). The zonation from nannofossil Zones CP13b through CP14a is difficult to resolve because of abundant reworking, but the magnetostratigraphy is consistent with a continuous depositional record. The corresponding magnetostratigraphic record in the APC cores from Hole 1049B shows the same general pattern, although it is more disturbed by coring (Fig. 18). The polarity chron assignments imply that the base of the Bartonian stage of the middle Eocene, which is coincident with the base of Chron C19n (Berggren et al., 1995), is in the lower portion of Core 171B-1049A-3H.

The biostratigraphy indicates a missing interval near the base of the middle Eocene between nannofossil Zones CP13b and CP12b. This hiatus has juxtaposed portions of Chrons C20r and C21r and omitted Chron 20n, for a total hiatus of ~4 m.y. (Fig. 18). Aubry (1995) recognized the same hiatus at nearby Site 390, where she proposed that nannofossil Zone NP15b (equivalent to CP13b) overlies Zone NP14a (equivalent to CP12a).

Uppermost lower Eocene polarity Chrons C22n-C22r-C23n appear to be present in Cores 171B-1049A-9H and 10X. Below this level, recovery of the lowermost Eocene and upper Paleocene interbedded chalk-chert-ooze facies was patchy, and therefore assignments of portions of Chrons C24n through C28n are based entirely on the shipboard biostratigraphic ages. The Paleocene/Eocene boundary interval was poorly recovered and may be condensed, or there may be a hiatus at this site.

K/T Interval and Cretaceous

The interval spanning the K/T boundary has a complex magnetization that is compounded by considerable sedimentary disturbances (synsedimentary slumping and/or drilling-induced disruption). The greenish layer of spherules at the K/T boundary is reversed polarity, which is consistent with the known age of the K/T event within Chron C29r. Cores 171B-1049A-16X and 17X appear to exhibit a complete but relatively condensed succession from upper Chron C30n (uppermost Maastrichtian) through lower Chron C28n (lowermost Paleocene).

The lower upper Maastrichtian in upper Core 171B-1049A-18X exhibits reversed polarity underlain by normal polarity. This interval may represent Chron C30r and uppermost Chron C30n.

The alternating reddish marls and white limestones of Aptian through early Albian age are dominated by the normal polarity of Chron C34 (Cretaceous Long Normal Chron). These facies were analyzed at high resolution for all holes in an effort to locate the brief polarity intervals of "M–1." (Isea polarity zone) through "M–3" observed at various DSDP/ODP sites and some land sections (reviewed in Gradstein et al., 1995). The "M–1" through "M–3" nomenclature was originally proposed by the DSDP Leg 40 scientific party (Ryan et al., 1978). A reversed-polarity zone observed near the top of the lower Albian succession in Holes 1049A (lower Section 19X-2) and 1049C (interval 10X-3, 10–40 cm) was assigned as "M–2." In Hole 1049C, this "M–2" reversed-polarity zone spans a complete white-red-white color alternation (100 k.y.).

A second reversed-polarity interval in the basal Albian was observed about 8 m lower, adjacent to a distinctive black shale layer. However, the coincidence of the reversed-polarity zone with an anomalous yellowish greenish staining of the sediments suggests that the apparent reversed magnetization is an artifact of post-Albian iron mobilization that occurred during diagenesis, induced by the redox contrasts near this black shale.

CORE-CORE INTEGRATION

At Site 1049, magnetic susceptibility and GRAPE density data from the multisensor track (MST) and reflectance data from the Minolta color scanner were available for attempting precise core-core integration (see Tables 11–13 on CD-ROM, back pocket, this volume). Several factors made it impossible to develop a complete composite section. First, there was an interval of about 5 m that contained chert layers; in this interval, coring was attempted only in Hole 1049A with only moderate recovery. Thus, there were many unrecovered intervals in the section drilled. Second, in the upper 50 m of the section (middle Eocene) the GRAPE density and magnetic susceptibility records are remarkably featureless. In addition, the seafloor depth was misestimated in Hole 1049A so that all cores in that hole require an initial offset of about −15 m. On the other hand, an

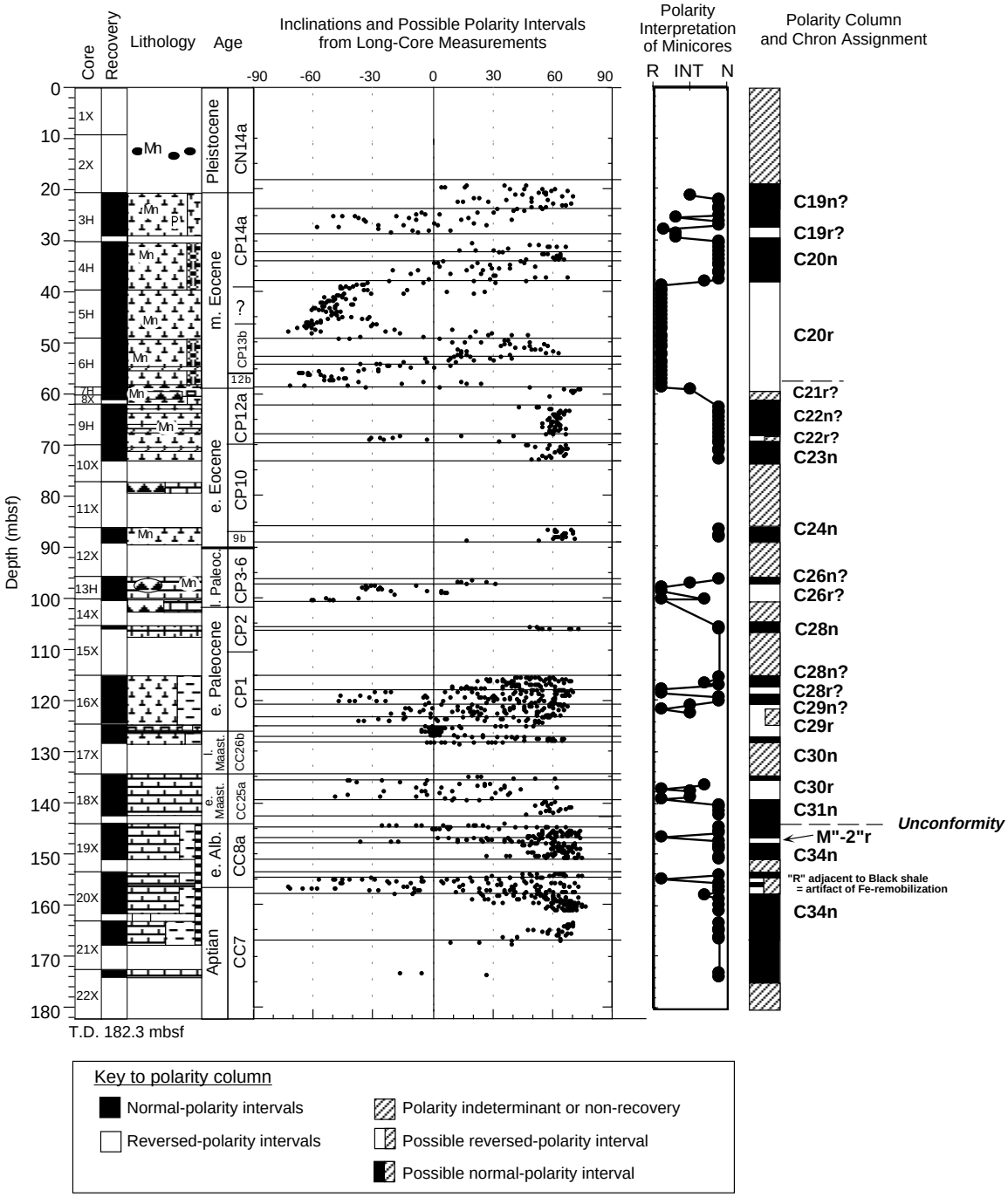

Figure 15. Magnetostratigraphy of Hole 1049A. Magnetic inclinations from long-core measurements are after AF demagnetization at 20 mT and were filtered using a three-point moving average. Measurements from the uppermost 20 cm of each core and those having anomalously high or low magnetic intensities were removed. Horizontal lines delineate clusters of predominantly positive, negative, or equally mixed magnetic inclinations that were used for a preliminary shipboard polarity column. Polarity of discrete minicores is from interpretation of progressive thermal demagnetization and is assigned relative degrees of certainty. These polarity interpretations from discrete samples are given priority in the compilation of the summary polarity column. Polarity chron assignments are based upon the polarity zone pattern and nannofossil biostratigraphy. Note that "0" on the depth scale in this hole is probably ~13 to 15 m above the top of the sediment surface.

excellent K/T boundary was recovered with similar characteristics at all three holes, and it was possible to develop a useful composite section below that point.

In view of these factors, we proceeded in the following manner. The depth of the K/T boundary in Core 171B-1049B-6X was arbitrarily taken as a fixed point (so that m composite depth [mcd] and mbsf depths are identical for Core 6X in Hole 1049B), and the depths of the correlative cores in Holes 1049A and 1049C were adjusted to align the boundaries to it on the basis of the minor magnetic susceptibility peak that is associated with the boundary. A partial composite section was built downward from that point. Even in this part of the section, the composite section is not complete because the probably

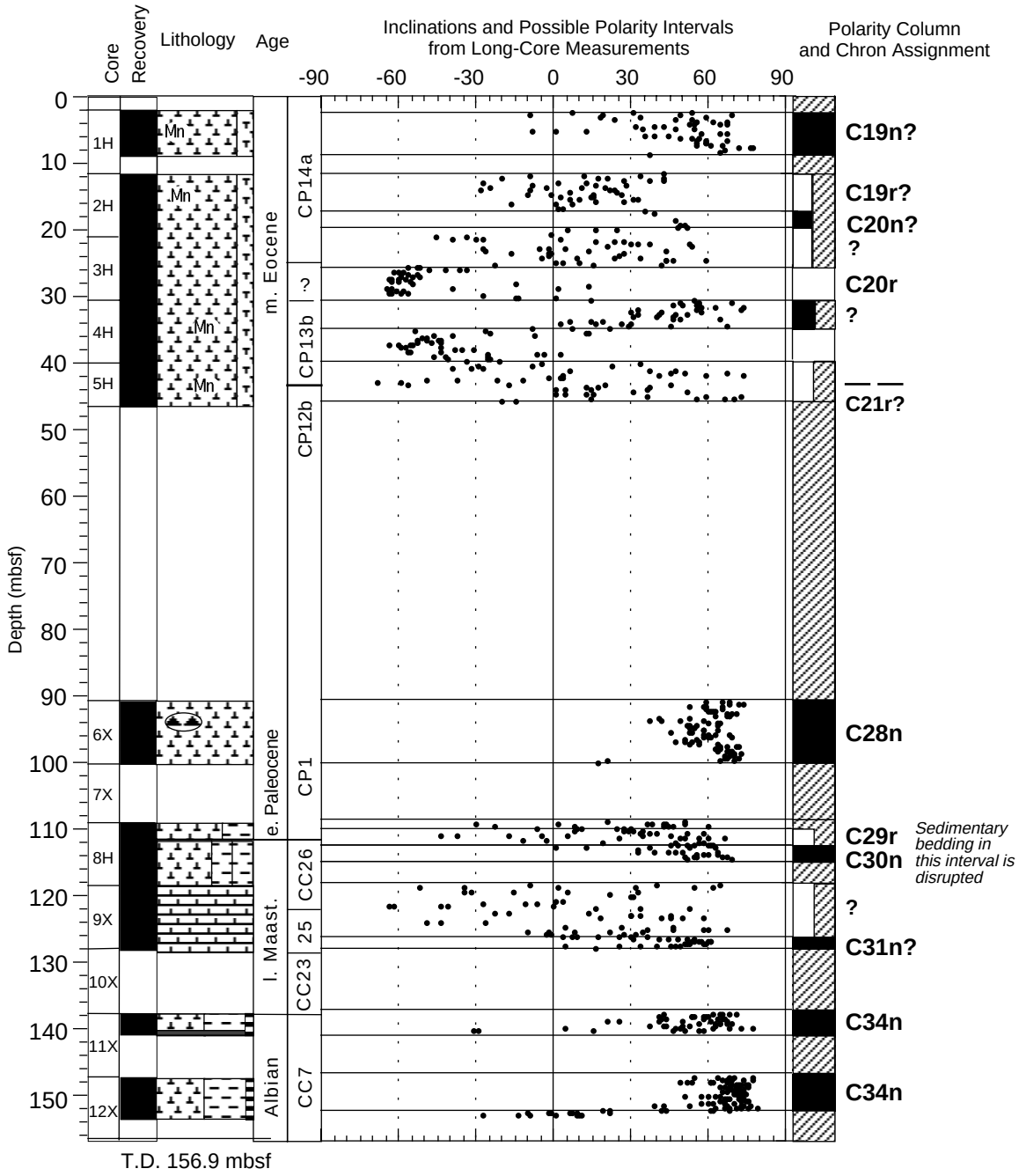

Figure 16. Magnetostratigraphy of Hole 1049B. Magnetic inclinations from long-core measurements are after AF demagnetization at 20 mT and were filtered using a three-point moving average. Measurements from the uppermost 20 cm of each core and those having anomalously high or low magnetic intensities were removed. Horizontal lines delineate clusters of predominantly positive, negative, or equally mixed magnetic inclinations that were used for a preliminary shipboard polarity column. Polarity chron assignments are based upon the polarity zone pattern and nannofossil biostratigraphy.

slumped or otherwise disturbed Maastrichtian does not contain any features that would make a composite section meaningful. However, the Aptian–Albian section shows excellent overlap among the holes, as is illustrated in Figure 19. Above the K/T boundary a few minor offsets were applied to individual cores where justified by the data, without achieving a composite section. The offsets applied are listed in Table 14.

The only interval for which the creation of a spliced record was warranted is the Aptian–Albian interval. Figure 20 shows a spliced magnetic susceptibility record from 131 to 152 mcd, composed of intervals from Holes 1049A, 1049B, and 1049C. This splice (Table 15) could be used as a guide for sampling the entire Aptain–Albian section without gaps or overlapping samples.

ORGANIC GEOCHEMISTRY

Gas Analyses

No clearly indigenous, natural thermogenic hydrocarbons were detected in the headspace samples from Hole 1049A. No vacutainer samples were required because no free gas was observed in the sediment. CO, CO_2, and H_2S gases were not measured at Hole 1049A.

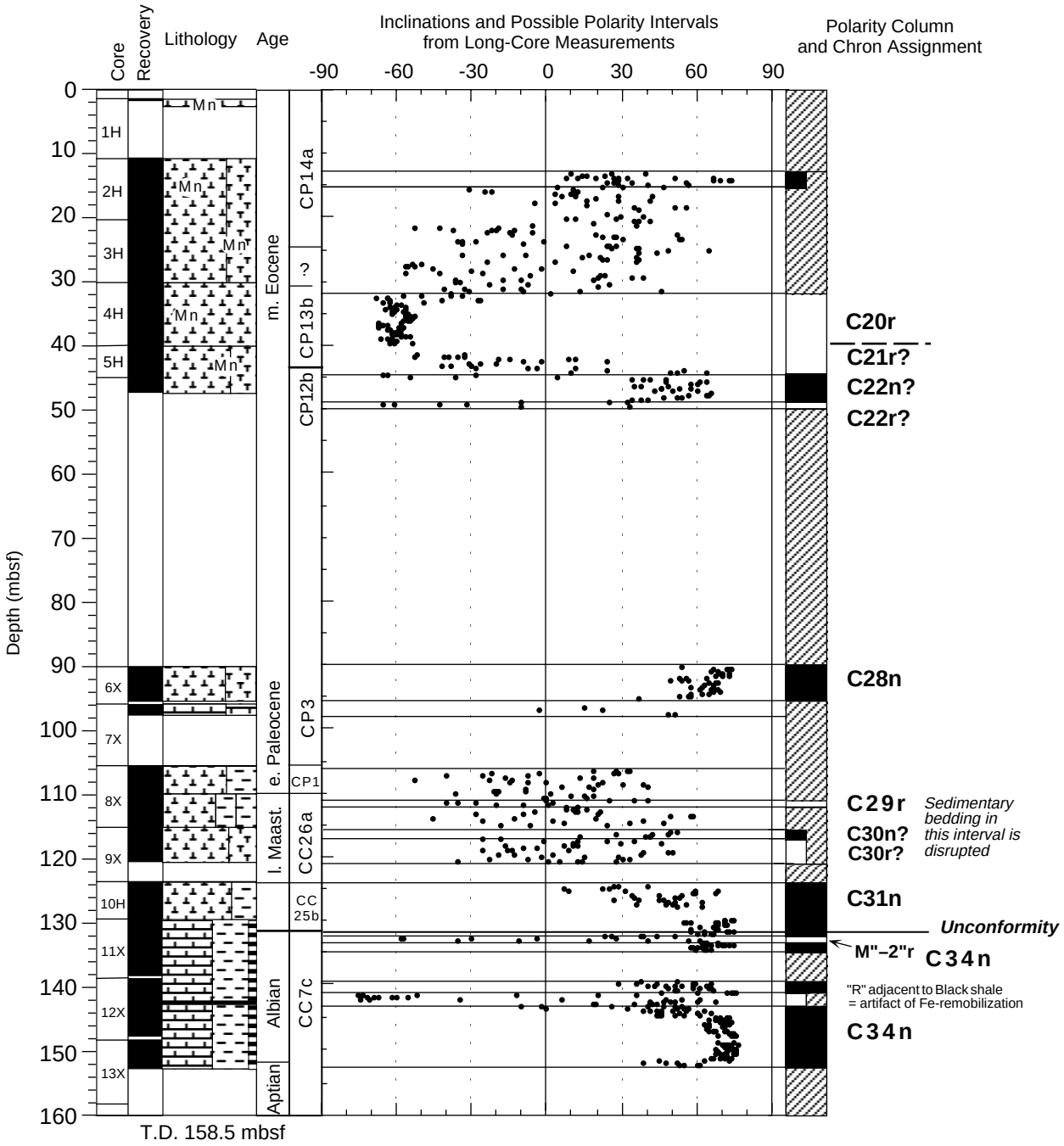

Figure 17. Magnetostratigraphy of Hole 1049C. Magnetic inclinations from long-core measurements are after AF demagnetization at 20 mT and were filtered using a three-point moving average. Measurements from the uppermost 20 cm of each core and those having anomalously high or low magnetic intensities were removed. Horizontal lines delineate clusters of predominantly positive, negative, or equally mixed magnetic inclinations that were used for a preliminary shipboard polarity column. Polarity chron assignments are based upon the polarity zone pattern and nannofossil biostratigraphy.

Gas chromatographic analysis of the Hole 1049A headspace samples detected mostly methane (C_1) and traces of ethane (C_2), ethylene (C_2=), propane (C_3), and propylene (C_3=) hydrocarbon gases, and propylene (C_3=). The C_1 data show three distinct groups related to depth. The surface group, near the present seafloor in Cores 171B-1049A-3H and 4H, contained 10.1 and 0.2 ppm methane, respectively (Table 16). These two cores were also the only ones with detectable C_{2+} hydrocarbons of 6.47 and 0.2 ppm, respectively. The middle group, at an intermediate depth in Cores 171B-1049A-5H through 13H, typically contained 2 to 2.5 ppm methane and no detectable C_{2+}. The deep group, which contained 43 to 50 ppm of methane, consists of samples from Cores 171B-1049A-15X through 22X.

The C_{2+} hydrocarbon content in the surface gas–analysis group is unusual in these cool, immature rocks and may be contamination. The middle gas–analysis group, containing 2 to 2.5 ppm methane, is similar to the background levels found in the laboratory air and, thus, is not considered to be significant for the headspace method. The deep gas–analysis group contains elevated methane values.

Overall, the sediment methane content is markedly lower than expected, based on results from several other sites (Emeis and Kven-

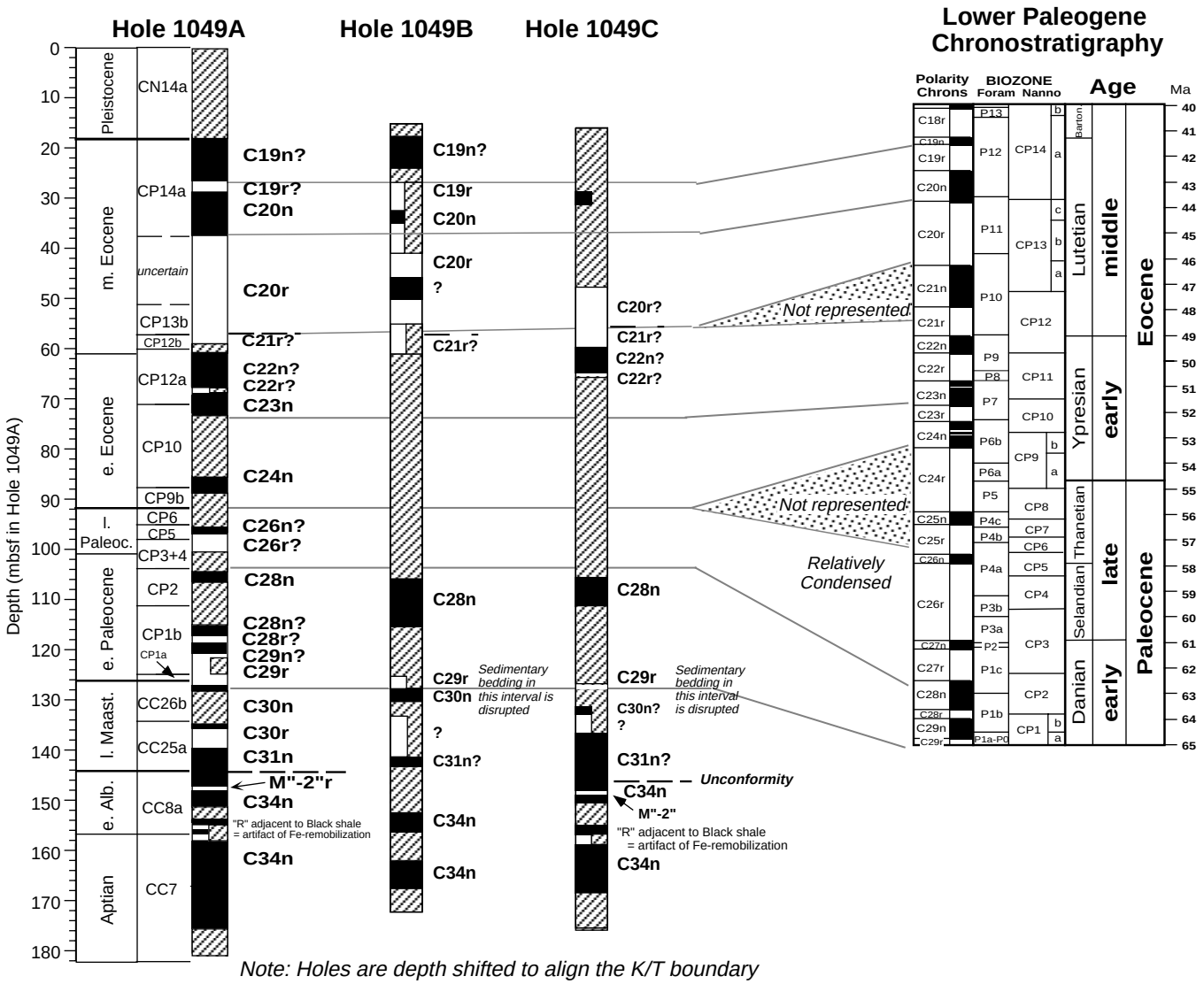

Figure 18. Comparison of polarity interpretations from the three holes at Site 1049 with Paleogene chronostratigraphy. Alignment of the three holes used the K/T boundary, implying that the upper 13–15 m of attempted coring in Hole 1049A was probably above the sediment surface. Polarity chron assignments are based upon the polarity zone pattern and nannofossil biostratigraphy.

volden, 1986). As shown in the "Elemental Analyses" section (this chapter), the reason for this exceptionally low gas content may be the low organic carbon content of these sediments.

Elemental Analyses

Carbonate and carbon analyses of about 50 samples from Hole 1049A (Table 17) show that middle Eocene to late Maastrichtian sediments (22–142 mbsf) from Hole 1049A are typically carbonate rich, ranging from 37 to 89 wt% $CaCO_3$ and averaging 69 wt% $CaCO_3$ (Fig. 21), and low in organic matter, ranging from below the detection limit of 0.3 wt% to 0.41 wt%. Lower Albian and Aptian strata from 144 to 158 mbsf are composed mostly of noncarbonate materials, ranging from 14 to 56 wt% $CaCO_3$ and averaging 34 wt% $CaCO_3$, that appear rich in clay minerals. Within this interval, a lower Albian black shale that occurs just below 140 mbsf in Hole 1049B is locally rich in sapropelic kerogen. This black shale was only partially recovered during drilling at Site 390, and, consequently, its significance was not recognized at that time (Erdman and Schorno, 1978). Most of the organic carbon–rich section was recovered in Holes 1049A, 1049B, and 1049C at Site 1049.

The black shale consists of medium gray claystone interbedded with sparse to locally abundant, cream-colored dolomite laminae and brownish black sapropelic layers (Fig. 22). In Hole 1049B, continuous samples of the black shale were taken over a 8-cm interval just below 140 mbsf.

The black shale and related strata were divided into facies Subunits A through I based on grouping similar lithology and considering the abundance of visible organic-rich layers (Table 18; Fig. 22). After sampling each subunit with a knife, the disturbed sediment in contact with the core liner was trimmed off, combined, and analyzed as pseudocomposite Sample 171B-1049B-11X-CC, 12.5–22 cm (Table 17). The sample is a pseudocomposite in that it may contain sediment slurry derived during drilling from strata outside the sample interval.

Rock-Eval Analyses

Rock-Eval results from five samples with >0.5 wt% TOC in an 8-cm interval show that the sediment is moderate to rich in kerogen, with TOC ranging from 1.2 to 10.1 wt% with a mean of 4.2 wt% (Table 19). TOC determined by the Carlo Erba model 1500 CNS analyzer from the same samples ranges from 1.7 to 11.5 wt%, with a

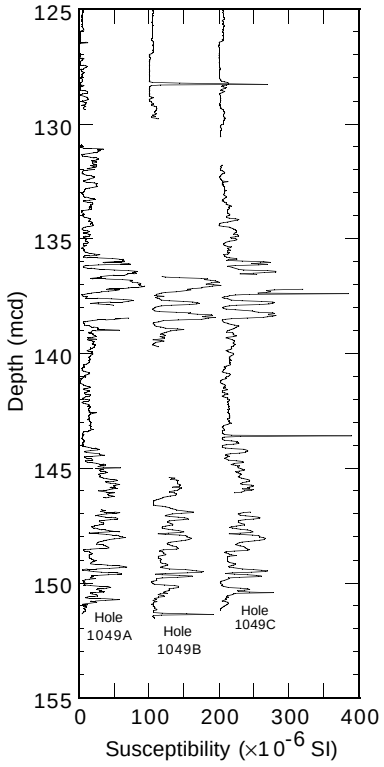

Figure 19. Magnetic susceptibility data from Holes 1049A, 1049B, and 1049C vs. depth (mcd). The data from Holes 1049B and 1049C have been shifted by 100×10^{-6} and 200×10^{-6} SI units, respectively.

mean of 4.8 wt% or about 10% higher relative TOC content compared with the values reported by Rock-Eval (Table 17). Because of the analytical approach, the TOC determined by the CNS analyzer and the total inorganic carbon analysis is considered more accurate. The organic matter in facies Subunits A through E is immature, as shown by a range of T_{max} values from 393° to 407°C. The indicated immaturity is corroborated by the lack of increased thermogenic hydrocarbon detected in headspace samples taken from cores bounding the black shale strata. Hydrogen indices (HIs) of the kerogen are high, ranging from 451 to 699 mg HC/g TOC with a mean of 556 mg HC/g TOC. The oxygen content of the kerogen was low, with oxygen indices (OIs) ranging from 45 to 152 mg CO_2/g TOC with a mean of 86 mg CO_2/g TOC. The HC index (S_2/S_3) of the kerogen ranges from 3.6 to 15.3 mg HC/mg CO_2 with a mean of 7.7 mg HC/mg CO_2, indicating the kerogen is oil generative. The genetic potential ($S_1 + S_2$) of the kerogen is moderate to excellent, ranging from 6.7 to 72.3 mg HC/g rock and averaging 24.4 mg HC/g rock.

Kerogen typing from the black shale bed in Hole 1049B (Fig. 23) indicates that the black shale layer contains mostly sapropelic (type II) kerogen. Smear-slide petrography indicates that overall the kerogen is composed of a type II sapropel and apparently is not a mixture of humic and type I kerogen. Facies Subunit B, with an HI of 699 mg HC/g rock and an OI of 45 mg CO_2/g rock, approaches the characteristics of a type I kerogen. This Rock-Eval analysis result and organic petrography suggest that the sample contains an amorphous organic matter apparently composed of detrital alginite and bituminite derived from cyanobacteria (Tyson, 1987). Smear slides and prepared paleontologic mounts show that traces of humic (woody) debris sporadically occur in the Cretaceous strata near the black shale beds. Such humic debris may be a minor component of the black shale beds, but it may be degraded to the point where it is not recognizable in the amorphous organic matter.

Table 14. Offsets applied to individual cores at Site 1049 to produce a partial composite record.

Core	Offset (m)
171B-1049A-	
3H	–15.88
4H	–14.90
5H	–13.86
6H	–14.06
7H	–13.02
8X	–13.02
9H	–13.02
10X	–13.02
12X	–13.02
13H	–13.02
15X	–13.02
16X	–13.02
17X	–13.02
18X	–13.02
19X	–13.02
20X	–15.15
21X	–16.32
22X	–16.32
171B-1049B-	
1H	0.00
2H	0.00
3H	0.00
4H	0.00
5H	0.00
6X	0.00
8H	1.81
9X	1.81
11X	–1.09
12X	–1.93
171B-1049C-	
2H	0.00
3H	0.24
4H	0.00
5H	0.00
6X	0.00
7X	0.00
8X	0.00
9X	0.00
10H	0.77
11X	2.07
12X	–2.18
13X	–2.03

Figure 23 also shows a strong correlation ($r^2 = 0.97$) of carbon content with hydrocarbon generation potential (S_2) in the kerogen from the black shale bed in Hole 1049B. This correlation is typical for marine sediments in the northern Atlantic Ocean (Summerhayes, 1987). This relationship is interpreted as an indication that the TOC content is dependent on the degree of preservation of the labile hydrogen-rich kerogen components, which is marked by an increasing S_2 content.

The interpretation that an increasing concentration of TOC in kerogen correlates with an increasing degree of preservation of kerogen can be used to interpret the TOC content of the facies subunits plotted as a function of depth (Fig. 24). The plotted TOC profile shows a sharp increase near the onset of black shale deposition, followed by a trend of ever-decreasing amounts of TOC to near-zero levels toward the top of the bed. The TOC profile suggests that the environment of deposition in the black shale initially produced a high degree of preservation in the kerogen, but, with time, the degree of preservation decreased to the point where little TOC was preserved, and carbonate deposition once again became dominant. Enhanced preservation is also indicated by the higher sulfur content near the base of the black shale interval (Table 17; Tyson, 1995).

Discussion

The lower Albian black shale bed in Hole 1049B contains a dominantly marine sapropelic kerogen in much greater amounts than reported from related strata in the nearby Blake-Bahama Basin (Cardoso et al., 1978; Dow, 1978; Kendrick et al., 1978; Herbin et al.,

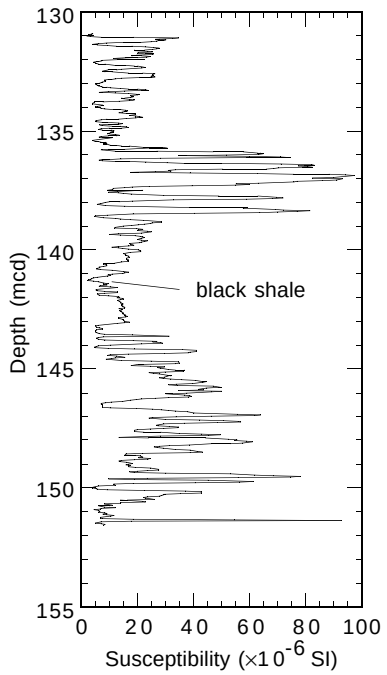

Figure 20. Spliced magnetic susceptibility record for the Aptian–Albian portion of Site 1049, using the intervals in Table 15.

1983; Katz, 1983; Summerhayes and Masran, 1983). The black shale from Hole 1049B is comparable in organic content and HI to the higher quality sapropels found throughout the North Atlantic (de Graciansky et al., 1987; Summerhayes, 1987). In comparison, Albian sediments from nearby Sites 390, 392, and 534 are far leaner in organic matter and hydrogen content. The Albian black shale within the Hatteras Formation in the Blake-Bahama Basin is thicker (95 m) and contains low to moderate amounts of mostly humic kerogen (about 0.8 to 4 wt% TOC) that is generally lower in hydrogen content (HI typically <200 mg HC/g rock). These geochemical differences are primary depositional characteristics and are not the result of the marginally higher thermal maturity of the beds in the Blake-Bahama Basin, which have a T_{max} of about 405° to 435°C (but still immature; Herbin et al., 1983; Katz, 1983) compared with the average T_{max} of 401°C in Hole 1049B on the Blake Nose.

The structural development and subsidence of the Blake Nose was largely complete in the latest Jurassic to Early Cretaceous, before the lower Albian black shale strata were deposited (see "Introduction" chapter, this volume). Furthermore, the area is now a positive topographic feature and the post–Early Cretaceous history of continuing pelagic sedimentation suggests that it was also a positive feature during deposition of the black shale in the early Albian. Therefore, continental sediment seems to have largely bypassed this positive area, allowing dominantly marine sapropels to be deposited. The minor amounts of continental-derived humic debris could have been deposited by eolian transport. In contrast, the Blake-Bahama Basin has been a negative feature since the Jurassic and, consequently, has received larger quantities of continent-derived humic debris that diluted the marine kerogen that was simultaneously deposited there.

INORGANIC GEOCHEMISTRY

Analytical Results

Interstitial waters were taken from 10 core samples in Hole 1049A. Shipboard interstitial-water data from Site 1049 are presented in Table 20. Salinity shows a relatively small range (35.0–36.5) and no systematic variation with depth (Fig. 25A). Chloride and sodium both show a slight overall decrease (~2%) with depth (Fig. 25B). Alkalinity shows a slight general increase with depth from 2.42 mM at 23.05 mbsf to 2.73 mM at 173.40 mbsf (Fig. 25C). The pH values show a slight decrease with depth.

Calcium increases from a minimum of 10.66 mM in the shallowest sample (23.05 mbsf) to 16.57 mM in the deepest sample (173.40 mbsf; Fig. 25A). Magnesium decreases from 54.15 to 47.18 mM over the same depth range (Fig. 25A). Potassium values show a general decreasing trend with depth (13.4 mM at 23.05 mbsf to 11.3 mM at 173.40 mbsf), but the highest concentration (14.7 mM) of this cation was recorded at 87.55 mbsf (Fig. 25C). These major cation data are consistent with seawater interaction with the upper oceanic crust at basement and/or volcaniclastic sediments (e.g., ash layers within Cores 171B-1049A-6H and 9H) within the overlying sediment column. Pore-water strontium concentrations generally show a small increase with depth from 85 µM at 23.05 mbsf to 100 µM at 173.40 mbsf (Fig. 25D). The Sr^{2+} data are consistent with the recrystallization of biogenic calcite in the sediment column at Site 1049. Pore-water lithium concentrations are nearly constant with depth (Fig. 25A). Pore-water rubidium concentrations are also nearly constant with depth, except for a relatively high (2.36 µM) value recorded at 87.55 mbsf (Fig. 25E). These data are broadly consistent with the pore-water potassium data.

Dissolved silica concentrations of the interstitial-water samples from Hole 1049A show an increase with depth to a peak of 937 µM (near saturation levels) at 87.55 mbsf, followed by a decrease to concentrations <150 µM below 148.35 mbsf (Sample 171B-1049A-19X-3, 145–150 cm; Fig. 25F). The peak in silica concentrations coincides with the occurrence of chert in this hole and is consistent with the fact that sediments in approximately the upper 100 m (lithologic Units I and II) still contain abundant biogenic (radiolarian) opal (see "Lithostratigraphy" section, this chapter).

Pore-water ammonium concentrations are low (<40 µM; Fig. 25G), and sulfate concentrations are relatively high (~26–29 mM; Fig. 25G). Sulfate concentrations throughout the section are consistent with the exceptionally low TOC content of lithology of the section (see "Organic Geochemistry" section, this chapter).

Pore-water boron concentrations are indistinguishable from the standard seawater value (~440 µM) in the upper 60 m of Hole 1049A, but they increase to larger values (as much as ~830 µM) below 100 mbsf (Fig. 25H).

Discussion

With the exception of the silica concentrations, the interstitial pore waters analyzed from Hole 1049A show relatively subtle chemical depth gradients. These data are consistent with the extreme distance between the bottom of the hole and the volcanic basement (>8 km; see "Introduction" chapter, this volume), the shallow core-top and burial depths of the sediments in the hole (2656 mbsl and 0–190 mbsf, respectively), and the possibility that the pore-water system at this site is in communication with adjacent open-ocean waters.

PHYSICAL PROPERTIES

Physical properties at Site 1049 were measured on both whole-round sections and discrete samples from split-core sections. Whole-round measurements included the determination of GRAPE bulk density, magnetic susceptibility, compressional *P*-wave velocity, and natural gamma radiation, as well as measurements of thermal conductivity. Index properties, compressional *P*-wave velocity, shear strength, and resistivity were measured on discrete samples from split-core sections at a typical frequency of three measurements per core.

Table 15. Makeup of splice for Aptian–Albian interval.

Hole, core, section, interval (cm)	Depth (mbsf)	Depth (mcd)	Whether tied	Hole, core, section, interval (cm)	Depth (mbsf)	Depth (mcd)
171B-						
1049A-19X-1, 3.0	143.93	130.91	Start	171B-		
1049A-19X-4, 143.00	149.83	136.81	Tie to	1049B-11X-1, 19.50	137.90	136.81
1049B-11X-2, 18.00	139.38	138.29	Tie to	1049C-12X-1, 117.00	140.47	138.29
1049C-12X-7, 12.00	148.22	146.04	Tie to	1049B-12X-1, 66.00	147.97	146.04
1049B-12X-5, 69.00	153.49	151.56	End			

Note: See Figure 20 for display of spliced data.

Table 16. Headspace gas composition for Hole 1049A.

Core, section, interval (cm)	Sample depth midpoint (mbsf)	Group	C_1	C_2=	C_2	C_3=	C_3
171B-1049A-							
3H-4, 0-5	23.13	Surface	10.1	1.3	3	2	0.17
4H-4, 0-5	34.73	Surface	0.2	0.2			
5H-4, 0-5	44.13	Middle	2.5				
6H-4, 0-5	53.63	Middle	2.4				
7H-1, 113-114	59.74	Middle	2.2				
8X-1, 0-5 ?	60.13	Middle	2.0				
9H-4, 0-5	66.43	Middle	2.2				
10X-2, 0-5	70.93	Middle	2.4				
12X-2, 0-5	87.63	Middle	2.2				
13H-2, 0-5	97.23	Middle	2.3				
15X-1, 45-50	105.48	Deep	46				
16X-3, 0-5	119.53	Deep	49				
17X-3, 128-129	128.10	Deep	50				
18X-5, 0-5	140.33	Deep	46				
19X-4, 0-5	148.43	Deep	45				
20X-4, 0-5	158.03	Deep	43				
21X-2, 0-5	164.63	Deep	44				
22X-2, 31-36	173.79	Deep	44				

Notes: In all cases the injected sample size was 5 cm^3. Concentration of gas is in ppm by volume. Where no values are reported, concentrations are below detection limits.

MST Measurements

It should be noted that MST measurements for Hole 1049A are plotted against a depth scale of 20 to 180 mbsf, whereas the measurements for Holes 1049B and 1049C are plotted against a depth scale of 0 to 160 mbsf. The differences in depth scale are to account for inaccuracies in the determination of depth to seafloor in Hole 1049A relative to Holes 1049B and 1049C (see "Operations" section, this chapter). These different depth scales aid in the visual comparison of the data sets.

GRAPE bulk density was measured on cores from all holes at Site 1049 (Fig. 26; Tables 21–23 on CD-ROM, back pocket, this volume). These data, along with magnetic susceptibility, were used in splicing the holes to form a composite Site 1049 stratigraphic section (see "Core-Core Integration" section, this chapter). These GRAPE data also have significance from a physical properties perspective.

At Site 1049, GRAPE bulk density shows a general increase in magnitude with depth below seafloor, from ~1.4 to 1.9 g/cm^3. Comparison of GRAPE bulk density with the defined lithologic units at Site 1049 (see "Lithostratigraphy" section, this chapter) highlights some features of this data set. In the upper 45 m of the sediment column (~20–55 mbsf in Hole 1049A), which corresponds to lithologic Unit I, bulk density is relatively constant at about an average of 1.45 g/cm^3. The boundary between lithologic Units I and II is represented by a sharp increase in bulk density at 45 mbsf (55 mbsf in Hole 1049A). Between 45 and 110 mbsf (55 and 125 mbsf in Hole 1049A), despite the low percentage recovery in this interval, it is apparent that bulk density shows some fluctuation about an average of 1.65 g/cm^3. This interval correlates to lithologic Unit II and the upper part of lithologic Unit III. At the K/T boundary, at ~110 mbsf in Holes 1049B and 1049C, the increase in bulk density with depth appears gradual, whereas in Hole 1049A (at 126 mbsf), this increase appears to be sharply defined. The K/T boundary itself is well defined by a negative excursion relative to general trends of GRAPE bulk density values between 1.3 and 1.4 g/cm^3. Between ~110 mbsf (125 mbsf in Hole 1049A) and total depth, bulk density values show considerable fluctuation about an approximate average of 1.7 to 2.0 g/cm^3. In Hole 1049C, the positive density spike in GRAPE bulk density labeled "Pyrite" corresponds with the early Albian black shale interval. It is impossible to distinguish the contacts between lithologic Units II and III and Units III and IV using the GRAPE bulk density data.

MST measurements of magnetic susceptibility from all holes at Site 1049 are shown in Figure 27 (also see Tables 24–26 on CD-ROM, back pocket, this volume). In the uppermost 40 m of the sediment column (above 60 mbsf in Hole 1049A), magnetic susceptibility fluctuations cannot be distinguished from background levels. Between 40 and 125 mbsf, magnetic susceptibility can be measured above background levels and shows some minor fluctuations. Within the correlative interval in Hole 1049A (between 60 and 145 mbsf), there are pronounced magnetic susceptibility "spikes" above 10^{-3} SI, which correlate either with ash or manganese-rich layers (see "Lithostratigraphy" section, this chapter). Below 120 mbsf (140 mbsf in Hole 1049A), magnetic susceptibility values show a significant increase in magnitude, $>10^{-4}$ SI units, and considerable fluctuation.

P-wave velocity data, measured with the MST *P*-wave logger on all holes drilled with the APC at Site 1049, are shown in Figure 28 (also see Tables 27–29 on CD-ROM, back pocket, this volume). This data set was edited to remove artificial and anomalous velocity values caused by section-end effects and the presence of void spaces. Despite additional scatter in this data set, which may be the result of cracking in the sediment or poor liner/sediment contact, it can be observed that *P*-wave velocity increases with depth, from ~1.40 to 1.47 km/s across the depth range 5 to 50 mbsf (20–60 mbsf in Hole 1049A). *P*-wave velocity data from 110 to 130 mbsf in Holes 1049B and 1049C, with values between 1.52 and 1.57 km/s, support the observation that *P*-wave velocity increases with depth at Site 1049.

Natural gamma-radiation counts measured on the MST for Holes 1049A and 1049C only are shown in Figure 29 (also see Tables 30, 31 on CD-ROM, back pocket, this volume). Natural gamma-radiation counts fluctuate at about background levels of 6 counts per second (cps) in the upper 40 m of the sediment column (20–60 mbsf in Hole 1049A) and increase in number with depth. The highest number of counts occurs between 120 mbsf (140 mbsf in Hole 1049A) and total depth, with a distinctive peak value of 25 cps associated with the early Albian black shale interval (see "Lithostratigraphy" section, this chapter) at ~156 mbsf in Hole 1049A and 143 mbsf in Hole 1049C.

Index Properties

Index properties were determined only for Hole 1049A. These data are listed in Table 32 and are shown in Figure 30. Index properties data primarily reflect progressive sediment compaction and fluid expulsion with depth in the sediment column. Bulk, dry, and grain density values show a steady increase with depth; porosity, water

Table 17. Elemental analyses for Holes 1049A and 1049B.

Core, section, interval (cm)	Midpoint (mbsf)	TIC (wt%)	$CaCO_3$ (wt%)	TC (wt%)	TOC (wt%)	N (wt%)	S (wt%)
171B-1049A-							
3H-2, 78.00-80.00	22.89	8.79	73.23	9.06	0.27		
3H-4, 49.00-55.00	25.62	8.93	74.36	8.95	0.02		
3H-5, 78.00-80.00	27.39	8.93	74.38	8.93	0.00		
4H-2, 78.00-79.00	32.385	8.98	74.80	9.11	0.13		
4H-3, 135.00-140.00	34.475	8.48	70.61	8.39	0.00		
4H-5, 74.00-75.00	36.845	7.98	66.51	7.93	0.00		
4H-6, 106.00-107.00	38.665	8.18	68.17	8.18	0.00		
5H-5, 77.00-78.00	46.375	8.36	69.64	8.27	0.00		
5H-6, 5.00-7.00	47.16	6.36	52.96	6.31	0.00		
6H-5, 77.00-78.00	55.875	8.34	69.47	8.75	0.41		
7H-1, 74.00-75.00	59.345	9.44	78.63	9.44	0.00		
8X-1, 9.00-10.00	60.195	9.55	79.54	9.58	0.03		
8X-1, 47.00-49.00	60.58	9.22	76.80	9.27	0.05		
9H-3, 135.00-137.00	66.26	7.86	65.51	7.85	0.00		
9H-5, 80.00-81.00	68.705	9.81	81.68	9.84	0.03		
10X-2, 78.00-79.00	71.685	9.61	80.05	9.86	0.25		
10X-3, 4.00-9.00	72.465	7.53	62.73	7.52	0.00		
10X-3, 14.00-15.00	72.545	7.90	65.77	8.00	0.10		
12X-1, 134.00-139.00	87.465	6.58	54.81	6.65	0.07		
13H-2, 78.00-79.00	97.985	4.43	36.91	4.43	0.00		
13H-3, 126.00-131.00	99.985	5.65	47.02	5.41	0.00		
16X-3, 135.00-140.00	119.375	9.12	75.94	8.87	0.00		
16X-5, 78.00-79.00	121.785	8.72	72.67	8.75	0.03		0.04
18X-3, 133.00-139.00	138.66	9.00	74.97	8.86	0.00		
18X-5, 75.00-76.00	141.055	10.69	89.03	10.39	0.00		
19X-1, 20.00-21.00	144.105	1.85	15.42	1.99	0.14	0.003	
19X-2, 23.00-24.00	145.635	2.67	22.23	2.64	0.00		
19X-3, 41.00-42.00	147.315	2.60	21.67	2.58	0.00		
19X-3, 53.00-55.00	147.44	1.71	14.26	1.55	0.00		
19X-3, 69.00-70.00	147.595	8.99	74.89	9.02	0.03		
19X-4, 107.00-108.00	149.475	2.91	24.25	2.88	0.00		
19X-5, 64.00-65.00	150.545	6.16	51.31	6.26	0.10		
20X-1, 45.00-47.00	153.96	4.46	37.18	4.25	0.00		
20X-2, 21.00-23.00	155.22	4.51	37.59	4.32	0.00		
20X-2, 51.00-53.00	155.52	3.85	32.09	3.71	0.00		
20X-2, 117.00-119.00	156.18	6.72	55.95	6.38	0.00		
20X-3, 96.00-97.00	157.465	3.66	30.52	3.57	0.00		
20X-3, 137.00-139.00	157.88	4.27	35.58	4.32	0.05		
20X-4, 21.00-23.00	158.22	2.76	22.98	2.58	0.00		
21X-2, 105.00-106.00	165.655	6.20	54.70	6.29	0.09		
21X-2, 116.00-117.00	165.765	9.97	88.04	10.06	0.09		
21X-CC, 28.00-33.00	167.515	7.08	59.01	7.17	0.09		
22X-2, 17.00-19.00	173.63	8.52	70.97	8.24	0.00		
22X-2, 27.00-29.00	173.73	9.88	82.33	9.60	0.00		
171B-1049B-							
11X-CC, 7.00-8.50	140.5525	3.56	29.66	3.64	0.08		
11X-CC, 8.50-12.50	140.5850	7.58	63.12	7.74	0.16		
11X-CC, 12.50-13.50	140.6085	6.66	55.44	8.34	1.68	0.014	
11X-CC, 13.50-16.00	140.6210	8.94	74.48	10.63	1.69	0.012	0.095
11X-CC, 16.00-17.50	140.6370	5.00	41.65	8.99	3.99	0.038	
11X-CC, 17.50-19.00	140.6515	5.97	49.76	17.42	11.45	0.16	0.62
11X-CC, 19.00-20.50	140.6665	6.15	51.20	11.54	5.39	0.085	
11X-CC, 20.50-22.00	140.6820	10.61	88.42	10.43	0.00		
Composite sample from core trim:							
11X-CC, 12.50-22.00	140.6425	6.19	51.53	9.16	2.97	0.04	

Notes: TIC = total inorganic carbon; TC = total carbon; TOC = total organic carbon computed by difference (TC – TIC). Negative TOC values are reported as 0.00. wt% = mass percent. Where no values are reported, concentrations are below detection limits.

content, and void ratio show a complementary decrease with depth. The clustering of grain density values at about 2.72 g/cm^3 below 135 mbsf is most likely related to compositional changes associated with lithologic Unit IV. Porosity values for the Eocene sediments at the seafloor are unexpectedly high, suggesting that a significant thickness of post-Eocene sediments was not deposited at Site 1049.

Comparison of discrete bulk density measurements with GRAPE bulk density for Hole 1049A (Fig. 31) shows good agreement between values generated using two distinctively different methods. Between 20 and 75 mbsf, which was drilled with the APC, the GRAPE bulk density data only slightly underestimate the true values, as obtained by discrete measurements. Below 75 mbsf, which was drilled with the XCB, the GRAPE bulk density values are lower than discrete measurements, although depth trends are still reproduced in both data sets. GRAPE bulk densities are most likely underestimates of true values because of the occurrence of void spaces, tension cracks created by sediment unloading or reduced core diameter, and the presence of slurry between drilling biscuits, which is common in the XCB cores. Figure 31 shows that GRAPE bulk density values are of considerable value even in sections where drilling techniques may result in an incompletely filled core liner.

P-wave Velocity

Discrete measurements of *P*-wave velocity were obtained on split-core sections using the Hamilton Frame velocimeter at Site 1049. These data are listed in Table 33 and are illustrated in Figure 32, which shows a composite data set from Holes 1049A and 1049B. These discrete measurements show an increase in velocity with depth that is similar to *P*-wave velocities measured with the MST PWL. Comparison of these two data sets shows that the MST PWL significantly underestimates the true values determined by discrete measurements. Figure 33 shows the expected positive relationship between *P*-wave velocity and bulk density. The lack of evidence for early diagenetic cementation near the seafloor, as shown by the high-percentage porosity (Fig. 30), suggests that the increase in *P*-wave

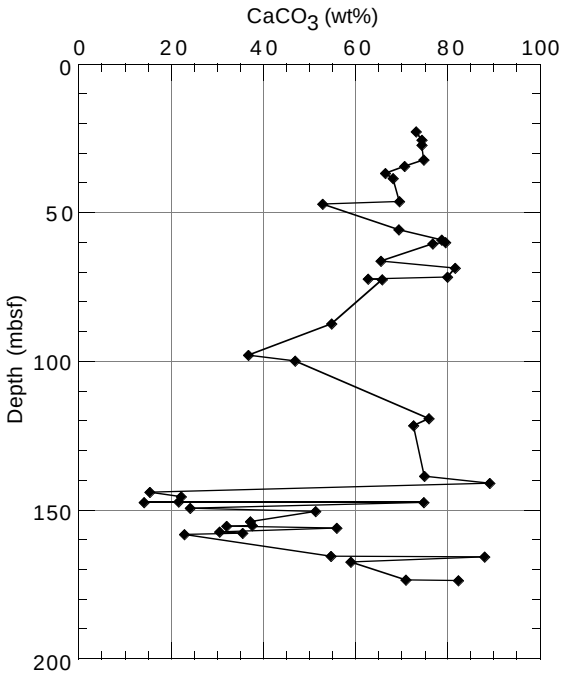

Figure 21. $CaCO_3$ content vs. sample depth midpoint in Hole 1049A. Decreases in $CaCO_3$ content are a guide to increases in clay minerals and other noncarbonate components such as silica.

velocity with depth is primarily the consequence of sediment compaction and pore-fluid expulsion.

Undrained Shear Strength

Undrained sediment shear strength was measured on sediments recovered from Hole 1049A by using the miniature vane-shear device and, when the sediment became too indurated to insert the vane-shear device, a pocket penetrometer. The shear strength data are listed in Table 34 and are shown in Figure 34. Although pocket penetrometer measurements are less accurate and less reproducible than data obtained using the vane-shear device, an increase in shear strength with depth is observed.

Normalized shear strength, the ratio of shear strength (S_u) to effective overburden pressure (P_0'), can be used to assess the stress history of a sediment column. Normalized shear strength ratios (S_u/P_0') determined for Hole 1049A are plotted against depth in Figure 35. A normally consolidated sediment has an S_u/P_0' between 0.2 and 0.22 (Ladd et al., 1977). Sediments below 60 mbsf in Hole 1049A have $S_u/P_0' < 0.2$, indicating that these sediments are underconsolidated. Such an underconsolidated state could have been maintained by the existence of excessive pore-fluid pressure within this interval in the sediment column. Chert stringers that occur in Hole 1049A between 60 and 80 mbsf (see "Lithostratigraphy" section, this chapter) may be responsible for maintaining elevated pore-fluid pressure below 60 mbsf. The peak S_u/P_0' at ~40 mbsf suggests that the middle Eocene sediments at this depth may have reached an overcompacted state from the accumulation of younger overburden, which has subsequently been removed by erosion. Assuming that the sediment at 40 mbsf was normally consolidated at maximum overburden pressure and that no changes in shear strength have occurred, estimation of the overburden thickness suggests that 75 m of sediment may have accumulated and been removed from above Hole 1049A between the Eocene and the present. The peak S_u/P_0' at 40 mbsf also coincides with a peak in sediment bulk density at ~45 mbsf, as shown in Figure 31.

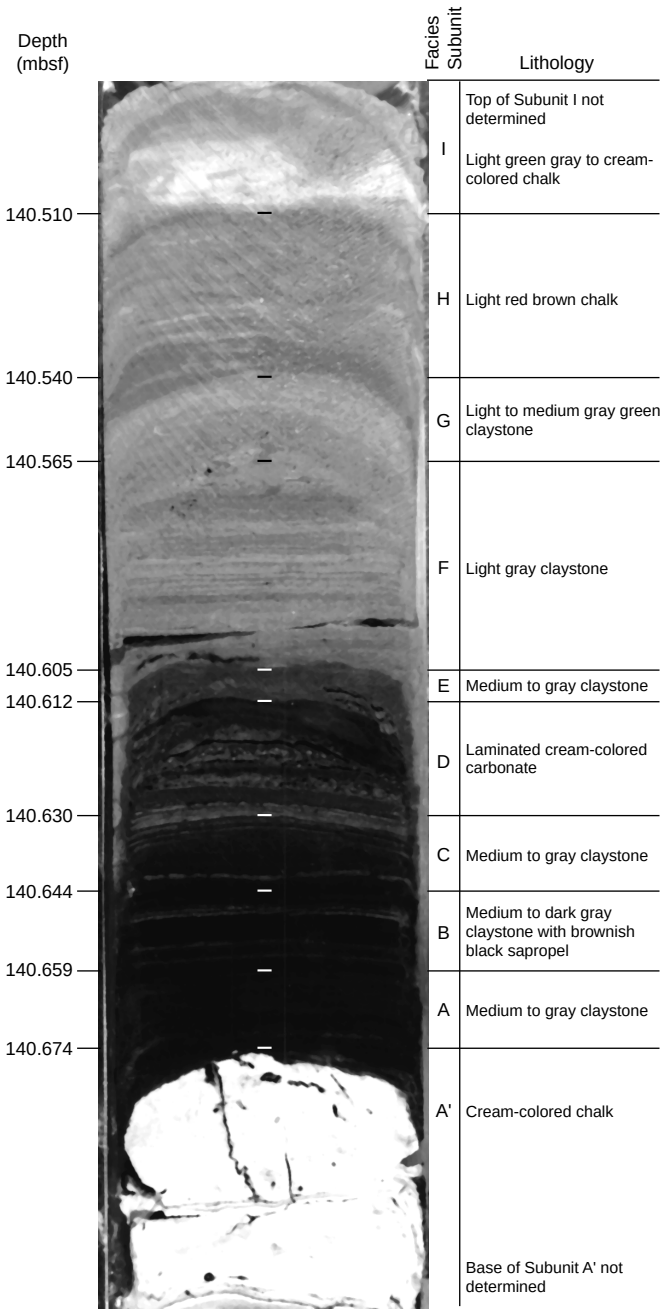

Figure 22. Section 171B-1049B-11X-CC, 0–36 cm (140.47–140.83 mbsf). Descriptions of the facies subunits are given in Table 18.

Resistivity

The resistivity data from Hole 1049A, measured using the Scripps Institution of Oceanography probe, are listed in Table 35 and are shown in Figure 36. Resistivity remains relatively constant at ~0.4 Ωm in the upper 70 m of the sediment column and increases to ~0.9 Ωm below 120 mbsf. Figure 37 illustrates the negative correlation between sediment resistivity and sediment porosity.

Table 18. Description of kerogen-rich and selected kerogen-lean subfacies units in Section 171B-1049B-11X-CC, 0 to 36 cm.

Depth of subunit top (mbsf)	Facies subunit	Organic facies	Lithologic description
	I	Barren	Chalk, light green gray to cream. Massive looking. Upper contact undulatory. Top of subunit not determined.
140.510	H	Barren	Chalk, light red-brown. Locally contains laminae of light green-gray claystone. Upper contact sharp.
140.540	G	Barren	Claystone, light to medium gray-green. Thinly bedded. Upper contact sharp.
140.565	F	Barren	Claystone, light gray. Interbeds of light brown to cream-colored carbonate laminae. Proportion of carbonate laminae increases toward the top. Upper contact sharp.
140.605	E	Low II	Claystone, medium gray. Increasing cream-colored carbonate laminae toward bottom of subunit. Upper contact sharp.
140.612	D	Low II	Carbonate, cream, laminated. Interbedded with thin laminae of medium gray claystone. Upper contact sharp.
140.630	C	Moderate II	Claystone, medium gray. Laminated. Upper contact sharp.
140.644	B	Moderate II	Claystone, medium to dark gray with brownish black sapropel. Laminated to 2- to 3-mm-thick bands. Proportion of sapropel increases toward the top. Upper contact sharp.
140.659	A	High I-s	Claystone, medium gray. Contains a few black, cream, and light brown colored laminae. Upper contact sharp.
140.674	A′	Barren	Chalk, cream colored. Massive. Upper contact sharp. Base of subunit not determined.

Notes: Section depth from 140.47 to 140.83 mbsf. The term subfacies refers to lithologically similar strata that were sampled from the black shale facies. The assignment of organic facies is assessed based on TOC content, kerogen type, and if the kerogen sulfur content is significant.

Table 19. Rock-Eval analyses for an early Albian-aged black shale cored just below 140 mbsf in Hole 1049B.

Facies (subunit)	Core, section, interval (cm)	Depth (sample midpoint, mbsf)	T_{max} (°C)	S_1 (mg HC/g rock)	S_2 (mg HC/g rock)	$S_1 + S_2$ (mg HC/g rock)	S_3 (mg CO_2/g rock)	PI	HC Index (S_2/S_3)	PC	TOC (wt%)	HI (mg HC/g TOC)	OI (mg CO_2/g TOC)
	171B-1049B-												
A′	11X-CC, 20.50-22.00	140.6820	445	0.03	0.8	0.8	0.61	0.04	1.3	0.06	0.06		1016
A	11X-CC, 19.00-20.50	140.6665	407	0.26	20.6	20.3	3.24	0.01	6.4	1.74	4.57	451	70
B	11X-CC, 17.50-19.00	140.6515	393	1.35	70.9	72.3	4.63	0.02	15.3	6.02	10.14	699	45
C	11X-CC, 16.00-17.50	140.6370	406	0.18	15.6	15.7	2.55	0.01	6.1	1.31	3.2	485	79
D	11X-CC, 13.50-16.00	140.6210	395	0.1	8.4	8.5	1.19	0.01	7.1	0.7	1.39	605	85
E	11X-CC, 12.50-13.50	140.6085	403	0.08	6.6	6.7	1.86	0.01	3.6	0.55	1.22	543	152
F	11X-CC, 8.50-12.50	140.5850	410	0	0.04	0.04	1.34	0	0.02	0	0.08	50	1675
G	11X-CC, 7.00-8.50	140.5525	413	0.02	0.1	0.1	1.92	0.25	0	0	0		
Composite:													
Subunit A to F (core trim)		140.6425	409	0.1	11.5		2.93	0.01	3.9	0.96	2.39	482	122
Chalk sample:													
171B-1049B-6H-5, 77-78 cm		55.85		0.01	0	0	0.81	0	0	0	0		
Statistics for facies Subunits A to E (samples with TOC >0.5 wt%):													
Minimum			393	0.1	6.6	6.71	1.2	0	3.56	0.55	1.22	451	45
Maximum			407	1.4	70.9	72.3	4.6	0	15.31	6.02	10.14	699	152
Mean			400.8	0.4	24.4	24.71	2.7	0	7.68	2.06	4.2	556	86
Standard deviation			6.42	0.5	26.6	27.16	1.3	0	4.47	2.26	3	9840	

Notes: The definitions of the reported values are given in the "Explanatory Notes" chapter (this volume). Blanks indicate that no value was reported from the Rock-Eval analysis.

Thermal Conductivity

Thermal conductivity data from Hole 1049A, obtained using the Thermcon-85, are listed in Table 36 and are shown in Figure 38. Average thermal conductivity for the 21 data points is 1.10 W/(m·K), with a standard deviation of 0.27. Thermal conductivity measurements for Hole 1049A display a large degree of scatter, although there may be a small increase in thermal conductivity with depth, as would be expected with a decrease in porosity. The randomness within this data set may be attributed to the insertion of different probes either into drilling slurry or drilling biscuits in the XCB-cored interval, which would result in inconsistent measurements. It is also possible that the anomalous measurements may be an artifact of temperamental Thermcon-85 needle probes, although no specific bias was observed for any specific probe.

Summary

Physical properties data at Site 1049 show variation with depth below seafloor that suggests progressive compaction and fluid expulsion as the dominant controlling factors. Large offsets in certain physical properties data, such as GRAPE bulk density, indicate that the dominant controls are also influenced by lithologic changes in the sediment column. The unexpectedly high-percentage porosity indicates that these sediments have little cementation and, hence, are valuable for paleoceanographic studies.

REFERENCES

Aubry, M.-P., 1995. From chronology to stratigraphy: interpreting the lower and middle Eocene stratigraphic record in the Atlantic Ocean. *In* Berggren, W.A., Kent, D.V., Aubry, M.-P., and Hardenbol, J. (Eds.), *Geochronology, Time Scales, and Global Stratigraphic Correlation: A Unified Temporal Framework for an Historical Geology.* Spec. Publ.—Soc. Econ. Palaeontol. Mineral., 54:213–274.

Berggren, W.A., Kent, D.V., Swisher, C.C., III, and Aubry, M.-P., 1995. A revised Cenozoic geochronology and chronostratigraphy. *In* Berggren, W.A., Kent, D.V., Aubry, M.-P., and Hardenbol, J. (Eds.), *Geochronology, Time Scales and Global Stratigraphic Correlation*. Spec. Publ.—Soc. Econ. Paleontol. Mineral., 54:129–212.

Cardoso, J.N., Wardroper, A.M.K., Watts, C.D., Barnes, J.R., Maxwell, J.R., Eglinton, G., Mound, D.G., and Speers, G.C., 1978. Preliminary organic geochemical analyses, Site 391, Leg 44 of the Deep Sea Drilling Project. *In* Benson, W.E., and Sheridan, R.E, et al., *Init. Repts. DSDP,* 44: Washington (U.S. Govt. Printing Office), 617–624.

Curry, W.B., Shackleton, N.J., Richter, C., et al., 1995. *Proc. ODP, Init. Repts.*, 154: College Station, TX (Ocean Drilling Program).

de Graciansky, P., Brosse, E., Deroo, G., Herbin, J.-P., Montadert, L., Müller, C., Sigal, J., and Schaaf, A., 1987. Organic-rich sediments and palaeoenvironmental reconstructions of the Cretaceous North Atlantic. *In* Brooks, J., and Fleet, A.J. (Eds.), *Marine Petroleum Source Rocks.* Geol. Soc. Spec. Publ. London, 26:317–344.

Dow, W.G., 1978. Geochemical analysis of samples from holes 391A and 391C, Leg 44, Blake-Bahama Basin. *In* Benson, W.E., and Sheridan, R.E, et al., *Init. Repts. DSDP,* 44: Washington (U.S. Govt. Printing Office), 625–634.

Emeis, K.-C., and Kvenvolden, K.A., 1986. Shipboard organic geochemistry on *JOIDES Resolution. ODP Tech. Note*, 7.

Erdman, J.G., and Schorno, K.S., 1978. Geochemistry of carbon: Deep Sea Drilling Project Leg 44. *In* Benson, W.E., and Sheridan, R.E., et al., *Init. Repts. DSDP,* 44: Washington (U.S. Govt. Printing Office), 605–615.

Gradstein, F.M., Agterberg, F.P., Ogg, J.G., Hardenbol, J., van Veen, P., Thierry, J., and Huang, Z., 1995. A Triassic, Jurassic and Cretaceous time scale. *In* Berggren, W.A., Kent, D.V., and Aubry, M.P. (Eds.), *Geochronology, Time Scales and Global Stratigraphic Correlation.* Spec. Publ.—Soc. Econ. Paleontol. Mineral., 54:95–128.

Herbin, J.P., Deroo, G., Roucaché, J., 1983. Organic geochemistry in the Mesozoic and Cenozoic formations of Site 534, Leg 76, Blake Bahama Basin, and comparison with Site 391, Leg 44. *In* Sheridan, R.E., and Gradstein, F.M., et al., *Init. Repts. DSDP,* 76: Washington (U.S. Govt. Printing Office), 481–493.

Katz, B.K., 1983. Organic geochemical character of some Deep Sea Drilling Project cores from Legs 76 and 44. *In* Sheridan, R.E., Gradstein, F.M., et al., *Init. Repts. DSDP,* 76: Washington (U.S. Govt. Printing Office), 463–468.

Kendrick, J.W., Hood, A., and Castano, J.R., 1978. Petroleum-generating potential of sediments from Leg 44, Deep Sea Drilling Project. *In* Benson, W.E., and Sheridan, R.E., et al., *Init. Repts. DSDP,* 44: Washington (U.S. Govt. Printing Office), 599–603.

Ladd, C.C., Foott, R., Ishihara, K., Schlosser, F., and Poulos, H.G., 1977. Stress-deformation and strength characteristics: state-of-the-art report. *Proc. 9th Int. Conf. Soil Mech. and Found. Eng.,* Tokyo, 2:421–482.

Langford, F.F., and Blanc-Valleron, M.M., 1990. Interpreting Rock-Eval pyrolysis data using graphs of pyrolizable hydrocarbons vs. total organic carbon. *AAPG Bull.*, 74:799–804.

Riedel, W.R., and Sanfilippo, A., 1978. Stratigraphy and evolution of tropical Cenozoic radiolarians. *Micropaleontology,* 24:61–96.

Ryan, W.B.F., Bolli, H.M., Foss, G.N., Natland, J.H., Hottman, W.E., and Foresman, J.B., 1978. Objectives, principle results, operations, and explanatory notes of Leg 40, South Atlantic. *In* Bolli, H.M., Ryan, W.B.F., et al., *Init. Repts. DSDP,* 40: Washington (U.S. Govt. Printing Office), 5–26.

Shipboard Scientific Party, 1978. Sites 389 and 390: North rim of Blake Nose. *In* Benson, W.E., Sheridan, R.E., et al., *Init. Repts. DSDP,* 44: Washington (U.S. Govt. Printing Office), 69–151.

Summerhayes, C.P., 1987. Organic-rich Cretaceous sediments from the North Atlantic. *In* Brooks, J., and Fleet, A.J. (Eds.), *Marine Petroleum Source Rocks.* Geol. Soc. Spec. Publ. London, 26:301–316.

Summerhayes, C.P., and Masran, T.C., 1983. Organic facies of Cretaceous and Jurassic sediments from Deep Sea Drilling Project Site 534 in the Blake Bahama Basin, Western North Atlantic. *In* Sheridan, R.E., and Gradstein, F.M., et al., *Init. Repts. DSDP,* 76: Washington (U.S. Govt. Printing Office), 469–480.

Tjalsma, R.C., and Lohmann, G.P., 1983. Paleocene-Eocene bathyal and abyssal benthic foraminifera from the Atlantic Ocean. *Micropaleontol. Spec. Publ.,* 4.

Tyson, R.V., 1987. The genesis and palynofacies characteristics of marine petroleum source rocks. *In* Brooks, J., and Fleet, A.J. (Eds.), *Marine Petroleum Source Rocks.* Geol. Soc. Spec. Publ. London, 26:7–67.

Tyson, R.V., 1995. *Sedimentary Organic Matter: Organic Facies and Palynofacies:* London (Chapman & Hall).

van Morkhoven, F.P.C.M., Berggren, W.A., and Edwards, A.S., 1986. Cenozoic cosmopolitan deep-water benthic foraminifera. *Bull. Cent. Rech. Explor.—Prod. Elf-Aquitaine,* Mem. 11.

Weaver, F.R., and Dinkleman, M.G., 1978. Cenozoic radiolarians from the Blake Plateau and the Blake-Bahama Basin, DSDP Leg 44. *In* Benson, W.E., Sheridan, R.E., et al., *Init. Repts. DSDP,* 44: Washington (U.S. Govt. Printing Office), 865–885.

Widmark, J.G.V., 1995. Multiple deep-water sources and trophic regimes in the latest Cretaceous deep sea: evidence from benthic foraminifers. *Mar. Micropaleontol.*, 26:361–384.

Widmark, J.G.V., and Speijer, R.P, in press. Benthic foraminiferal ecomarker species of the terminal Cretaceous deep-sea Tethys. *Mar. Micropaleontol.*

Ms 171BIR-103

NOTE: Core-description forms ("barrel sheets") and core photographs can be found in Section 4, beginning on page 363. Forms containing smear-slide data can be found on CD-ROM, back pocket, this volume. See Table of Contents for material contained on CD-ROM.

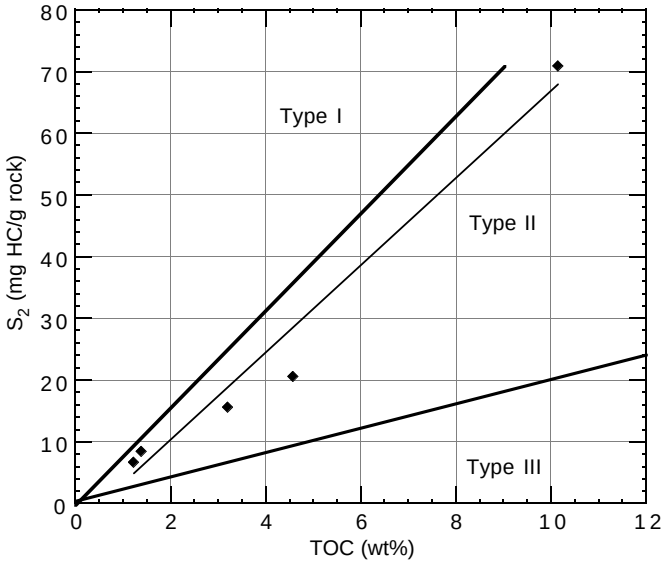

Figure 23. Rock-Eval analysis S_2 vs. TOC for interpreting kerogen type at Hole 1049B. The thick lines indicate the boundaries between kerogen types as proposed by Langford and Blanc-Valleron (1990). See text for discussion of the correlation between TOC and S_2. The thin line is a linear curve fit of the variables, with a correlation coefficient of 0.97.

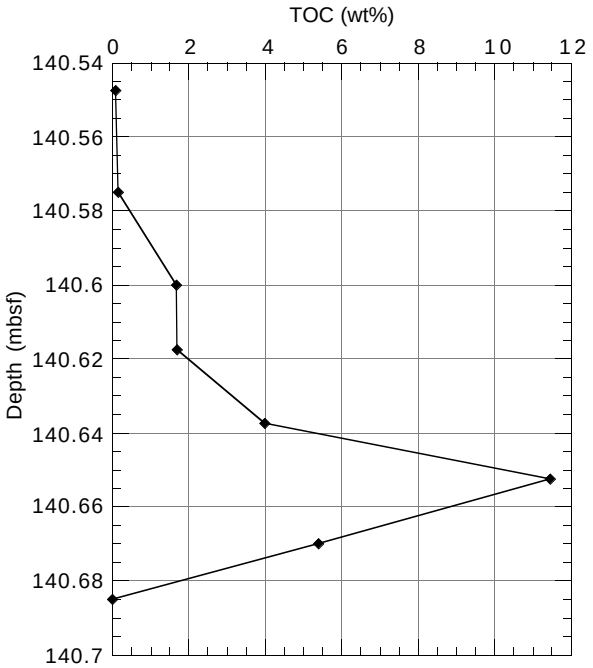

Figure 24. TOC vs. sample depth in Hole 1049B. TOC values are given in Table 17.

Table 20. Interstitial-water geochemical data for Hole 1049A.

Core, section, interval (cm)	Depth (mbsf)	pH	Alkalinity (mM)	Salinity (g/kg)	Cl (mM)	Na (mM)	Mg (mM)	Ca (mM)	SO_4 (mM)	NH_4 (µM)	H_4SiO_4 (µM)	K (mM)	Sr (µM)	Li (µM)	Rb (µM)	B (µM)
171B-1049A-																
3H-3, 145-150	23.05	7.63	2.42	36.0	561	477	54.15	10.66	28.4	10	546	13.4	85	29	2.09	499
4H-3, 145-150	34.55	7.61	2.47	36.0	557	474	53.45	10.95	27.6	32	728	12.0	87	27	1.95	531
5H-3, 145-150	44.05	7.57	2.54	36.5	555	474	52.67	11.16	28.3	32	807	12.3	87	28	2.03	459
6H-3, 145-150	53.55	7.52	2.58	36.5	554	474	52.71	11.61	28.8	28	681	11.7	88	30	2.01	491
9H-3, 145-150	66.35	7.65	2.84	35.5	557	476	52.00	12.32	28.5	14	743	11.7	94	28	1.99	475
10X-3, 145-150	70.85	7.63	2.70	35.5	553	472	51.85	12.38	28.1	21	757	11.5	97	31	2.01	499
12X-1, 145-150	87.55	7.58	2.74	35.3	553	470	49.85	13.09	27.5	17	937	14.7	93	33	2.36	507
16X-1, 145-150	117.95	7.58	2.79	35.0	547	465	47.63	14.50	26.0	25	549	12.9	99	33	2.08	675
19X-3, 145-150	148.35	7.56	2.73	36.5	549	470	45.79	16.02	26.6	28	148	11.8	100	37	2.00	834
22X-1, 70-75	173.40			35.5	548		47.18	16.57	28.3	38	134	11.3	100	30	2.07	611

Notes: Insufficient water was recovered from the sample in Core 171B-1049A-22X to determine pH and alkalinity and, therefore, sodium (by charge balance). Where no values are reported, data are absent.

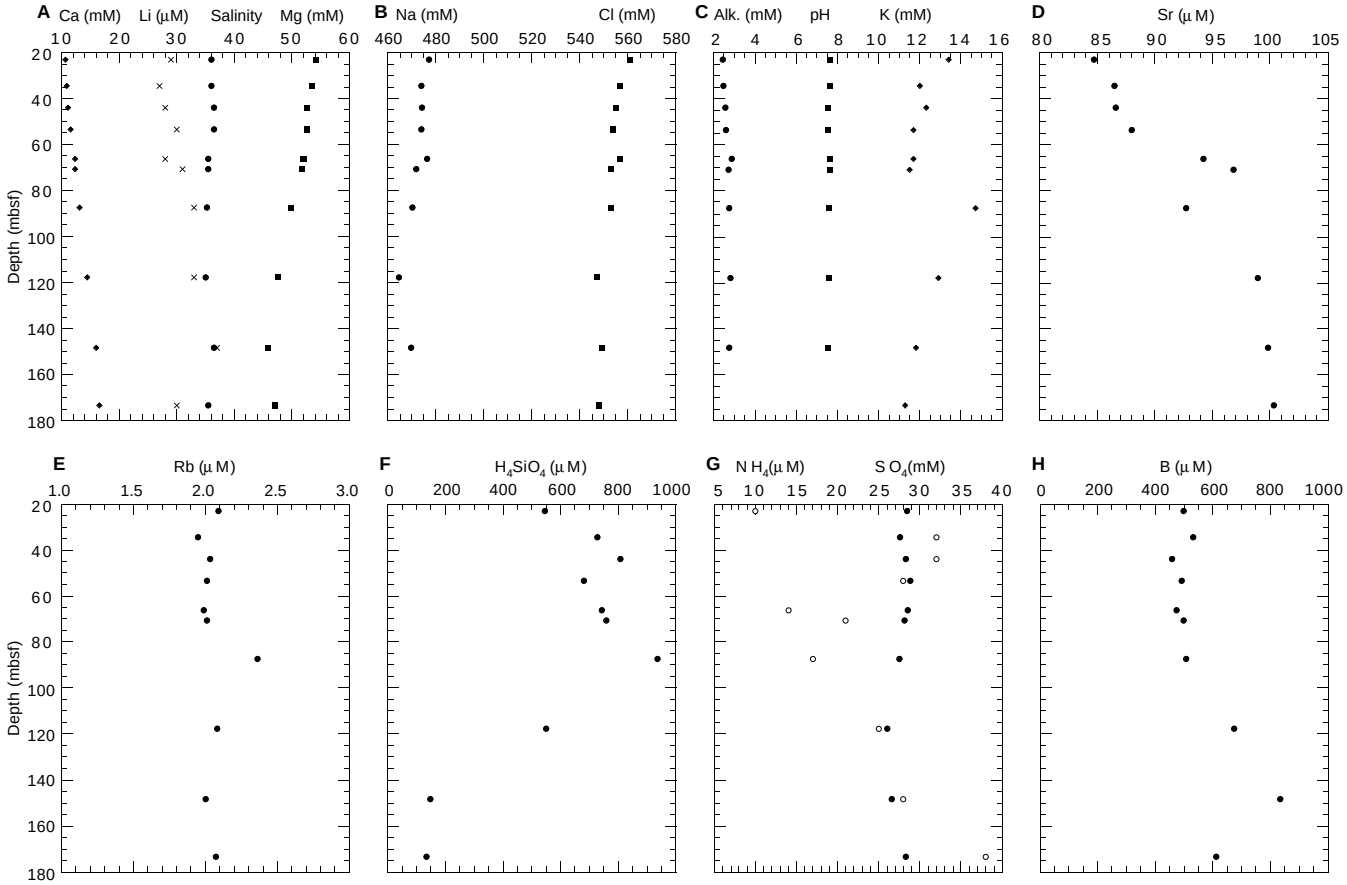

Figure 25. Interstitial-water geochemical data for Hole 1049A vs. depth. **A.** Calcium, lithium, salinity, and magnesium. **B.** Sodium and chloride. **C.** Alkalinity, pH, and potassium. **D.** Strontium. **E.** Rubidium. **F.** Silica. **G.** Ammonium and sulfate. **H.** Boron.

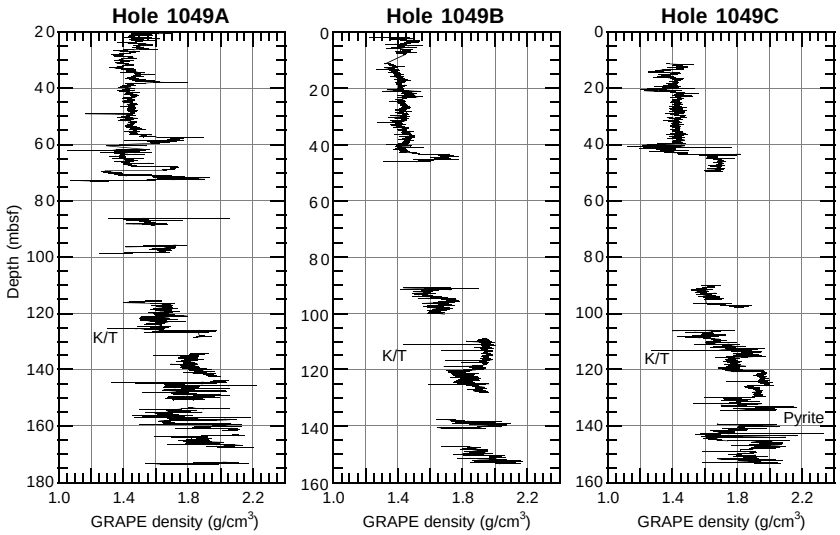

Figure 26. GRAPE bulk density for Holes 1049A, 1049B, and 1049C (see Tables 21–23 [CD-ROM, back pocket, this volume] for data). See text for discussion of the different depth scales.

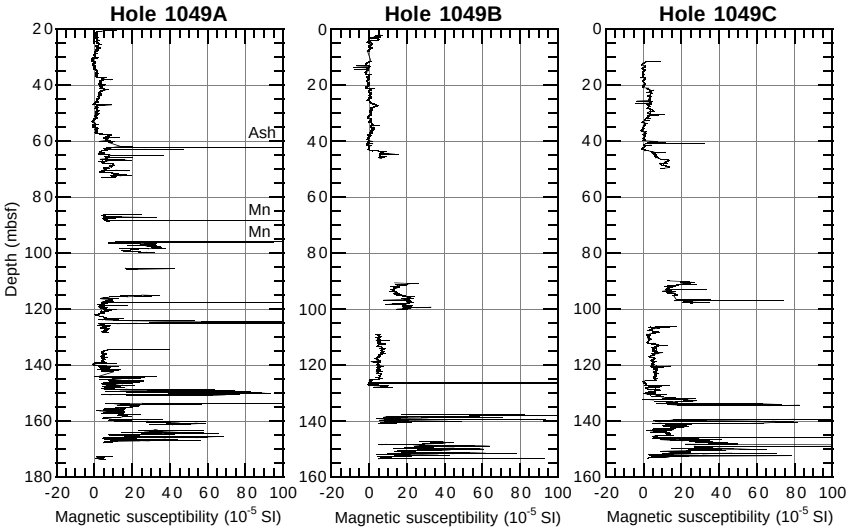

Figure 27. Magnetic susceptibility for Holes 1049A, 1049B, and 1049C (see Tables 24–26 [CD-ROM, back pocket, this volume] for data). See text for discussion of the different depth scales.

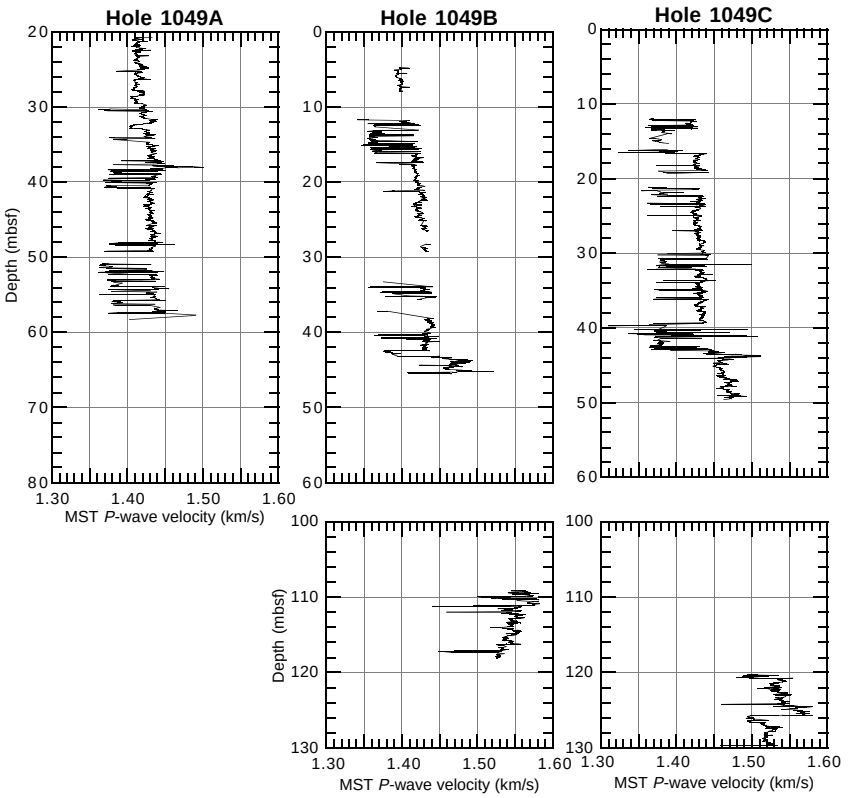

Figure 28. MST *P*-wave velocity for Holes 1049A, 1049B, and 1049C (see Tables 27–29 [CD-ROM, back pocket, this volume] for data). *P*-wave velocity was measured on APC cores only. See text for discussion of the different depth scales.

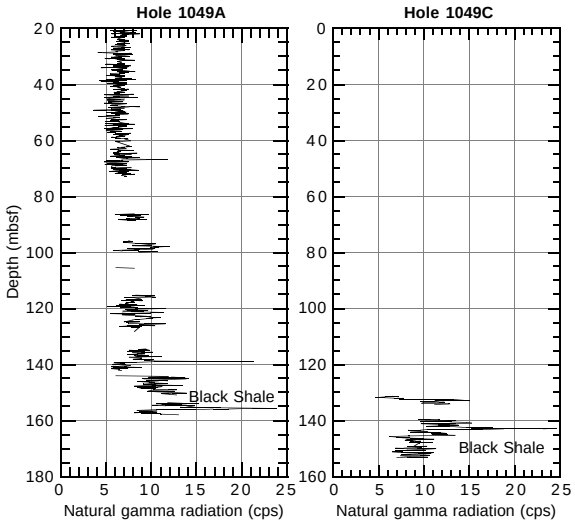

Figure 29. Natural gamma radiation for Holes 1049A and 1049C (see Tables 30, 31 [CD-ROM, back pocket, this volume] for data). See text for discussion of the different depth scales.

Table 32. Discrete index properties measurements for Hole 1049A.

Core, section, interval (cm)	Depth (mbsf)	Water content (total mass wt%)	Water content (solid mass wt%)	Bulk density (g/cm^3)	Grain density (g/cm^3)	Dry density (g/cm^3)	Porosity (%)	Void ratio
171B-1049A-								
3H-1, 75-77	21.35	47.2	89.4	1.51	2.65	0.80	69.8	2.31
3H-2, 75-77	22.85	48.2	93.0	1.50	2.66	0.78	70.7	2.42
3H-3, 75-77	24.35	45.0	81.8	1.55	2.67	0.85	68.1	2.13
3H-4, 75-77	25.85	47.0	88.4	1.52	2.65	0.81	69.6	2.29
3H-5, 75-77	27.35	50.0	99.9	1.48	2.67	0.74	72.3	2.61
3H-6, 75-77	28.85	52.5	110.5	1.45	2.65	0.69	74.1	2.86
4H-1, 74-76	30.84	52.7	111.3	1.43	2.56	0.68	73.5	2.78
4H-2, 75-77	32.35	55.1	122.7	1.42	2.66	0.64	76.1	3.19
4H-3, 74-76	33.84	48.5	94.0	1.48	2.56	0.76	70.2	2.36
4H-4, 75-77	35.35	45.8	84.3	1.53	2.62	0.83	68.3	2.15
4H-5, 71-73	36.81	48.5	94.0	1.48	2.57	0.76	70.2	2.36
4H-6, 75-77	38.35	46.9	88.3	1.51	2.62	0.80	69.3	2.26
5H-1, 75-77	40.35	49.1	96.4	1.47	2.56	0.75	70.6	2.41
5H-2, 75-77	41.85	49.9	99.5	1.46	2.55	0.73	71.3	2.48
5H-3, 75-77	43.35	43.6	77.5	1.54	2.54	0.87	65.8	1.92
5H-4, 75-77	44.85	52.6	111.0	1.43	2.53	0.68	73.3	2.75
5H-5, 77-79	46.37	46.3	86.3	1.51	2.57	0.81	68.4	2.16
5H-6, 75-77	47.85	48.7	95.1	1.48	2.57	0.76	70.4	2.38
6H-1, 77-79	49.87	49.1	96.6	1.48	2.59	0.75	70.9	2.44
6H-2, 75-77	51.35	49.6	98.5	1.47	2.58	0.74	71.3	2.48
6H-3, 75-77	52.85	48.7	95.0	1.48	2.54	0.76	70.2	2.36
6H-4, 75-77	54.35	47.0	88.8	1.50	2.57	0.80	69.0	2.23
6H-5, 75-77	55.85	47.0	88.9	1.50	2.58	0.80	69.1	2.24
6H-6, 75-77	57.35	43.5	77.1	1.56	2.61	0.88	66.2	1.96
7H-1, 77-79	59.37	39.4	64.9	1.64	2.67	0.99	62.9	1.69
9H-1, 75-77	62.65	50.2	100.8	1.46	2.57	0.73	71.6	2.53
9H-2, 75-77	64.15	53.5	115.1	1.42	2.56	0.66	74.2	2.88
9H-3, 77-79	65.67	49.4	97.5	1.47	2.58	0.75	71.0	2.45
9H-4, 75-77	67.15	50.5	102.0	1.45	2.54	0.72	71.6	2.53
9H-5, 76-78	68.66	35.7	55.4	1.70	2.68	1.09	59.2	1.45
10X-1, 66-68	70.06	52.2	109.0	1.44	2.57	0.69	73.2	2.73
10X-2, 75-77	71.65	37.6	60.3	1.67	2.69	1.04	61.3	1.58
12X-1, 72-74	86.82	40.6	68.3	1.61	2.64	0.96	63.7	1.76
12X-2, 73-75	88.33	37.2	59.2	1.68	2.70	1.06	61.0	1.56
13H-1, 93-95	96.63	36.0	56.1	1.68	2.64	1.08	59.1	1.45
13H-2, 75-77	97.95	40.0	66.6	1.61	2.61	0.97	62.9	1.70
15X-1, 41-43	105.71	31.9	46.8	1.76	2.66	1.20	54.8	1.21
16X-1, 68-70	115.68	31.1	45.1	1.78	2.68	1.23	54.2	1.18
16X-2, 75-77	117.25	29.4	41.7	1.82	2.68	1.28	52.2	1.09
16X-3, 74-76	118.74	32.8	48.9	1.76	2.70	1.18	56.3	1.29
16X-4, 71-73	120.21	35.8	55.6	1.71	2.72	1.10	59.7	1.48
16X-5, 75-77	121.75	30.3	43.4	1.81	2.72	1.26	53.5	1.15
18X-2, 85-87	136.65	24.2	31.9	1.94	2.71	1.47	45.8	0.84
18X-3, 85-87	138.15	23.6	30.9	1.95	2.71	1.49	45.0	0.82
18X-4, 87-89	139.67	28.2	39.3	1.85	2.71	1.33	51.0	1.04
18X-5, 78-80	141.08	26.1	35.2	1.90	2.72	1.41	48.3	0.94
19X-1, 64-66	144.54	29.6	42.1	1.83	2.74	1.29	53.0	1.13
19X-2, 75-77	146.15	22.0	28.2	1.99	2.72	1.56	42.8	0.75
19X-3, 51-53	147.41	27.1	37.3	1.88	2.74	1.37	49.9	1.00
19X-4, 75-77	149.15	23.0	29.8	1.97	2.73	1.52	44.3	0.79
19X-5, 15-17	150.05	27.2	37.4	1.88	2.74	1.37	50.0	1.00
20X-1, 81-83	154.31	27.4	37.7	1.88	2.74	1.37	50.2	1.01
20X-2, 41-43	155.41	28.1	39.2	1.86	2.73	1.34	51.1	1.05
20X-3, 98-100	157.48	29.3	41.5	1.83	2.72	1.29	52.4	1.10
20X-4, 39-41	158.39	26.4	35.9	1.89	2.71	1.39	48.8	0.95
20X-5, 78-80	160.28	21.2	26.9	2.02	2.73	1.59	41.7	0.72
21X-1, 75-77	163.85	20.5	25.7	2.02	2.70	1.61	40.4	0.68
21X-2, 75-77	165.35	21.3	27.1	2.01	2.72	1.58	41.8	0.72
21X-3, 75-77	166.85	22.7	29.4	1.98	2.72	1.53	43.9	0.78

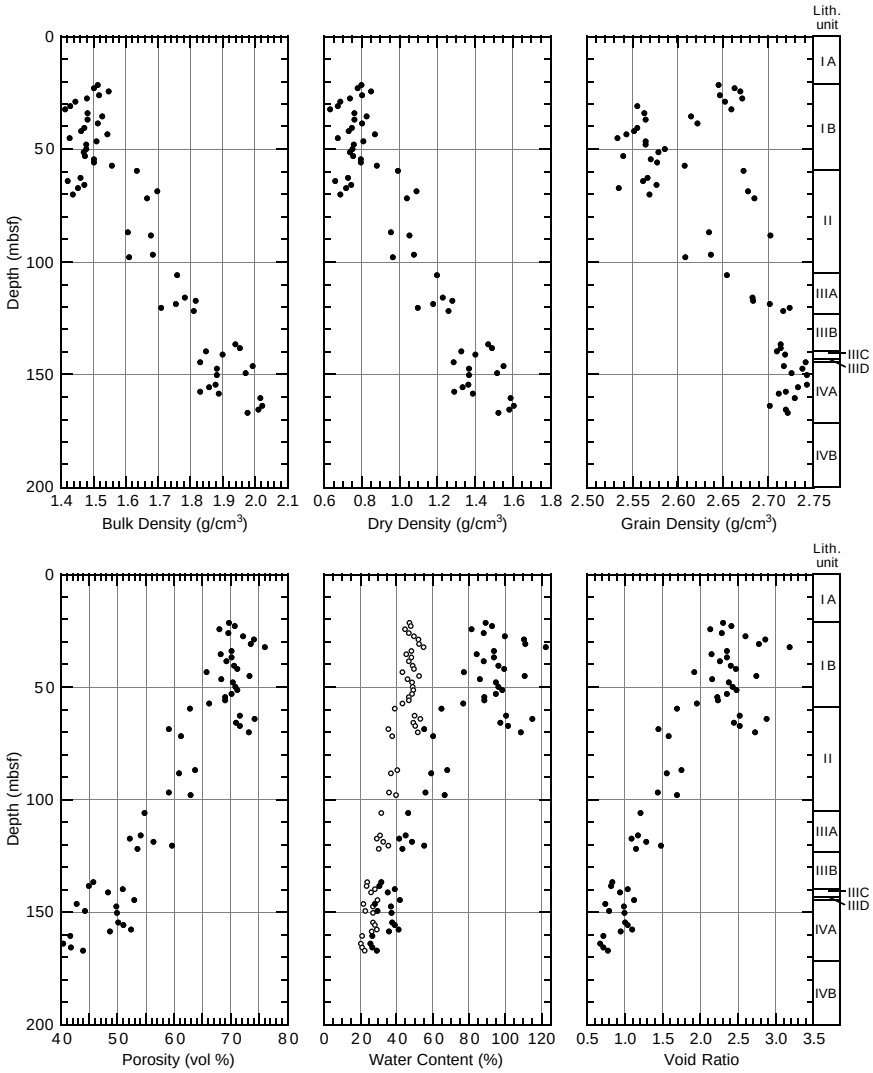

Figure 30. Discrete measurements of bulk density, dry density, grain density, porosity, water content, and void ratio for Hole 1049A. In the water content plot, open circles = values expressed in terms of total mass; solid circles = values expressed in terms of the total mass of solids.

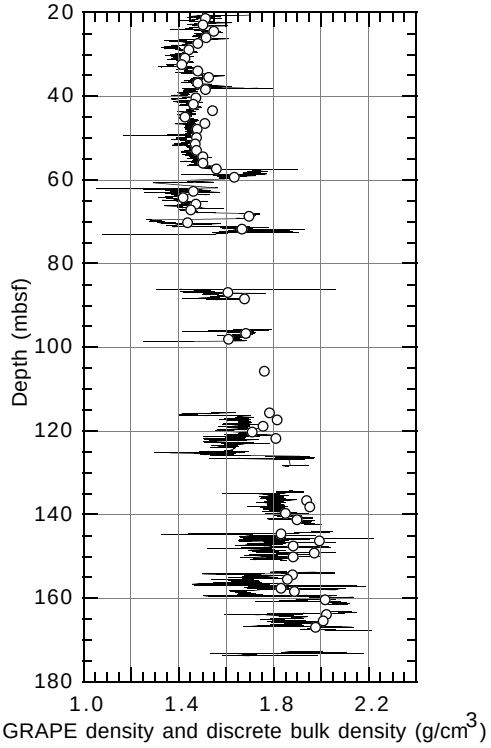

Figure 31. Comparison of GRAPE bulk density (line) with discrete measurements of bulk density (open circles) for Hole 1049A.

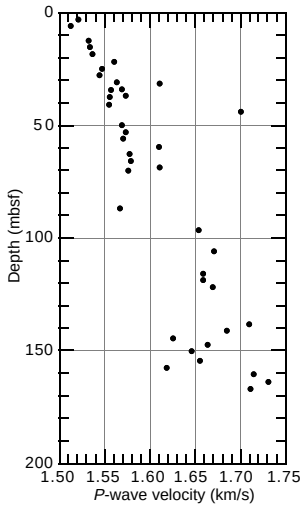

Figure 32. Composite plot of discrete *P*-wave velocity using data from Holes 1049A and 1049B.

Table 33. Discrete measurements of uncorrected transverse *P*-wave velocity for Site 1049.

Core, section, interval (cm)	Depth (mbsf)	Transverse *P*-wave velocity (km/s)
171B-1049A-		
4H-1, 74-76	30.84	1.564
4H-3, 74-76	33.84	1.569
4H-5, 71.1-73.1	36.81	1.573
6H-1, 74-76	49.84	1.569
6H-3, 74-76	52.84	1.574
6H-5, 74-76	55.84	1.571
7H-1, 74-76	59.34	1.611
9H-1, 71-73	62.61	1.578
9H-3, 74-76	65.64	1.579
9H-5, 74-76	68.64	1.611
10X-1, 64-66	70.04	1.576
12X-1, 74-76	86.84	1.567
13H-1, 70.6-72.6	96.41	1.654
15X-1, 42.6-44.6	105.73	1.671
19X-1, 64.3-66.3	144.54	1.626
19X-3, 50.8-52.8	147.41	1.664
19X-5, 15.7-17.7	150.06	1.647
20X-1, 80.8-82.8	154.31	1.655
20X-5, 79-81	160.29	1.715
20X-3, 98.6-100.6	157.49	1.619
16X-1, 70.9-72.9	115.71	1.659
16X-3, 74-76	118.74	1.659
16X-5, 79.1-81.1	121.79	1.669
18X-3, 74-76	138.04	1.710
18X-5, 74-76	141.04	1.685
21X-1, 74-76	163.84	1.731
21X-3, 74-76	166.84	1.712
171B-1049B-		
1H-1, 79-81	2.79	1.522
1H-3, 74-76	5.74	1.513
2H-1, 74-76	12.24	1.533
2H-3, 74-76	15.24	1.534
2H-5, 74-76	18.24	1.537
3H-1, 74-76	21.74	1.561
3H-3, 74-76	24.74	1.548
3H-5, 74-76	27.74	1.545
4H-1, 74-76	31.24	1.611
4H-3, 74-76	34.24	1.557
4H-5, 74-76	37.24	1.556
5H-1, 74-76	40.74	1.556
5H-3, 74-76	43.74	1.701

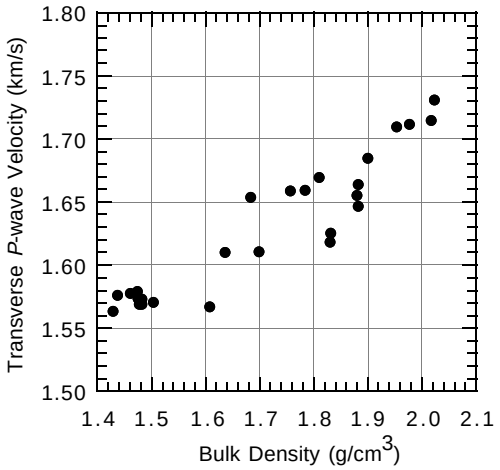

Figure 33. Comparison of discrete *P*-wave velocity and discrete bulk density for Hole 1049A. The *P*-wave velocity values are uncorrected for in situ pressure and temperature conditions (r^2 = 0.880).

Table 34. Discrete measurements of shear strength for Hole 1049A.

Core, section, interval (cm)	Depth (mbsf)	Peak (kPa)	Residual (kPa)	Penetrometer (kPa)
171B-1049A-				
3H-1, 74.5-75.5	21.35	14.18		
3H-3, 74.5-75.5	24.35	15.36	8.25	
3H-5, 34.5-35.5	26.95	20.78	8.03	
4H-1, 71.4-72.4	30.81	29.75	9.42	
4H-3, 71.7-72.7	33.82	33.19	15.16	
4H-5, 68.2-69.2	36.78	46.50	24.18	
5H-1, 71.7-72.7	40.32	55.09	26.92	
5H-3, 71-72	43.31	58.15	26.65	
5H-5, 71.9-72.9	46.32	68.12		
6H-1, 74.5-75.5	49.85	41.14	17.69	
6H-3, 74.5-75.5	52.85	36.85	12.16	
6H-5, 74.5-75.5	55.85	47.55	23.14	
7H-1, 74.8-75.8	59.35	95.17	29.19	
9H-1, 71.5-72.5	62.62	26.92	10.59	
9H-3, 74.5-75.5	65.65	47.87	11.97	
9H-5, 74.5-75.5	68.65	43.19	27.21	
10X-1, 64.5-65.5	70.05	8.97	3.95	
12X-1, 69.2-70.2	86.79	51.97	21.29	
13H-1, 92.2-93.2	96.62	72.96	19.46	
19X-1, 64.8-65.8	144.55			112.8
19X-3, 51.3-52.3	147.41			95.1
19X-5, 16.2-17.2	150.06			110.3
20X-1, 81.3-82.3	154.31			34.3
20X-1, 83.5-84.5	154.34	86.65	50.09	
20X-5, 79.5-80.5	160.30			159.4
20X-3, 99.1-100.1	157.49			129.9
16X-1, 71.4-72.4	115.71			142.2
16X-3, 74.5-75.5	118.75			112.8
16X-5, 79.6-80.6	121.80			66.2
18X-5, 77.5-78.5	141.08			120.1
21X-1, 72-73	163.82			117.7
21X-3, 72-73	166.82			161.8

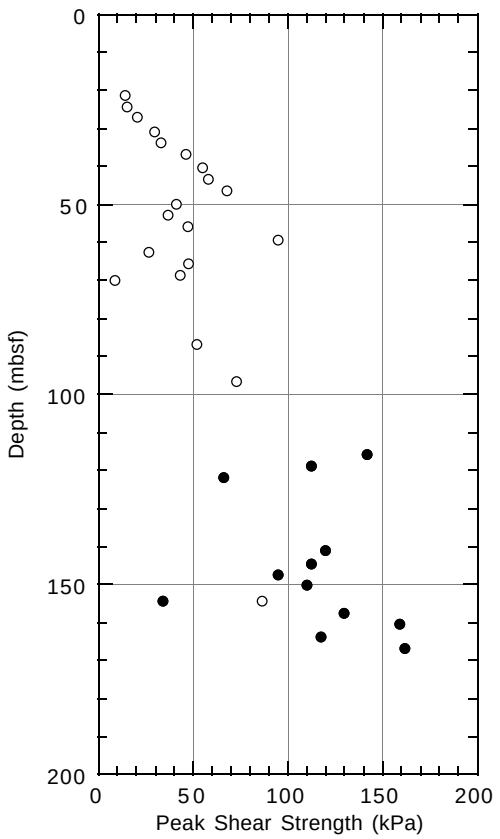

Figure 34. Shear strength for Hole 1049A. The open circles = vane-shear device measurements; the solid circles = pocket penetrometer measurements.

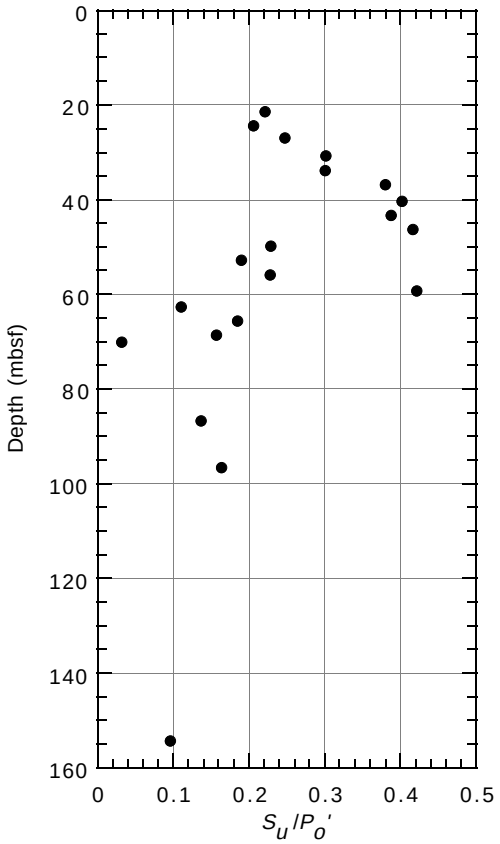

Figure 35. S_u/P_0' for Hole 1049A. The S_u/P_0' are calculated from bulk density and undrained shear strength data (see text for further details).

Table 35. Discrete measurements of resistivity for Hole 1049A.

Core, section, interval (cm)	Depth (mbsf)	Longitudinal resistivity (Ωm)	Transverse resistivity (Ωm)
171B-1049A-			
3H-1, 73.5-76.5	21.34	0.473	0.432
3H-3, 73.5-76.5	24.34	0.457	0.445
3H-5, 33.5-36.5	26.94	0.420	0.421
4H-1, 73.5-76.5	30.84	0.356	0.426
4H-3, 73.5-76.5	33.84	0.400	0.400
4H-5, 73.5-76.5	36.84	0.417	0.400
5H-1, 73.5-76.5	40.34	0.370	0.366
5H-3, 73.5-76.5	43.34	0.386	0.498
5H-5, 73.5-76.5	46.34	0.374	0.364
6H-1, 73.5-76.5	49.84	0.363	0.347
6H-3, 73.5-76.5	52.84	0.379	0.401
6H-5, 73.5-76.5	55.84	0.349	0.351
7H-1, 73.5-76.5	59.34	0.474	0.452
9H-1, 73.5-76.5	62.64	0.376	0.341
9H-3, 73.5-76.5	65.64	0.362	0.340
9H-5, 73.5-76.5	68.64	0.485	0.492
10X-1, 63.5-66.5	70.04	0.392	0.364
12X-1, 73.5-76.5	86.84	0.512	0.575
13H-1, 85.5-88.5	96.56	0.608	0.694
19X-1, 63.8-66.8	144.54	0.968	0.894
19X-3, 50.3-53.3	147.40	1.048	1.008
19X-5, 15.2-18.2	150.05	0.907	0.899
20X-1, 84.5-87.5	154.35	0.850	0.799
20X-5, 78.5-81.5	160.29	0.847	0.843
20X-3, 98.1-101.1	157.48	0.983	0.919
16X-1, 70.4-73.4	115.70	0.912	0.882
16X-3, 73.5-76.5	118.74	0.940	1.005
16X-5, 78.6-81.6	121.79	0.961	0.802
18X-3, 70.5-73.5	138.01	0.915	0.946
18X-5, 70.5-73.5	141.01	0.762	0.679
21X-1, 68.5-71.5	163.79	0.909	0.916
21X-3, 69.5-72.5	166.80	0.919	0.893

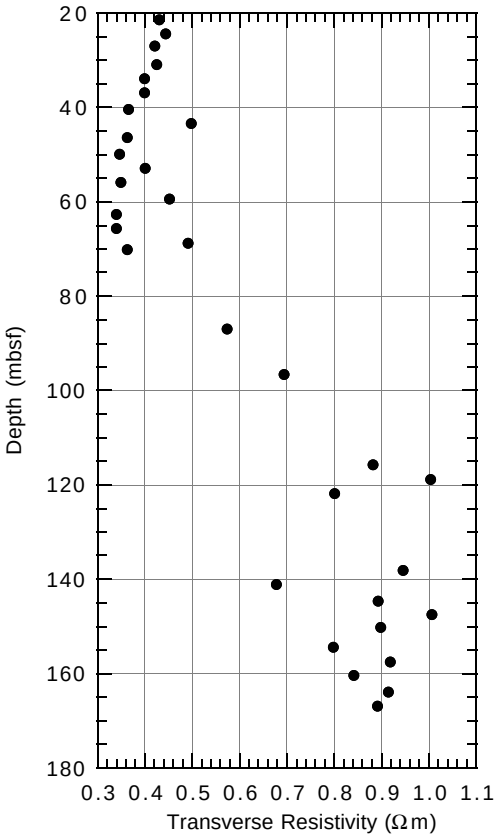

Figure 36. Sediment resistivity for Hole 1049A. Transverse resistivity measurements are considered more reliable than longitudinal measurements, because planar unloading cracks that are perpendicular to the core axis bias longitudinal resistivity measurements to higher values.

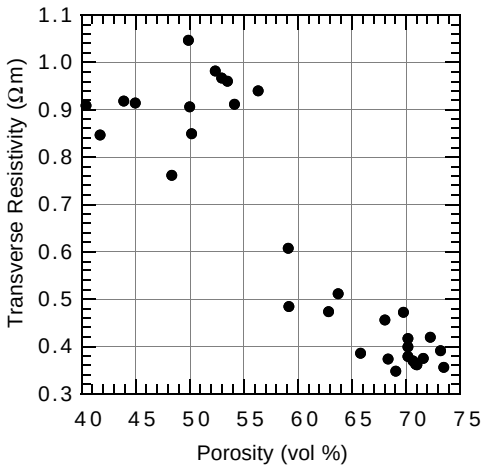

Figure 37. Comparison of transverse resistivity and sediment porosity for Hole 1049A.

Table 36. Discrete measurements of thermal conductivity for Hole 1049A.

Core, section, interval (cm)	Depth (mbsf)	Thermal conductivity (W/m·K)
171B-1049A-		
1H-1, 75-75	2.75	1.03
1H-3, 75-75	5.75	1.07
2H-1, 75-75	12.25	0.78
2H-3, 75-75	15.25	1.01
2H-5, 75-75	18.25	1.04
3H-1, 75-75	21.75	0.83
3H-3, 75-75	24.75	1.02
3H-5, 75-75	27.75	1.08
4H-1, 75-75	31.25	0.80
4H-3, 75-75	34.25	1.19
4H-5, 75-75	37.25	1.10
5H-1, 75-75	40.75	0.54
5H-3, 75-75	43.75	1.57
6X-1, 75-75	91.45	0.94
6X-3, 75-75	94.45	1.49
6X-5, 75-75	97.45	1.20
9X-3, 75-75	122.25	1.46
9X-5, 55-55	125.05	1.17
11X-1, 50-50	138.20	0.91
11X-2, 75-75	139.95	1.56
11X-1, 100-100	138.70	1.41

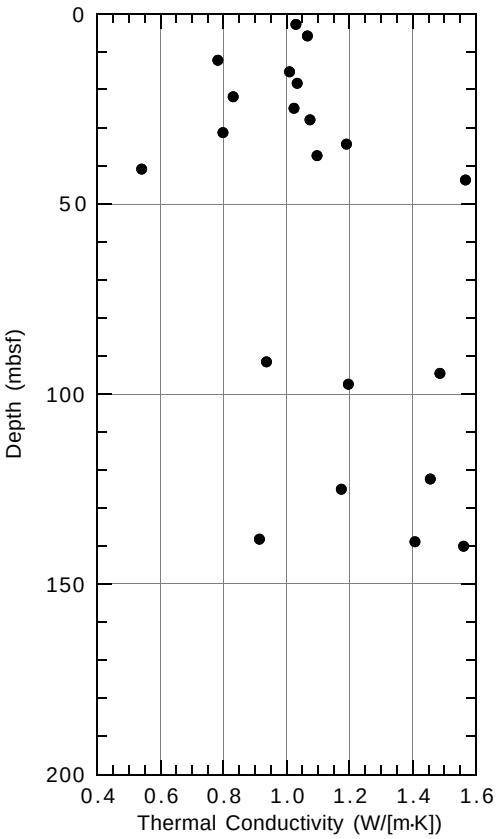

Figure 38. Thermal conductivity for Hole 1049A.